MICROCOPY RESOLUTION TEST CHART
NATIONAL BUREAU OF STANDARDS-1963-A

ROBOT-ASSISTED TOTAL KNEE ARTHROPLASTY: Investigation of the
  Feasibility and Accuracy of the Robotic Process

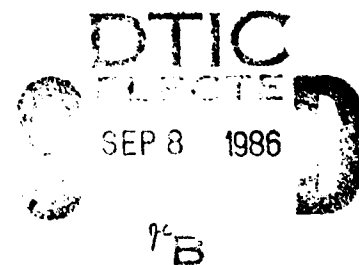Richard Gosaku Kaiura, 03
HQDA, MILPERCEN (DAPC-OPA-E)
200 Stovall Street
Alexandria, Virginia 22332

Final Report   21 August 1986

A thesis submitted to the University of Washington
in partial fulfillment of the requirements for the degree of
MASTER OF SCIENCE IN MECHANICAL ENGINEERING

86   01

REPORT DOCUMENTATION PAGE		READ INSTRUCTIONS BEFORE COMPLETING FORM
1. REPORT NUMBER	2. GOVT ACCESSION NO. AD-A171 669	3. RECIPIENT'S CATALOG NUMBER
4. TITLE (and Subtitle) ROBOT-ASSISTED TOTAL KNEE ARTHROPLASTY: Investigation of the Feasibility and Accuracy of the Robotic Process		5. TYPE OF REPORT & PERIOD COVERED Final Report 21 August 1986
		6. PERFORMING ORG. REPORT NUMBER
7. AUTHOR(s) Richard G. Kaiura		8. CONTRACT OR GRANT NUMBER(s)
9. PERFORMING ORGANIZATION NAME AND ADDRESS Student,HQDA, MILPERCEN (DAPC-OPA-E), 200 Stovall Street Alexandria, Virginia 22332		10. PROGRAM ELEMENT, PROJECT, TASK AREA & WORK UNIT NUMBERS
11. CONTROLLING OFFICE NAME AND ADDRESS HQDA,MILPERCEN ATTN: DAPC-OPA-E 200 Stovall Street,Alexandria,Virginia 22332		12. REPORT DATE 21 August 1986
		13. NUMBER OF PAGES 195
14. MONITORING AGENCY NAME & ADDRESS(If different from Controlling Office)		15. SECURITY CLASS. (of this report) UNCLASSIFIED
		15a. DECLASSIFICATION/DOWNGRADING SCHEDULE

16. DISTRIBUTION STATEMENT (of this Report)

Approved for public release; distribution is unlimited.

17. DISTRIBUTION STATEMENT (of the abstract entered in Block 20, if different from Report)

18. SUPPLEMENTARY NOTES

Document is a thesis submitted in partial fulfillment of the requirements for the Master of Science in Mechanical Engineering Degree. Degree is awarded by the Department of Mechanical Engineering, University of Washington, Seattle, Washingtion.

19. KEY WORDS (Continue on reverse side if necessary and identify by block number)

ROBOT-ASSISTED SURGERY: Total Knee Arthroplasty

20. ABSTRACT (Continue on reverse side if necessary and identify by block number)

The technique of total knee arthroplasty could be improved if there existed a method for making bone cuts on the distal end of the femur which were (1) an exact pres,-fit to the femoral prosthetic component, (2) smooth, and (3) in proper alignment with respect to bones and soft tissues. Using an industrial robot, current mathematical concepts and specially designed fixtures, a robotic process was developed which achieved near press-fit cuts. The resultant cuts were smooth to within a few thousandths of an

DD 1 JAN 73 1473 EDITION OF 1 NOV 65 IS OBSOLETE

ROBOT-ASSISTED TOTAL KNEE ARTHROPLASTY

Investigation of the Feasibility and

Accuracy of the Robotic Process

By

Richard Gosaku Kaiura

A thesis submitted in partial fulfillment
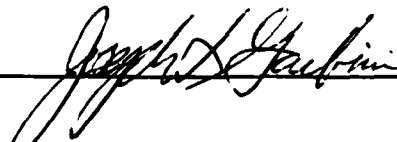of the requirements for the degree of

Master of Science

in

Mechanical Engineering

University of Washington

1986

Approved by _____

Program Authorized
to Offer Degree ___Department of Mechanical Engineering___

Date _____8/21/86_____

In presenting this thesis in partial fulfillment of the requirements for a Master's degree at the University of Washington, I agree that the Library shall make its copies freely available for inspection. I further agree that extensive copying of this thesis is allowable only for scholarly purposes, consistent with "fair use" as prescribed in the U.S. Copyright Law. Any other reproduction for any purposes or by any means shall not be allowed without my written permission.

Signature _Richard G Kamin_

Date _8/21/56_

TABLE OF CONTENTS

LIST OF FIGURES

LIST OF PLATES

LIST OF TABLES

LIST OF SYMBOLS

x, y, z   Scalars; components of a given point; specific component values are indicated with subscripts (e.g. x_i).

c,r,p   Subscripts or superscripts; indicate the coordinate system a certain point is given with respect to; associated with CCS, RCS and PCS respectively.

ϕ, θ, ψ Euler angles phi, theta and psi respectively; when used separately, theta refers to a singular rotation angle which describes the magnitude of a rotation vector, $\vec{\theta}$.

$\vec{p}$, $\vec{m}$, $\vec{n}$, $\vec{o}$ Position and orientation vectors used to describe a tool location in space; $\vec{n}$ also used as an axis of rotation vector in conjunction with the rotation vector, $\vec{\theta}$.

$\vec{s}$, $\vec{t}$, $\vec{u}$, $\vec{r}$, $\vec{1}$ Vectors; general vectors used for illustration purposes.

$\vec{a}$, $\hat{b}$ Vectors; used to refer to the columns of A and B respectively; associated with one point in a set of fiducial points.

N   Scalar; the number of fiducial points used in computing a transformation matrix, $^{r}T_p$.

A   Matrix; a 4 x N matrix whose columns are the x, y, z coordinates of the points contained in a set of points given with respect to the RCS and whose bottom row consists of 1's.

B   Matrix; a 4 x N matrix whose columns are the x, y, z coordinates of points contained in a set of points given with respect to the PCS or CCS and whose bottom row consists of 1's.

$^{r}T_p$ Matrix; a 4 x 4 matrix which is the transformation matrix between two coordinate systems or a coordinate system and a reference frame; subscript indicates

	initial coordinate system, superscript indicates resultant coordinate system or reference frame.
R	Matrix; a 3 x 3 matrix which is the rotation matrix between two sets of points; used to compute ^rT_p.
L, K, J	Matrices; general 4 x 4 matrices used in computing ^rT_p.
RCS	Robot Coordinate System
PCS	Planning Coordinate System
CCS	Measurement Test Cube Coordinate System
BRF	Bone Reference Frame
MTE	Mean Translational Error
MRE	Mean Rotational Error
RMS	Root Mean Squared
AI32	The controller for the AID 600 robot, built by Automatix, Inc.
AID 600	The industrial robot used in this investigation, also built by Automatix, Inc.

ACKNOWLEDGEMENTS

CHAPTER 1

INTRODUCTION

1.1 Preliminary Remarks

Total knee arthroplasty encompasses the replacement of the contact surfaces of the femur, tibia and patella in the knee joint of a patient with prosthetic components designed for this purpose. Of chief concern to orthopaedic surgeons and manufacturers of prosthetic devices is the question regarding the relationship between the functional characteristics in knee arthroplasty and certain intra-operative variables which affect them [1]. Research being conducted at the University of Washington jointly by the Departments of Mechanical Engineering and Orthopaedics [2] has produced a method of studying these characteristics and variables and predicting their relationship. Moreover, preliminary assessments of this research are being confirmed and indications are promising that orthopaedic surgeons will be able to utilize these results to assist them in optimizing the functional capabilities of their knee arthroplasty patients. However, while inroads are being made in this area of knee arthroplasty, the means for precisely and accurately achieving the desired physical positioning of prosthetic components on to their respective knee joint locations remain undeveloped.

The improper positioning and alignment of the femoral prosthetic component on the distal end of the femur is a problem frequently encountered during clinical evaluations of total knee arthroplasty. This problem established the central focus for this investigation. An understanding of this problem requires an explanation of the anatomy and geometry of the femur and its corresponding prosthetic component. The terms used to describe the different parts of the femur are shown in Figures 1.1 and 1.2. Figure 1.1 shows the location of the femur in a human leg. Figure 1.2 identifies the different features of the distal end of the femur. On the femur, the surfaces of the condyles and the anterior side of the femur near the condyles are replaced in total knee arthroplasty. These surfaces are replaced by those of a femur-shaped prosthetic component. Figure 1.3 illustrates such a component and identifies its various surface and part names. Figure 1.4 shows the relationship between the femur and this component after completion of total knee arthroplasty.

The femoral prosthetic component position and alignment errors encountered in clinical evaluations of total knee arthroplasties manifest themselves in all, or part of, four variables. These variables are

      (1) the tibiofemoral angle of the knee in extension,

      (2) the flexion/extension rotation of the femoral pros-
             thetic component,

PROXIMAL END OF THE FEMUR ——————

FEMUR ———————

DISTAL END OF THE FEMUR—

KNEE JOINT AREA —
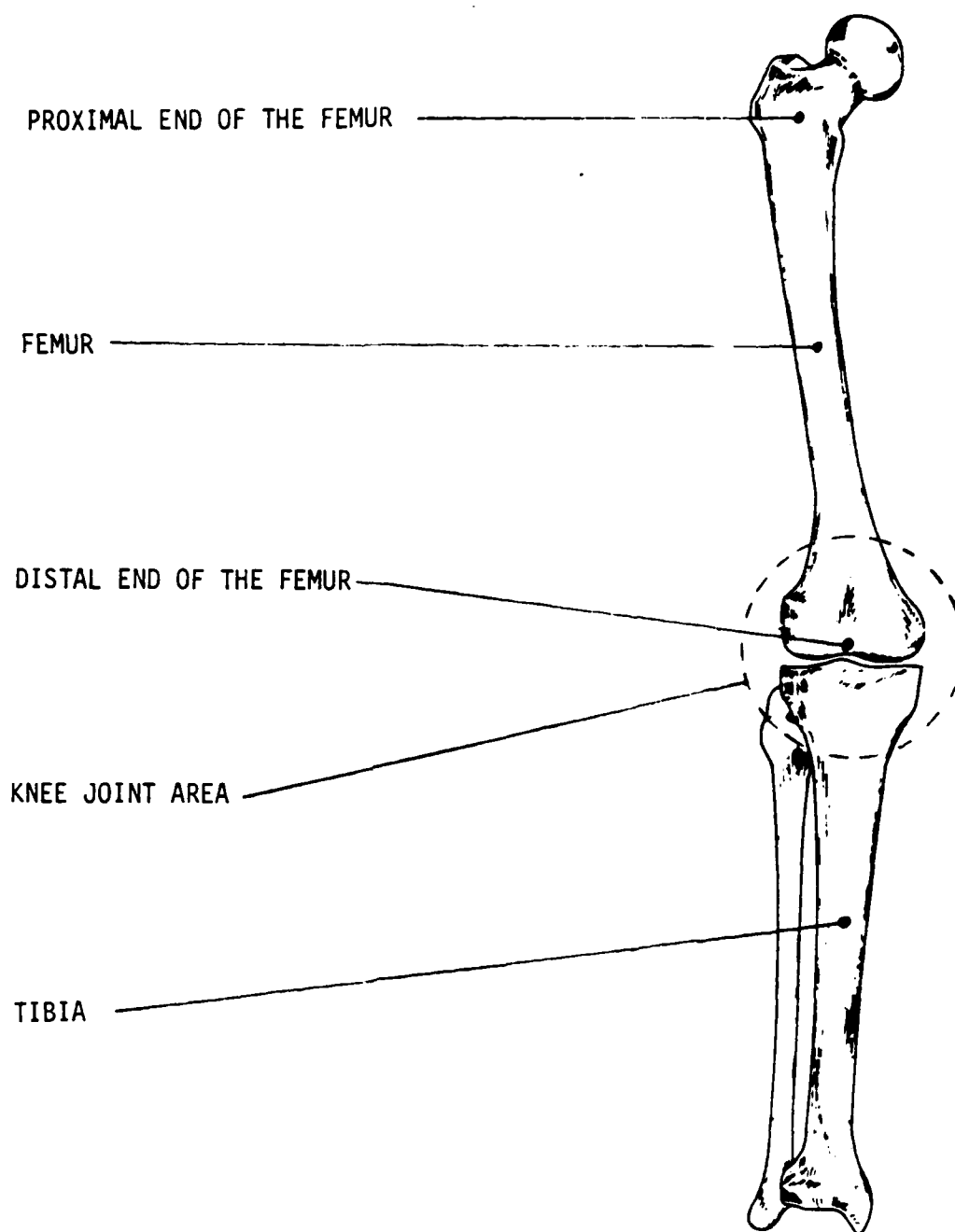
TIBIA —

Figure 1.1 Illustration of the femur and tibia in the human leg[*]

ANTERIOR SIDE OF THE FEMUR

EPICONDYLE

CONDYLE

CONDYLE

POSTERIOR SIDE OF THE FEMUR

NOTCH MARGIN
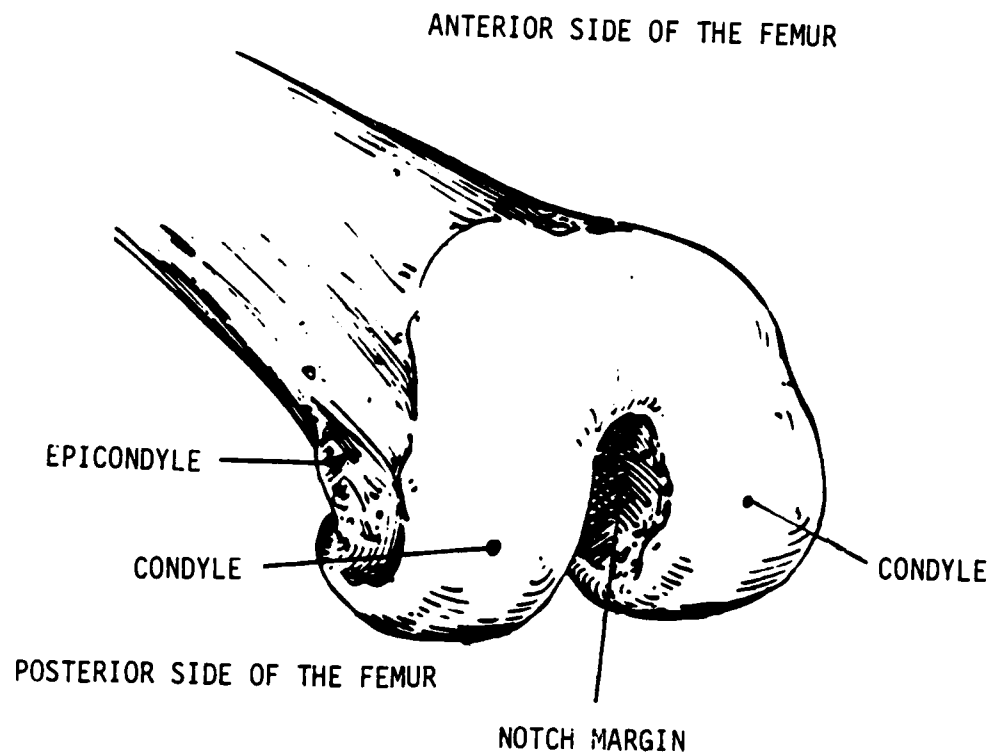
Figure 1.2 Illustration of the distal end of the femur[*]

---

[*]This is a modification of an illustration taken from "Robert Brigham Total Knee Operative Technique," written by F. C. Ewald and published for the Johnson and Johnson Orthopaedics Products Division.

INNER, POROUS SURFACE

STUD

STUD

OUTER CONTACT SURFACE
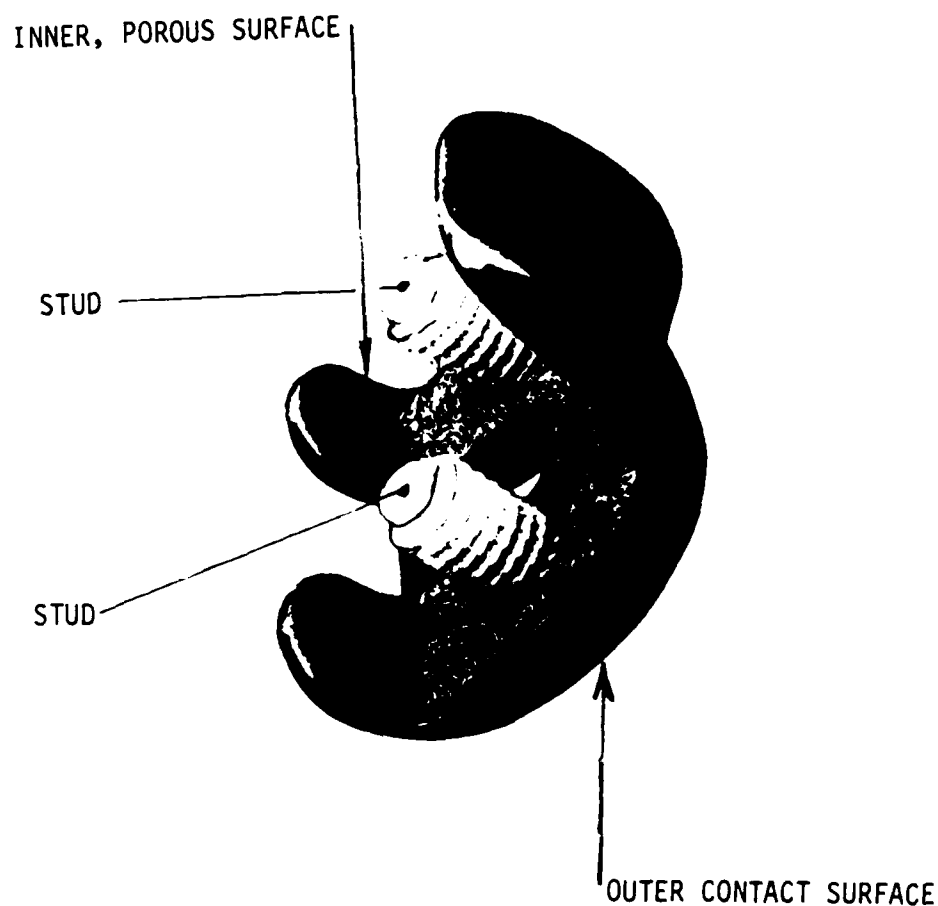
Figure 1.3 Illustration of the femoral prosthetic component [*]

---

[*] This is a modification of an illustration taken from the pamphlet "TOTAL KNEE REPLACEMENT WITH THE TRICON-M SYSTEM," written by Richard S. Laskin, M.D., and published for the Richards Medical Company.

FEMORAL PROSTHETIC COMPONENT

FEMUR
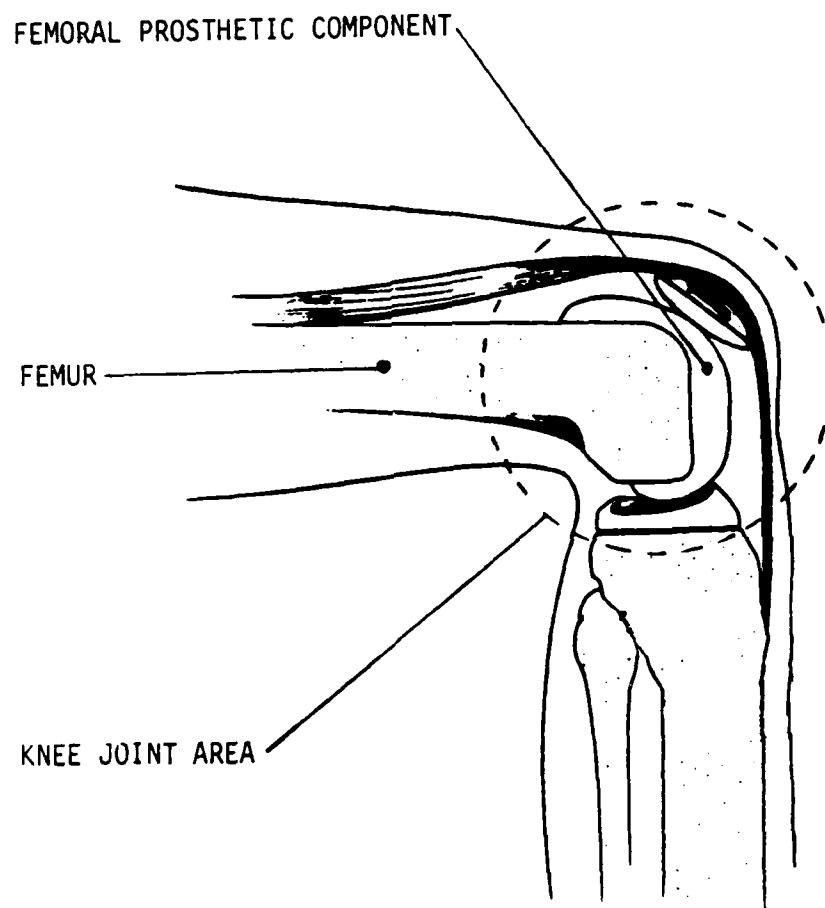
KNEE JOINT AREA

Figure 1.4   Illustration of an implanted femoral prosthetic component
in a human knee joint *

*This is a modification of an illustration taken from the pamphlet
"TOTAL KNEE REPLACEMENT WITH THE TRICON-M SYSTEM," written by Richard
S. Laskin, M.D., and published for the Richards Medical Company.

(3) the axial rotation of the femoral prosthetic component, and

(4) the translation deviation of the prosthetic component from its intended position.

These errors are illustrated in Figures 1.5 through 1.8 respectively. In these figures, both correct and incorrect placements of the prosthetic component are shown. Note that these variables are associated with all six degrees of freedom characterizing a rigid body's location in three-dimensional space.

In Figure 1.5, the tibial axis, shown by a solid line, passes through the center of the prosthetic component and is aligned with the long axis of the tibia. The femoral axis is indicated by a dashed line and is aligned with the long axis of the femur. The tibiofemoral angle is generally accepted to be 7 degrees. Although this may vary widely from person to person, it is based on the results of many clinical studies and is the standard used by industrial manufacturers of prosthetic devices. Both a correct and an incorrect tibiofemoral alignment angle illustration are given.

In Figure 1.6, the flexion/extension angle of the prosthetic component on the femur is shown. Though not an established standard, the generally accepted alignment criterion for this angle is that the plane containing the inner, porous surface of the prosthesis which ingrafts on to the distal cut of the femur should be

INCORRECT

FEMUR

PROSTHESIS

7°

CORRECT

——— tibial axis
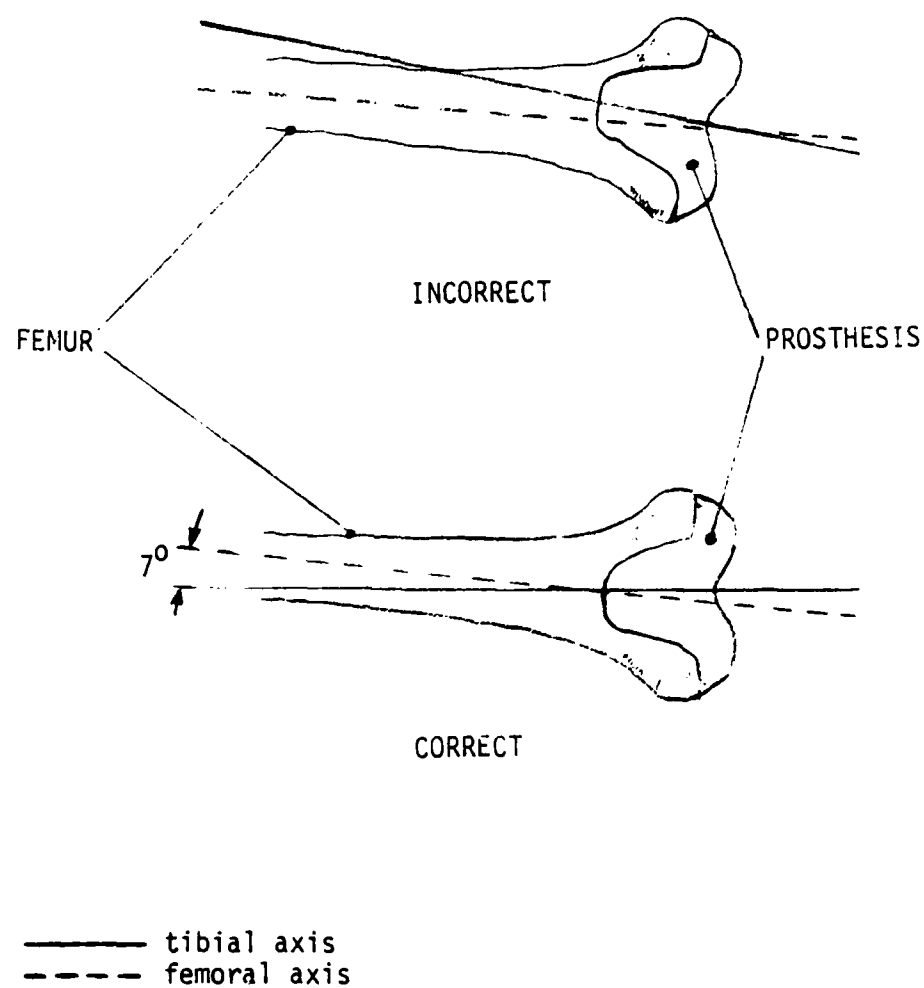
– – – femoral axis

Figure 1.5 Illustration of the tibiofemoral alignment angle for
a correct total knee arthroplasty and an incorrect
knee(exaggerated)
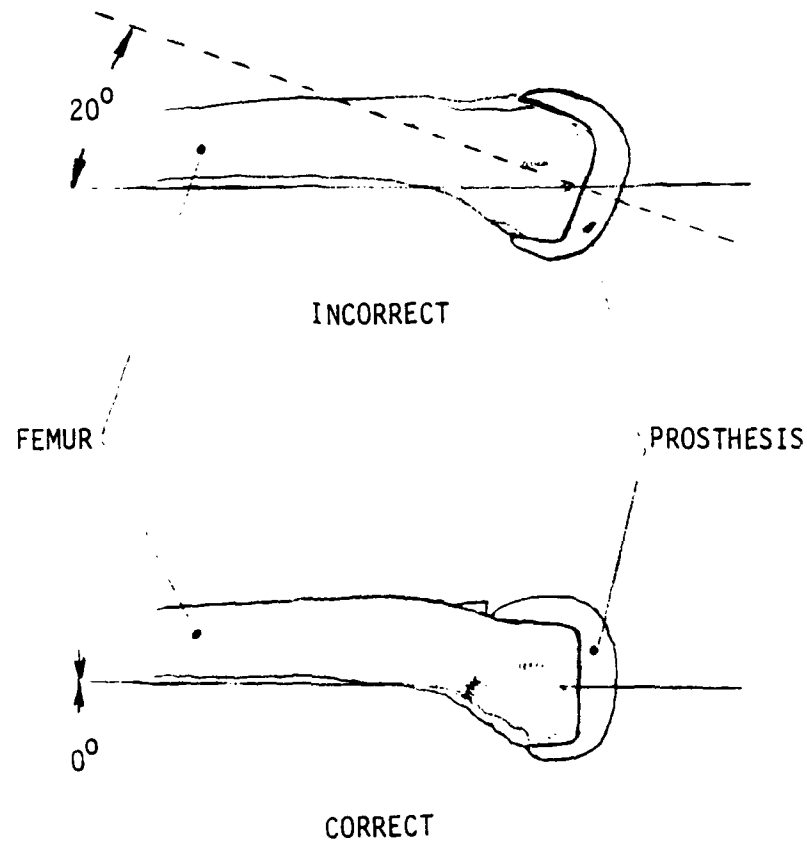
Figure 1.6   Illustration of the flexion/extension angle for a
correct total knee arthroplasty and an incorrect
knee

perpendicular to an imaginary axis which runs from the center of this surface to the center of the ball shaped proximal end of the femur. The correct alignment of the prosthetic component on the femur is shown below a greatly exaggerated, incorrectly aligned prosthetic component.

The axial rotation angle of the prosthetic component on the distal end of the fermur is illustrated in Figure 1.7. Because the prosthesis is designed to replace the contact surfaces on the femur, great care must be taken to insure the cuts affecting this angle are accurately made. This generally involves taking equal portions of bone off the posterior surfaces of the femoral condyles and insuring a parallel anterior cut. When this is done, the imaginary line, which bisects both mounting studs of the prosthetic component and is contained in the plane of the inner, porous surface of the prosthetic component that ingrafts on to the distal cut surface of the femur, will be aligned parallel to another imaginary line which is parallel to the cut posterior surfaces of the femoral condyles and which bisects, perpendicularly, the imaginary line running from the ball portion of the proximal end of the femur to the center of the distal cut surface of the femur. Both correct and incorrect alignments of the axial rotation angle are shown.
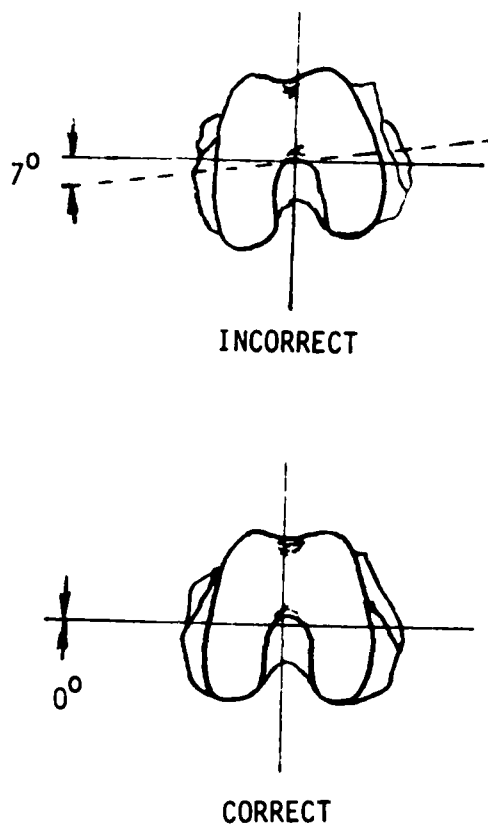
Figure 1.7 Illustration of the axial rotation angle for a correct total knee arthroplasty and an incorrect knee

In Figure 1.8, the last type of placement error associated with the femoral prosthetic component on the femur is illustrated. This error is positional in nature and is the result of either removing too much bone material or not enough when the distal femoral cut is made.

Instances of improper femoral prosthetic component placement and alignment on the distal end of the femur are not isolated. In one clinical study, fewer than 10% of the 76 total knee arthroplasty patients evaluated were judged to have perfectly positioned prosthesis [3]. Moreover, improper positioning of knee prostheses has been shown to predispose the implanted prostheses to loosening and failure [4]. Furthermore, statistics show the number of total knee arthroplasties done in the United States in 1983 was approximately 30,000 [5]. Current estimates, however, are much higher. These facts all serve to underscore the need for more accurate and precise methods of conducting total knee arthroplasties.

The source of the position and alignment problem is known. Currently, complex techniques for knee arthroplasty utilize surgical fixtures, cutting guides and tools. While these techniques and instruments embody the best currently "in-use" approaches to solving the position and alignment problem, they depend heavily on the experience and intuition of the surgeon and clinically established "rules-of-thumb." The resultant surgical burden is tremendous. Without the aid of any precision devices which would insure the

INCORRECT

TRANSLATIONAL ERROR
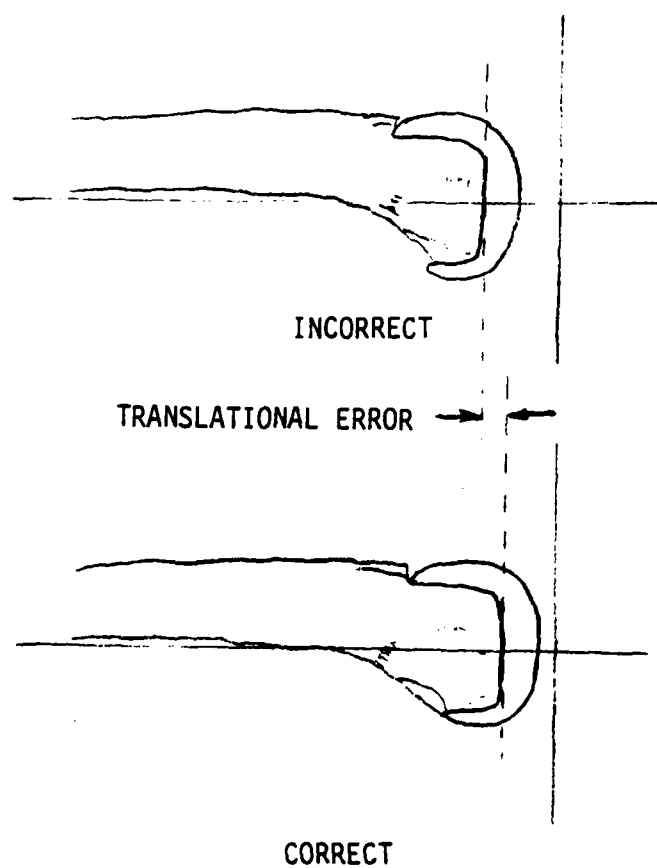
CORRECT

Figure 1.8 Illustration of the translational position for a correct total knee arthroplasty and an incorrect knee

levels of accuracy so urgently required to solve the position and alignment problem, significant reductions in total knee arthroplasty failures cannot be reasonably expected.

Since the position and alignment of the femoral prosthetic component is directly related to the cuts made on the distal end of the femur, it can be reasoned that by generating the femoral cuts more accurately, the position and alignment errors can be reduced. The attainment of precision cutting in industry is obtained using computer-controlled precision cutting machines. If this technology can then be adapted to the operating room, a possible solution to the position and accuracy problem has been identified.

1.2 Current Related Research

The results of total knee arthroplasty could be vastly improved if a means for accurately locating and making the cuts to the components of the knee joint existed. The problems of accuracy discussed so far suggest the source of a possible solution--robot assisted surgery. While the involvement of computers in the medical field is widespread, robotic processes are scarce. Computers are playing an increasing role in tomography, database management, structuring medical diagnostics, bionics and medical modeling and simulation. Surprisingly enough, however, the involvement of robots in the medical field is extremely rare. For example, computer searches of the COMPENDEX, INSPEC and MEDLINE databases from 1982 to

the present turned up only a handful of articles indicating areas in which robots were utilized in the medical field. Out of these only one was directly related to an applied robotic process; the stereotactic neurosurgery being done in Long Beach, California [6]. Additional hand searches indicated that research at the University of Tokyo was pursuing the development of a microsurgery robot system to be used in keratoplasty [7].

1.3 Research Goals

The goals established for the research conducted in this thesis were:

(1) To demonstrate the feasibility of using a robot controlled cutting tool to generate the cuts on the femur component of the knee joint necessary to mount the corresponding prosthetic device; and

(2) To experimentally assess the accuracy of the resulting robotic process.

The demonstration of feasibility was accomplished through the definition, explanation, development and demonstration of a robotic process which utilizes a robot controlled cutting tool to generate the cuts on the femur. The assessment of accuracy of the robotic process was accomplished through the identification and analysis of all possible factors which might contribute to the overall system

error. Further examination of all significant error sources was then conducted to establish their actual values and relationship to the overall system error.

CHAPTER 2

PRELIMINARY EQUIPMENT/SOFTWARE DESCRIPTION

2.1 General Comments

Research conducted in this study involved the extensive use of
equipment and computer languages already available. The integration
of an industrial robot required the writing of additional software
and the incorporation of at least two of the AI32's controller ports
into an existing computer switching system. In addition, the
fabrication of several fixtures was required before any programming
work could be accomplished. Descriptions of the computer equipment
and languages used, preliminary software and fixture requirements and
the Automatix AID 600 robot with AI32 controller are provided below.

2.2 Computer Equipment and Languages Used

Much of the analytical work associated with transformation
matrix programming was accomplished on the Mechanical Engineering
Department's PDP-11 computer system using the FORTRAN 77 programming
language. In addition to this, many of the programs developed on the
PDP-11 were edited on this computer before being transferred to the
AI32. The AI32 used the RAIL computer language. RAIL stands for
"Robot Automatix Incorporated Language." RAIL can be characterized
as being similar to Pascal, but with many other commands contained in

it which allow it to:

- move the AID 600 robot.

- input and output data and control signals.

- load, store, and edit programs.

- handle a variety of data types which include not only integers, real numbers, character strings, arrays and logical data, but also points, paths and reference frames.

- use a built in library of special functions.

For a more detailed descriptions of RAIL, see the RAIL Software Reference Manual [8].

2.3 Preliminary Software and Fixture Requirements

Several programs were written to enhance the interaction between the AI32, PDP-11, and user.

These programs:

- configured the ports of the AI32.

- allowed the user to operate from a remote terminal.

- printed out listings of variable values and names, programs and data.

- transferred files between the AI32 and PDP-11 computer.

- loaded files into the AI32 and set robot speeds.

Several fixtures were required in order for the robotic process established in this thesis to be implemented. These fixtures were developed to aid the robot in defining the tips, edges or surfaces of tools which would be employed in the robotic process as well as to immobilize the femur in the work volume of the robot. Descriptions of the various types of fixtures developed are listed below:

- brackets which mounted specific tooling onto the end of the robot.

- brackets which restrained the femur in the work volume of the robot.

- fixtures which were used to calibrate the tools used in the robotic process.

- fixtures which were used to assess the accuracy of the robotic process.

2.4 Automatix Robot Characteristics

The Automatix AID 600 robot proved to be an excellent choice for the tool manipulator in this research. The robot possessed a large work envelope enabling the tools used in the research effort to be moved about the femur in a variety of different positions. The built-in functions of the robot coupled with the flexibility of being

able to run computation programs using the AI32 made the AID 600 a highly convenient, self contained robot system. Many of the programs written for the control of the cutting tool relied on several built-in functions organic to the AID 600 robot; most notably the BUILDFRAME function. Figure 2.1 contains a diagram of the AID 600. Table 2.1 contains a listing some of the hardware characteristics of this robot system.
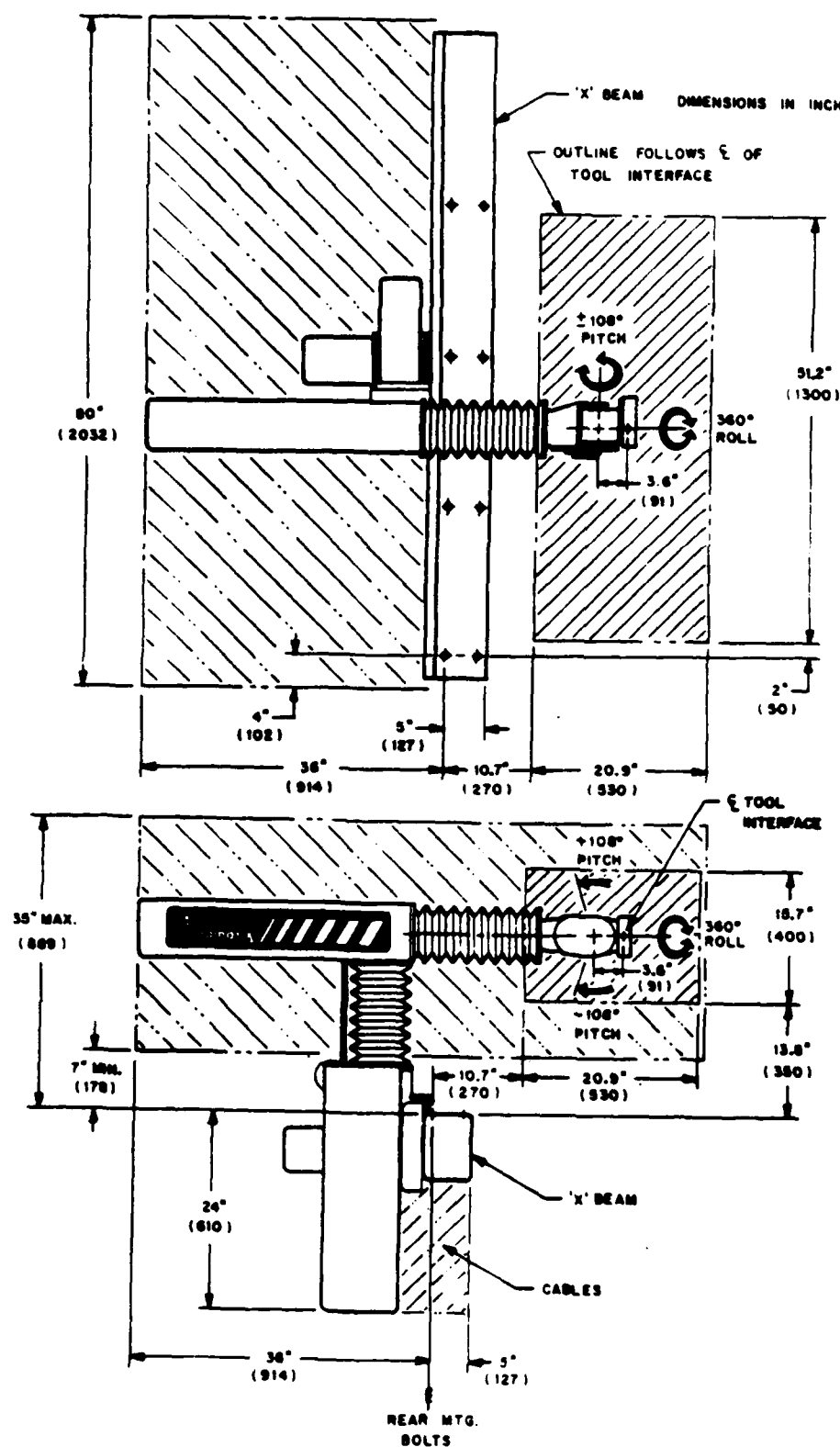
Figure 2.1 Diagram of Automatix Robot [9]

Table 2-1 Automatix AID 600 Robot [10]

Axes   Three Cartesian Axes, Two Rotary Axes (wrist)
Work Volume   .28 M^3
Axes Range   x - 1300 mm   Ry - +/- 108 deg
                          y - 530 mm   Ry - +/- 180 deg
                          z - 400 mm

Maximum Work Weight   8 kg (17.6 lbs)

Axes Velocities   x - 60 M/min   Rx - 135°/sec
   (maximum)   y - 60 M/min   Ry - 360°/sec
                          z - 60 M/min

Drive   DC Permanent Magnet Motors with
                          Brushed Commutation

Resolution   Linear: .02 mm
                          Rotary: .3 mrad

Linearity   Linear: +/- .025 mm
                          Rotary: +/- .6   mrad

Backlash   Linear: .01 mm
                          Rotary: .3 mrad

CHAPTER 3

DEFINING THE ROBOTIC PROCESS

3.1 General Comments

The robotic process developed in this investigation took advantage of the precision motion control characteristics of an industrial robot in its application to a specific medical problem. The first goal of this research was to determine the feasibility of generating knee arthroplasty bone cuts on the femur using a robot. This involved three distinct phases of what was envisioned to be robotic surgery in the near future: (1) planning (2) orientation, and (3) cut generation.

The demonstration of the feasibility of using robots to assist orthopaedic surgeons in total knee arthroplasty was accomplished using the AID 600 robot, manufactured by Automatix, Inc. Additional equipment necessary for the robotic process was either designed and fabricated or procured locally. The cutting tool was a modified 2-1/4" helically-fluted routing cutter mounted in an air motor and driven at a speed of 18,000 RPM. The cutting tool was mounted at the end of the robot wrist using a fabricated bracket. Hardshell plastic femurs with foam cores were used as the test bones on which all cuts were generated. Proof of feasibility was considered to be the development and demonstration of a reasonable procedure for the

execution of this specific application of robotic surgery; cost was not considered in this investigation.

Prior to this investigation, much of the work in the planning phase was already developed and in the advanced stages of refinement. This investigation was considered the next, logical step in the pursuit of an applied robotics process which would enable the orthopaedic surgeon to significantly improve the quality of his knee arthroplasty techniques.

The intent of this investigation is to determine the usefulness and practicality of applying robots as a surgical aid in total knee arthroscopy to increase the accuracy of this procedure. It is not suggested that robots are capable of replacing the surgeon in the operating room.

3.2 Calibration

The calibration of the robot and the tools used by the robot was a critical aspect of this investigation. Values for the accuracy of tool definitions were necessary in order to make any conclusive statement concerning the resultant accuracy of the robotic process developed in this study. A complete description of the calibration procedure is contained in Appendix A. Tool definitions were required for: (1) wrist extension, (2) stylus, (3) cutter, and (4) dial indicator.

3.3   The Robotic Process

3.3.1   Planning

This first phase of the robotic process obtained and processed the information utilized to execute the remaining two phases.   This phase was therefore critical to the successful outcome of the knee arthroplasty.   It involved a computer graphics analysis of the positioning of the prosthesis and the resultant prediction of knee joint performance.   In this phase, the femoral surface anatomy of the knee joint was digitized.   Approximately 2000 points were taken of the femoral surface and subsequently displayed as a three-dimensional image on a computer graphics terminal.   A similar three-dimensional image of the prosthesis was also digitized, with both bearing surfaces and inner bone adhesion surfaces being modeled on the same computer graphics terminal.

The position of the prosthesis image relative to that of the femur on a computer graphics terminal was controlled by the six-degree-of-freedom motion of a hand-held stylus.   The resultant position and orientation of the inner bone adhesion surfaces and load bearing surfaces relative to the femur surface anatomy were then inspected and iteratively adjusted as necessary to obtain the final desired alignment.   This final bone-to-component alignment was then defined numerically by specifying in a common, planning coordinate system (PCS): (1) the location of fiducial landmarks on the surface

anatomy of the bone (epicondyles, notch margin, etc.), and (2) the femur reference points used to describe the position and orientation of the prosthetic component. This resultant data was then transferred to the AI32 controller of the AID 600 robot for the next phase of the robotic process.

3.3.2 Orientation

This phase was characterized by the transfer of data from the Planning Phase and the development of the final path of points necessary for the AID 600 to move the cutter. It was in this phase where the greatest sources of error in the robotic process were found. This phase began with the mounting of the bone within the work volume of the robot. The femur was immobilized using special fixtures in a manner which would not obstruct conventional surgical approaches to the knee joint area. These approaches included the area of space immediately above and to the side of the knee joint.

The location of the bone in the robots work volume was determined using tactile methods. The robot, using a stylus mounted to the end of its wrist, touched each of the fiducial landmarks, or points, specified in the previous planning phase. These points were touched in the same sequence in which they were entered into the AI32 controller.

Using these two sets of corresponding coordinates, the appropriate transformation matrix between the planning coordinate

system (PCS) and robot coordinate system (RCS) was computed. The resultant transformation was applied to the femur reference points, which were then used to compute the final Bone Reference Frame of the femur in the RCS. A previously specified path of points for the cutter, defined relative to the origin of the RCS, was then transformed to this Bone Reference Frame and the final cutting path established.

3.3.3 Cut Generation

At this point in the robotic process, the robot possessed the desired path information necessary for generating the cuts on the femur. The robot was to generate in succession the distal, anterior chamfer, anterior, posterior chamfer and posterior bone cuts (see Figure 4.1). The stud hole cuts for the studs on the inner, porous surface of the prosthesis were also made (see Figure 1.3). Protocol for making each of the required cuts was predetermined and designed to minimize robot backlash effects.

3.4 Definitions and Equations

3.4.1 Definitions

Certain definitions were used throughout this thesis to assist in explaining procedures and concepts used in the robotic process. These definitions are established here in an effort to make the reading of this thesis as succinct as possible.

COORDINATE SYSTEM: A system in which three orthogonal, linearly scaled axes are established at a fixed position in space for the purpose of defining the location of points relative to that fixed position, referred to as an origin with its coordinates being (0, 0, 0). Three coordinates are used and the axes are nominally designated as the x, y, and z axes. This form of coordinate system is commonly referred to as the Cartesian coordinate system. In this thesis three such coordinate systems were used. They were the robot coordinate system (RCS), planning coordinate system (PCS) and the measurement test cube coordinate system (CCS).

REFERENCE FRAME: A location within a specified coordinate system, other than the origin, which is established by applying an orthogonal transformation to the origin. The reference frame may be used to transform points, defined with respect to the origin of the specified coordinate system, to locations relative to the desired reference frame. The important concept to note is that reference frames do not establish new coordinate systems; they operate within the coordinate system in which they are defined.

HOME: A built-in variable of the RAIL language defined as the location where all robot joint variables are zero. For the AID 600 robot, the home position is in the lower-right, rear corner of the working volume when facing the robot.

TOOL: A built-in variable of the RAIL language that describes the tool tip location and tool orientation of the tool attached to the robot. The TOOL definition is related to the wrist of the robot arm. It is specified in coordinate transformation form:

$$TOOL = [D_x, D_y, D_z, \phi, \theta, \psi]$$

The D_x, D_y, D_z parameters are the RCS coordinates to the tool tip, from the wrist flange reference frame, when the robot arm is in the HOME position. The ϕ, θ, ψ parameters are the orientation angles of the tool. They also correspond to a set of Euler angles. The Tool definition may be changed to define a stylus, cutter, dial indicator or wrist extension. For more information see Appendix A.

COORDINATE TRANSFORMATION FORM: A six parameter row matrix of the form $[D_x, D_y, D_2, \phi, \theta, \psi]$ which contains all the essential information necessary to construct a transformation matrix. The parameters D_x, D_y and D_z correspond to the elements of the transformation matrix p_x, p_y and p_z respectively. The parameters ϕ, θ, and ψ are Euler angles which, when substituted into equation (4) yields the direction cosines n_x, n_y, n_z, o_x, o_y, o_z, m_x, m_y and m_z. When these elements are entered into equation (3) the homogeneous transformation matrix, ^rT_p is obtained.

LOCATION: The spatial position and orientation of an object relative to a specified coordinate system or reference frame. The same

coordinate transformation form format used to define TOOL is used to define points and objects in the RCS. Point locations require only the first three parameters of the coordinate transformation form. Object locations, on the other hand, require all six parameters. In order for the ϕ, θ, ψ angles to have meaning, an object must have at least one of its axis designated. (e.g. the z-axis of the cutter is located along the centerline of its longest axis).

BUILDFRAME: A built-in function of the RAIL langugae that allows a reference frame to be created in the robot coordinate system by identifying three existing point locations. The first point is the "origin" of the reference frame. The second point is a point located along the positive x-axis of the new reference frame. The third point is any point in the positive quadrant of the XY plane of the new reference frame. For an explanation of this function see reference [11].

REFERENCE POINTS: Points which are used to assist in establishing reference frames using the BUILDFRAME function described above. Femur reference points are used in the Orientaticn Phase of the robotic process to establish the Bone Reference Frame of the femur in the RCS.

FIDUCIAL POINTS: Physical points on the surface of the femur selected by the surgeon for use in computing the transformation between the

PCS and the RCS. The number of points used varied between 4 and 10, though any number of points greater than 4 may be used.

PATH: A connected series of points along which the tip of the tool mounted on the wrist of the AID 600 robot is to move.

SPATIAL ERROR: The dissimilarity in the spatial arrangement of two corresponding sets of measurements taken from one set of physical points. The coordinate systems of each set of measurements may be different. Spatial error is considered to be the result of random error which exists in the robotic process.

3.4.2 Equations

The following equations were relied on heavily throughout this study to explain certain numerical relationships and are established here for later reference.

STANDARD MATRIX EQUATION: $$A \vec{x} = \vec{b} \qquad (1)$$

This matrix equation is used to represent a system of linear algebraic equations. A is the coefficient matrix while $\vec{x}$, $\vec{b}$ are column vectors.

TRANSFORMATION MATRIX EQUATION: $$A = {}^{r}T_{p}\, B \qquad (2)$$

This matrix equation is the principle equation used in the transformation process. A is a 4 x N matrix whose columns contain the x, y, z components of each fiducial point with reference to the

RCS. Similarly, **B** is a 4 x N matrix whose columns contain the x, y, z components of each fiducial point with reference to the PCS. The fourth row in both matrices consists of 1's. $^{r}T_p$ is the transformation matrix to be determined. In this thesis, $^{r}T_p$ is a homogeneous transform which insures the retention of spatial relationships (e.g. distances and angles remain unchanged).

GENERAL FORM OF TRANSFORMATION MATRIX:

$$^{r}T_{p} = \begin{bmatrix} n_x & o_x & m_x & p_x \\ n_y & o_y & m_y & p_y \\ n_z & o_z & m_z & p_z \\ 0 & 0 & 0 & 1 \end{bmatrix} \tag{3}$$

This establishes the convention used for referring to each component of the 4 x 4 transformation matrix which creates a rotation and translation of any vector or matrix it pre-multiplies from one coordinate system or reference frame to any other. The physical relevance of the components is best illustrated in Figure 3.1.

The tool tip in this example is the origin of the tool reference frame. The vector, $\vec{p}$, describes the difference between the origin of the initial coordinate system and the origin of the tool tip. There is no restriction on the components of $\vec{p}$. The z - axis of the tool lies in a direction from which the tool would approach an object and is known as the approach vector, $\vec{m}$. The y - axis of the tool is known as the orientation vector, $\vec{o}$, and normally specifies the orientation of the tool. For the tool illustrated, this direction vector does not matter. The last vector, $\vec{n}$, known as the normal vector, is specified by the vector cross product, $\vec{n} = \vec{o} \times \vec{a}$. $\vec{n}$, $\vec{o}$, and $\vec{a}$ are unit vectors. They are also orthogonal with respect to each other.
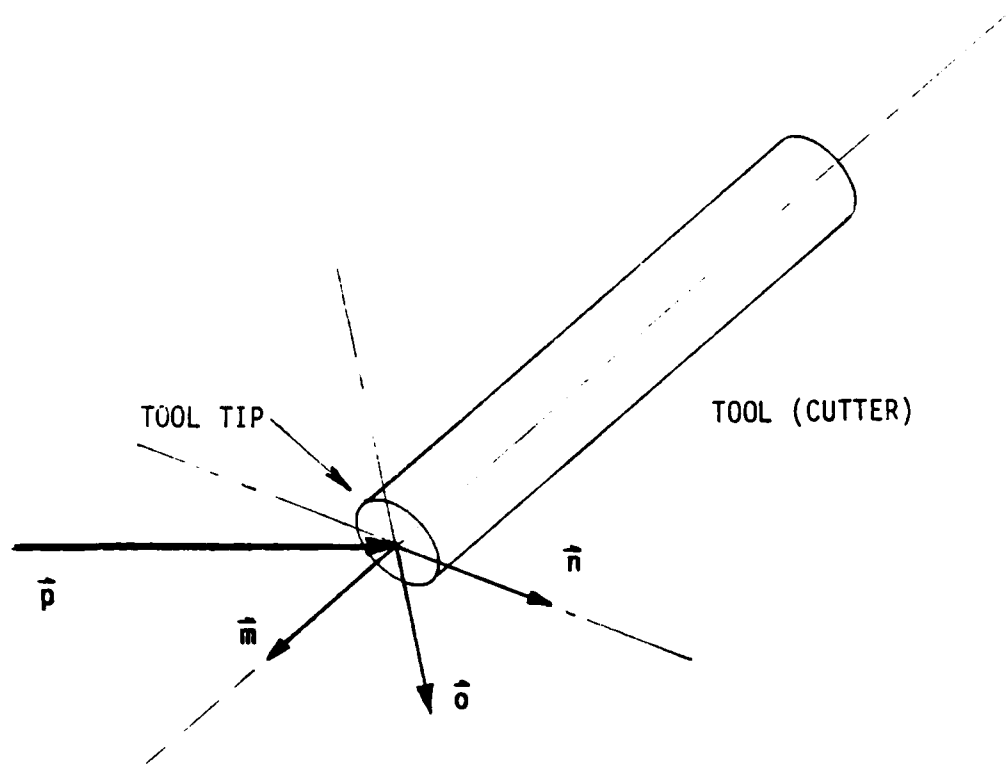
Figure 3.1 Tool Orientation Vectors

EULER ANGLES (ϕ, θ, ψ):

$$^r T_p = \begin{bmatrix} c\phi c\theta c\psi - s\phi s\psi & -c\phi c\theta s\psi - s\phi c\psi & c\phi s\theta & 0 \\ s\phi c\theta c\psi + c\theta s\psi & -s\phi c\theta s\psi + c\phi c\psi & s\phi s\theta & 0 \\ -s\theta c\psi & s\theta s\psi & c\theta & 0 \\ 0 & 0 & 0 & 1 \end{bmatrix} \quad (4)$$

where c = cosine

s = sine

This equation establishes the relationship between the Euler angle parameters used and the formulation of an orthogonal transformation matrix. The Euler angles establish the rotation about certain axes of a coordinate system which will change the orientation of an object in a certain manner. The relationship between the old and new orientation of an object and its Euler angles is illustrated in Figure 3.2

The first angle, ϕ, is created by a rotation of the x, y, z axes about the z - axis forming the x', y', z' reference frame. The second angle, θ, is a rotation about the new y'-axis forming the x", y", z" reference frame. Finally, the third angle, ψ, is a rotation about the new z" axis forming the x''', y''', z''' reference frame [12].
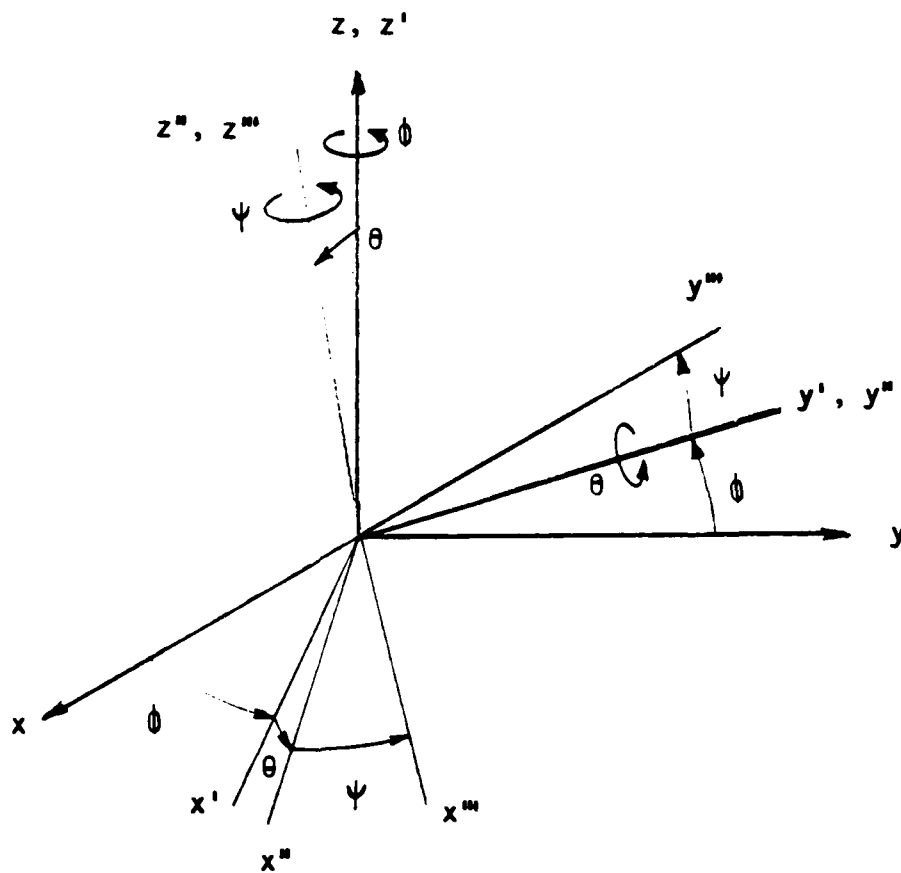
Figure 3.2 Euler Angles

INVERSE KINEMATIC EQUATIONS TO THE EULER ANGLES [13].

Given a transformation, ^rT_p, whose components are those listed in equation (3) above, it is possible to compute the euler angles which are related to them as well as the translation vector, $\overline{p}$.

$$\vec{p} = p_x \, \vec{i} + p_y\vec{j} + p_z\vec{k} \tag{5}$$

$$\phi = \arctan \ (m_y/m_x) \tag{6}$$

$$\theta = \arctan \ ((m_x.\cos\phi + m_y.\sin \phi)/m_z) \tag{7}$$

$$\psi = \arctan \ ((n_y.\cos\phi - n_x.\sin\phi)/(o_y.\cos\phi - o_x.\sin \phi)) \tag{8}$$

ROTATION VECTOR, $\vec{\theta}$:

Given a transformation matrix, ^rT_p, it is possible to compute a rotation vector, $\vec{\theta}$, which describes an axis of rotation, $\vec{n}$, about which a rigid body is rotated θ degrees. Equation (3) above and the following equations are utilized.

$$\theta = \arccos \ ((Tr.R - 1)/2), \text{ where}$$

$$Tr.R = n_x + o_y + m_z$$

Also: $\quad n_1 = (o_z - m_y)/2 \sin \theta$

$$n_2 = (m_x - m_z)/2 \sin \theta$$

$$n_3 = (n_y - o_z)/2 \sin \theta$$

Hence: $\quad \vec{\theta} = \theta \, \vec{n}, \text{ where}$

$$\vec{n} = (n_1, n_2, n_3)$$

To obtain the direction cosine elements of ^rT_p given a rotation vector, $\vec{\theta}$, the following equations may be used:

$$n_x = 1 + (n_1{}^2 - 1) \cdot (1 - \cos \theta)$$

$$o_x = -n_3 \cdot \sin \theta + n_1 \cdot n_2 \cdot (1 - \cos \theta)$$

$$m_x = n_2 \cdot \sin \theta + n_1 \cdot n_3 \cdot (1 - \cos \theta)$$

$$n_y = n_3 \cdot \sin \theta + n_1 \cdot n_2 \cdot (1 - \cos \theta)$$

$$o_y = 1 + (n_2{}^2 - 1) \cdot (1 - \cos \theta)$$

$$m_y = -n_1 \cdot \sin \theta + n_2 \cdot n_3 \cdot (1 - \cos \theta)$$

$$n_z = -n_2 \cdot \sin \theta + n_1 \cdot n_3 \cdot (1 - \cos \theta)$$

$$o_z = n_1 \cdot \sin \theta + n_2 \cdot n_3 \cdot (1 - \cos \theta)$$

$$m_z = 1 + (n_3{}^2 - 1) \cdot (1 - \cos \theta)$$

The following properties concerning the rotation vector, $\overset{\frown}{\theta}$, are also noted:

$$\theta_x = \theta n_1$$

$$\theta_y = \theta n_2$$

$$\theta_z = \theta n_3$$

$$n_1{}^2 + n_2{}^2 + n_3{}^2 = 1$$

$$(\theta_x{}^2 + \theta_y{}^2 + \theta_z{}^2)^{1/2} = \theta$$

These equations are used extensively in the RMS Method (see Appendix C) to compute $\overset{\frown}{\theta}$ and to insure the resulting transformation matrix is constrained to be orthogonal.

CHAPTER 4

PLANNING PHASE

4.1 General Comments

In order to apply robots to any operation, the object to be worked on has to be numerically defined or digitized. Any other component which affects the resultant robotic process must also be described in terms of its surface geometry. While this geometric description may be obtained in different ways, the simplest means of gathering this data is with a digitizing device.

Having digitized the surfaces of both the femur and prosthesis, their relative locations were then determined. The selection of a location for the prosthesis on the femur was accomplished through the use of a computerized simulation discussed in Section 4.3.

Once a position for the prosthesis was selected, a method of passing the locations of both femur and prosthesis relative to each other had to be established. However, prior to this the location of the femur had to have been identified to the robot. To accomplish this, fiducial points were selected which characterized the bone surface. Then femur reference points were specified which served to orient the robot tool to make the correct cuts on the femur.

4.2 Digitization of the Femur and Prosthesis

A knowledge of the surface geometries of the femur and the prosthesis to be attached to it were required to implement this robotic process. Data used to define the surface anatomy of both structures was obtained using two methods: (1) a POLHEMUS digitizer and (2) conventional hand measurement techniques.

The data necessary to conduct the analysis and subsequent determination of the relative positioning between the femur and its prosthesis was gathered using a POLHEMUS digitizer. A stylus was fabricated for this device and calibrated so that the location of the tip of this stylus was known at all times. The stylus tip was then placed in contact with and passed over the surface of the femur. The location of the stylus tip was recorded at uniform time intervals. The resultant set of points, when displayed on a computer graphics terminal, gave the three-dimensional image of the femur. A similar process was used to determine the surface anatomy of the prosthesis with the only difference being the use of a non-metallic model of the prosthesis in the digitizing process.

The data required to compute the path which the cutter followed was obtained using calipers, a ruler and a protractor to construct a two-dimensional profile of the inside, porous surfaces of the prosthesis. Figure 4.1 shows the resulting dimensions used to characterize these inner surfaces. A total of five planar surfaces
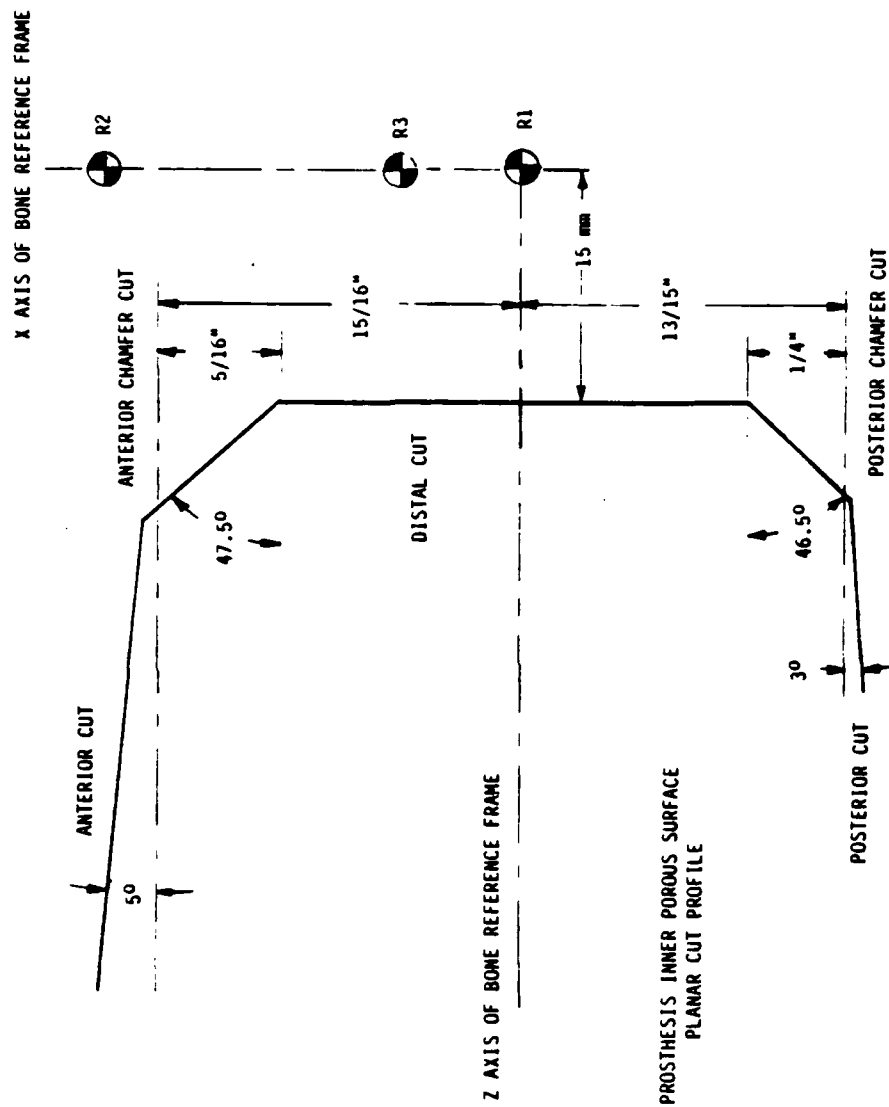
Figure 4.1 Prosthesis Pourous Inner Surface Geometry

was used, although any increased number of surfaces could have also been utilized.

4.3 Positioning of the Prosthesis on the Femur

Using a computerized biomechanical simulation of the prosthetic knee, with the data taken by the POLHEMUS digitizer employed, a desired relationship between the femur and prosthesis was established. In arriving at this desired relationship several intraoperative variables which affect knee function were considered. These included:

(1) The proximal/distal and anterior/posterior position of the tibial prosthetic component.

(2) The medial/lateral and anterior/posterior tilt of the tibial prosthetic component.

(3) The flexion/extension and axial rotation of the femoral prosthetic component.

(4) The thickness and position of the patellar prosthetic component.

(5) The retention or sacrifice of one or both cruciate ligaments.

The functional characteristics of the knee arthroplasty evaluated in conjunction with the above variables included:

(1) a range of motion from full extension to at least 105 degrees of flexion.

(2) stability throughout the range of joint motion.

(3) a tibiofemoral angle of about 7 degrees when the knee is loaded in extension.

(4) tibial loads which are balanced mediolaterally and anteroposteriorally.

(5) adequate mechanical efficiency of the extensor mechanism of the knee.

The end result of this simulation was to produce a location for the placement of the femoral component of the prosthesis which addressed current concerns for the satisfactory functioning of the knee upon completion of the knee arthroplasty. A more comprehensive discussion of this simulation and the associated research in this area is contained in reference [2].

4.4 Selection of Fiducial Points

The selection of fiducial points to be used in the orientation phase was an arbitrary process subject to the following constraints:

(1) Fiducial points had to be accessible to the surgeon as well as the robot.

(2) Fiducial points could not be coplanar. They had to

possess enough spatial dispersion to firmly establish their orientation in space.

(3) Fiducial points were to be selected as far apart as possible.

(4) A minimum of 4 to as many as 10 fiducial points were used in this thesis. The effect of the number of fiducial points used on the transformation process was examined closely (see Chapter 6).

(5) Fiducial points had to be identifiable. This constraint had a significant impact on the transformation process and is addressed in much detail in Chapter 6.

4.5 Calculation of the Femur Reference Points

The computation of the femur reference points was accomplished after analyzing the positional relationship between prosthesis and femur. The femur reference points were calculated in the PCS after the determination of the prosthesis location had been made.

The femur reference points were used to establish the Bone Reference Frame (BRF) of the femur in the RCS. Three such points were used. Their significance is defined as follows:

Point 1: the origin of the BRF

Point 2: a point along the positive x - axis of the BRF

Point 3: a point in the positive xy - plane of the BRF.

By using this format, these points could be, upon transformation into the RCS, entered directly into the built-in function, BUILDFRAME.

The relationship between the desired planar cuts of the femur and the femur reference points is illustrated in Figure 4.1. The corresponding relationship between the femur and the femur reference points is shown in Figure 4.2.

R1 - ORIGIN
R2 - POINT ON POSITIVE X AXIS
R3 - POINT ON POSITIVE XY QUADRANT
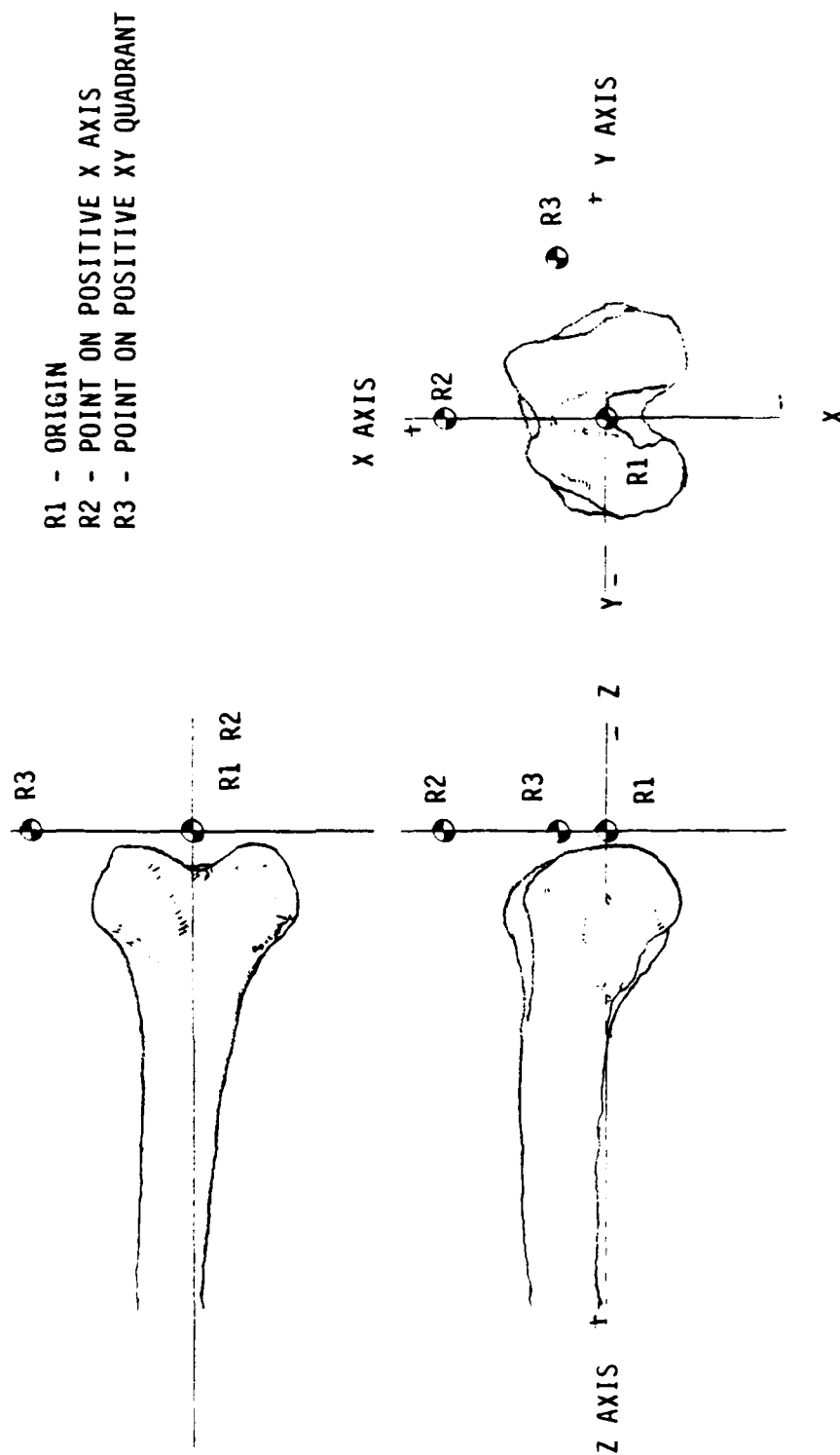
Figure 4.2 Femur Reference Points

CHAPTER 5

ORIENTATION PHASE

5.1 General Comments

In order to mill or drill holes in the femur using a robot, the robot had to acquire information regarding the location of the femur. The procedure developed in this study utilized the following sequence of steps:

(1) Transfer the Cartesian coordinates of the fiducial points and the femur reference points with reference to the PCS to the AI32.

(2) Mount the femur in the work space of the robot.

(3) Locate the fiducial points of the femur using the stylus of the robot to touch each fiducial point.

(4) Compute ^rT_p, the transformation matrix between the PCS and the RCS.

(5) Compute the coordinates of the femur reference points in the coordinate system of the robot using ^rT_p.

(6) Calculate the Bone Reference Frame (BRF) of the femur using the intrinsic Automatix function, BUILDFRAME, and the transformed femur reference points.

(7) Transform the coordinates which describe the path of
the cutter relative to the origin of the RCS into the
Bone Reference Frame (BRF).

5.2 Determination of the Fiducial Points in the Coordinate System of
the Robot

Once the femur was mounted in the work space of the AID 600, the
determination of the RCS fiducial points was made.   This was
accomplished through the use of a stylus previously mounted to the
wrist of the AID 600 robot arm and calibrated so that the exact
location of its tip was known to the robot (See Appendix A).   By
selecting the working tool of the AID 600 to be the stylus, the AI32
was able to obtain feedback as to the position and orientation of the
stylus upon request.   Moreover, by placing the tip of the stylus on a
particular fiducial point, that point's location was immediately
determined by simply recording the location of the stylus.   This
tactile method of determining the RCS fiducial point coordinates
proved highly effective.

It was noted that the greatest sources of error in the accuracy
of the robotic process were introduced in the Orientation Phase.   The
amount of spatial error between RCS and PCS fiducial point
coordinates was directly affected by the operator's ability to place
the stylus tip on the fiducial points of the femur.   Without any
system of marking definite locations on the femur, spatial errors of

as much as 4 millimeters were induced. These spatial errors had a significant impact on the output of the transformation process.

5.3 Computing the Transformation Matrix

With two sets of coordinates describing the location of the fiducial points of the femur available, the transformation matrix between the PCS and the RCS was computed. Three different methods for calculating this transformation were developed and evaluated. Two of these methods yielded satisfactory, orthogonal transformation matrices. All three methods are described below along with an explanation of the steps each used to obtain the transformation matrix. The relative merit of each of these transformation methods is discussed in Chapter 6.

The data entered into each of these methods was (1) N, the number of fiducial points used, (2) A, the 4 x N matrix of fiducial points in the RCS, and (3) B, the corresponding set of fiducial points in the PCS, also formed into a 4 x N matrix.

5.3.1 Tensor Method [14]

This method reduced each set of fiducial points down to a simpler form by computing the centroid of each fiducial point set and subtracting the resultant centroids from all points in their corresponding fiducial point set. This had the effect of translating both sets of fiducial points to one common origin. Each point was then treated as a point mass within a rigid body. The inertia tensor

of this rigid body was computed for both sets of points. The resultant inertia tensors are real, symmetric 3 x 3 matrices which characterize each set of points. Because these inertia tensors are real symmetric matrices their eigenvalues and corresponding eigenvectors are real valued.

Using the Jacobi method of finding the eigenvalues and eigenvectors of a real symmetric matrix, the inertia tensors for each set of points were solved for their eigenvalues (principle moments of inertia) and eigenvectors (principal directions). The eigenvectors were stored column-wise in 3 x 3 matrices which formed the modal matrices for each inertia tensor. P_p designates the modal matrix associated with the PCS. P_r designates the modal matrix associated with the RCS. The correspondence of eigenvectors in the modal matrix for each set was checked by matching each eigenvector with its eigenvalue. Each eigenvector was stored in the modal matrix in descending order according to the value of its eigenvalue. Jacobi's method also insured the formation of orthonormal eigenvectors.

These modal matrices could then be viewed as transformations from the coordinate system whose basis was composed of unit vectors in the principal x, y, z directions into the coordinate system characterizing the orientation of each set of points.

By utilizing the relationship, $P_p^{-1} = (P_p)^T$, for an orthonormal basis, an initial rotation matrix was constructed by inverting the modal matrix associated with the planning coordinate system and pre

multiplying it by the modal matrix associated with the robot coordinate system. In other words, $R = P_r (P_p)^T$. This 3 x 3 R matrix was expanded to 4 x 4 size with the addition of a row and a column of zeroes, except for the unity value added to the fourth row, fourth column element. The effects of the translation of each set of points to a common origin were accounted for and the final transformation matrix, ^rT_p , was complete. For a detailed presentation of the determination of the characteristic roots of a matrix by the Jacobi Method, see reference [15].

5.3.2 Best Approximate Solution Method

This method was developed from current matrix theory in the field of generalized inverses of m x n matrices, where $m \neq n$. The theory on which this method is based [16] states that:

The "best approximate solution" for the matrix equation $A = BX$, where B is an m x n matrix, X is an n x k matrix, and A is an m x k matrix, is:

$$X = B^+ A$$

where B^+ is the Moore-Penrose Inverse of the B matrix [17]. Furthermore, B^+ may be defined by $B^+ = B^* (B B^*)^{-1}$ for B an m x n matrix with m   n. In this thesis, m will always be less than or equal to n.

Now, because X was the transformation solution to the matrix equation, $A = BX$, we had to modify this approach to obtain the

solution, ^rT_p, to the equation $A = {}^rT_pB$. This was done by setting

up the matrix equation $BX = {}^rT_pB$ and solving for ^rT_p. We then

obtain $^rT_p = BXB^+$ where B^+ was previously calculated. Therefore,

the transformation was obtained by:

$$^rT_p = B[B*(BB*)^{-1}] A [B(BB*)^{-1}] \qquad (10)$$

This equation reduces to:

$$^rT_p = AB*(BB*)^{-1} \qquad (11)$$

The drawback to using this method is that it fails to produce a

homogeneous transformation matrix.

5.3.3 Root Mean Squared Method [18]

The Root Mean Squared (RMS) Method computed the transformation

matrix between two corresponding sets of points minimizing the root

mean squared error between them, much as the name suggests. The

transformation was achieved in a step-wise manner which first

captures the translational differences between A and B and then

iteratively computes an approximation for the rotation difference.

This approximation was improved with each iteration until a minimal

derivative of the rotation change was obtained.

To obtain the translational difference between the two

corresponding sets of points represented by A and B, the centroids of

both sets were computed and recorded. Each set of points was then

translated by subtracting the value of its corresponding centroid

from each individual point in the set. This process aligned the centroid of each set of points with a common origin. The only remaining transformation difference involved rotation.

The matrix equation to be solved is similar to equation (2), except that only the rotational transformation is left to be determined. Because of this, equation (2) was simplified by reducing A and B to 3 x N matrices through the elimination of the fourth row of 1's, and computing only the 3 x 3 rotation transformation matrix, R. The modification to equation (2) may be expressed here as **A'** = **R** **B'**, or by transforming each column vector in **A'** and **B'** separately as shown by the equation:

$$\sum_{i=1}^{N} \vec{a^i} = \sum_{i=1}^{N} R \, \vec{b^i} \qquad (12)$$

The necessity of distinguishing the individual column vectors of **A'** and **B'** is due to the method for computing **R**. The procedure for computing **R** is described in Appendix C.

Upon computing the rotation matrix, **R**, everything needed to compute ^rT_p was available. The 4 x 4 matrix, **L**, was formed by subtracting the x, y, and z components of the centroid of **B** from the first, second, and third rows of the fourth column of an identity matrix of rank, 4. That is,

$$L = \begin{bmatrix} 1 & 0 & 0 & -x \\ 0 & 1 & 0 & -y \\ 0 & 0 & 1 & -z \\ 0 & 0 & 0 & 1 \end{bmatrix} \qquad \text{where } (x, y, z) \text{ was}$$

where (x, y, z) was the centroid of **B**

In a similar manner, the 4 x 4 matrix, **J**, was formed by adding the x, y, and z components of the centroid of **A** to the first, second, and third rows of the fourth column of an identity matrix of rank, 4. That is,

$$J = \begin{bmatrix} 1 & 0 & 0 & x \\ 0 & 1 & 0 & y \\ 0 & 1 & 0 & z \\ 0 & 0 & 0 & 1 \end{bmatrix} \qquad \text{where } (x, y, z) \text{ was}$$

where (x, y, z) was the centroid of **A**

The matrix, **K**, was formed by adding **R** to a null matrix of rank 4 and then adding a 1 to the fourth column, fourth row of **K**. Finally, the orthogonal transformation matrix, $^{r}T_{p}$ was computed by:

$$^{r}T_{p} = J \; K \; L$$

5.4 Establishing the Bone Reference Frame

With $^{r}T_{p}$ computed, the femur reference points were now transformed into the RCS. These transformed points were then entered into the AI32 controller to obtain the Bone Reference Frame. This

was done using the intrinsic function, BUILDFRAME. BUILDFRAME accepted three points in the RCS according to the format specified in Section 4.5 and returned a location. This location was given in coordinate transformation form (see definition in Section 3.4.1), in which the first three numbers specified the position vector from the origin of RCS to the Bone Reference Frame and the last three numbers specified the Euler angle relationship between the axes of the RCS and those of the Bone Reference Frame (BRF). This BRF did not establish another coordinate system, but was instead defined in the coordinate system of the robot, RCS. The format is identical to that used by the robot to specify the definition of its tools.

5.5 Establishing the Path of the Cutter

With the Bone Reference Frame established, the final step in the fixation and orientation process was to transform the coordinates which controlled the motion of the robot's cutter from the origin of the RCS to the BRF. The important concept to understand here was that the coordinates which defined a path for the cutter to follow in relation to the origin of RCS were related in the same manner that the femur reference points were related to the desired cuts of the femur discussed in Section 4.5.

The femur reference points were selected to define a reference point and orientation with respect to the femur in PCS. The coordinates stored as path information for the cutter were also

selected to have the same relation to the origin of the RCS.

By transforming the coordinates for the cutter path from the origin of RCS to the BRF, the orientation process was now complete. The protocol for the execution of these cuts is addressed in Chapter 7.

CHAPTER 6

ANALYSIS OF THE TRANSFORMATION PROCESS

6.1 General Comments

Because of the importance of the transformation process, and its influence on the resulting cuts made to the femur, it was important to assess the performance of the methods used to compute the transformations. Since the measurements made by the digitizer and by the robot were taken from the same corresponding physical points on a rigid body, the expectation was that the spatial arrangement of each set of measurements would be identical. However, this was not the case. Some spatial error always exists because of the inaccuracies contained in human handling of probes and subjectivity and due to the lack of precision in machinery being used to make the measurements.

In this study, the performance of the three transformation methods described in Section 5.3 were evaluated on the basis of their (1) orthogonality of the resultant transformation matrix, (2) acceptance of different spatial arrangements of fiducial points, (3) effect of strain on transformations, (4) root mean squared error, and (5) execution time.

6.2 Orthogonality

The property of orthogonality in a transformation is important. When it exists in a transformation, the linear mapping of points from one coordinate system to another also preserved the spatial orientation of those points. Angular and distance relationships between sets of points are preserved. Since the preservation of angular and distance relationships is critical to the accuracy of the process developed in this thesis it was the first property to be checked.

The test procedure is straightforward. Each transformation program was tested by entering the data in Table 6.1 into it. The program was required to compute the transformation between the two sets of points. The resultant transformations produced were then checked to see if they were orthogonal.

Orthogonality of a transformation matrix is checked by taking the inner product of any two of the first three columns. The resultant scalar should be nearly zero. (Discrete systems, such as computers, will not always produce scalar values which are identically zero). Tables 6.2, 6.3, and 6.4 show the transformations obtained when the data in Table 6.1 was used. The actual solution is contained in Table 6.5.

Both the Tensor Method and the Root Mean Squared (RMS) Method produced orthogonal transformation. The Best Approximate Solution

Table 6.1   Set of values used in the analysis of
            the Transformation Process (Set A)

Number of fiducial points used (N) - 4

A matrix:

$$\begin{bmatrix} 2.000000 & 2.000000 & -2.000000 & -2.000000 \\ 3.000000 & 3.000000 & 3.000000 & 3.000000 \\ 1.000000 & -1.000000 & -1.000000 & 1.000000 \\ 1.000000 & 1.000000 & 1.000000 & 1.000000 \end{bmatrix}$$

B matrix:

$$\begin{bmatrix} 10.18321 & 9.426181 & 6.281714 & 7.691098 \\ 23.28539 & 23.97223 & 22.07981 & 21.61304 \\ 30.70685 & 29.26226 & 29.93393 & 32.23779 \\ 1.000000 & 1.000000 & 1.000000 & 1.000000 \end{bmatrix}$$

Comments: The **A** matrix was produced by selecting a simple set of
            points which was not symmetric about the origin.   The
            coordinates of these points were then entered as column vectors
            in the **A** matrix, with the bottom row of A containing 1's.   See
            the List of Symbols for further information.   **B** was computed by
            pre-multiplying the **A** matrix by an orthogonal transformation
            matrix whose coordinate transformation form is:

$$[10, 20, 30, 10, 20, 30]$$

            As defined in Chapter 3, the coordinate transformation form is a
            six parameter row matrix which contains all the data necessary
            to construct an orthogonal transformation matrix. The parameters
            shown were selected for their simplicity.

Usage: Set A was used to test the orthogonality of all three
         transformation methods developed in Chapter 5.

Table 6.2   Transformation computed using Set A data and the Tensor
            Method

0.8137979	0.4698463	-0.3420199	-7.274309
-0.4409692	0.8825641	0.1631769	-18.13690
0.3785226	0.1802719E-01	0.9254164	-31.90826
0.0000000	0.0000000	0.0000000	1.000000

Table 6.3   Transformation computed using Set A data and the BAS
            Method

1.1900	-.2890	-.4820	11.0000
-.0352	-.0586	.0029	2.2500
.4730	-.1680	.8940	-27.5000
-.0117	.0195	.0010	.7500

Table 6.4   Transformation computed using Set A data and the RMS
            Method

0.8137978	0.4698462	-0.3420201	-7.274302
-0.4409691	0.8825642	0.1631770	-18.13690
0.3785228	0.1802719E-01	0.9254164	-31.90826
0.0000000	0.0000000	0.0000000	1.000000

Table 6.5   Actual Transformation Solution for Set A data

0.8137977	0.4698463	-0.3420202	-7.274299
-0.4409696	0.8825642	0.1631760	-18.13687
0.3785224	0.1802831E-01	0.9254166	-31.90829
0.0000000	0.0000000	0.0000000	1.000000

(BAS) Method did not produce an orthogonal transformation. This was because the BAS Method lacked any constraining relationships which guaranteed orthogonality. The orthogonality of transformations produced by the Tensor Method was assured by the employment of an eigenvector solving algorithm to compute two orthonormal modal matrices which, when processed and multiplied together, produced a resultant orthogonal transformation matrix. Orthogonality of transformations produced by the RMS method was assured through the use of a rotation matrix-rotation vector relationship which was constrained to be orthogonal. The rotation matrix was made to be the function of a single, independent variable, $\vec{\theta}$. For any $\vec{\theta}$ an orthogonal matrix was produced. Because of its failure to meet this first required, the BAS Method was rejected from any further testing.

6.3 Acceptance of Different Fiducial Point Geometries

The question arose as to whether or not any restrictions exist on the configuration of points which could be processed by the different transformation programs. The answer to this question is yes. Depending upon the method used to determine the transformation matrix, certain restrictions did exist.

The Tensor Method was found to have difficulty with certain configurations of points. It was found that for inertia tensors having two or three principal moments of inertia which were exactly equal that the resultant transformation matrix would deviate from the

correct transformation by a large amount. Small differences in the principal moments of inertia, however, could be differentiated without any problem.

To test this out, a set of points was developed in which symmetry existed about the z - axis (See Table 6.6). This set of points was then entered into the transformation testing programs using the Tensor Method and the RMS Method. The resultant transformations are shown in Tables 6.7 and 6.8. The actual solution is contained in Table 6.9.

The RMS Method was able to handle symmetrical configurations of fiducial points without producing transformations which deviated significantly from the actual solutions of the transformation matrix equation (2); this was not true for the Tensor Method. Because of its dependence on the magnitude of the principal moments of inertia obtained from the inertia tensor, the Tensor Method was sensitive to situations in which two or more equal principal moments of inertia were encountered. The RMS Method did not have this dependence, mainly because it was able to maintain the correspondence between points in each set, even when spatial error was induced into the transformation process.

The likelihood of encountering a set of fiducial points which are exactly symmetric about some axis is small. In fact, the geometry of the femur portion of the knee joint is highly asymmetric. Moreover, given the surgeon's preference for selecting points on the

Table 6.6   Set of values used in the analysis of
            the Transformation Process (Set B)

Number of fiducial points used (N) - 4

A matrix:

2.000000	2.000000	-2.000000	-2.000000
2.000000	-2.000000	2.000000	-2.000000
0.0000000	0.0000000	0.0000000	0.0000000
1.000000	1.000000	1.000000	1.000000

B matrix:

10.74566	12.50953	7.490466	9.254344
22.70482	19.17456	20.82544	17.29518
29.64231	28.98961	31.01039	30.35769
1.000000	1.000000	1.000000	1.000000

Comments: The **A** matrix was produced by selecting a set of fiducial
           points which was symmetric about the origin of its associated
           coordinate system. In a manner identical to the one used in
           Table 6.1, the coordinates of these points were entered as
           column vectors in the **A** matrix, with the bottom row of **A**
           containing 1's. (See the List of Symbols for an explanation of
           the **A** matrix.) **B** was computed by pre-multiplying the **A** matrix
           by an orthogonal transformation matrix whose coordinate
           transformation form was:

$$[10, 20, 30, 10, 20, 30]$$

           See the definition for coordinate transformation form in Chapter
           3.

Usage: Data Set B was used to test the effect of symmetrical   point
         arrangements on the Tensor and RMS Methods.

Table 6.7   Transformation computed using Set B data and the Tensor
Method

-0.457402E-01	0.9989530	-0.7525422E-03	-19.49908
0.9244615	0.4204393E-01	-0.3789503	1.283014
-0.3785219	-0.1802897E-01	-0.9254168	31.90830
0.0000000	0.0000000	0.0000000	1.000000

Table 6.8   Transformation computed using Set B data and the RMS
Method

0.8137982	0.4698452	-0.3420203	-7.274278
-0.4409689	0.8825647	0.1631748	-18.13685
0.3785220	0.1802898E-01	0.9254167	-31.90830
0.0000000	0.0000000	0.0000000	1.000000

Table 6.9   Actual Transformation Solution for Set B data

0.8137977	0.4698463	-0.3420202	-7.274299
-0.4409696	0.8825642	0.1631760	-18.13687
0.3785224	0.1802831E-01	0.9254166	-31.90829
0.0000000	0.0000000	0.0000000	1.000000

bone which are easy to identify, the probability the set of points he selects will be perfectly symmetric about the same axis is expected to be zero. In light of this, the Tensor Method is still considered a useful method subject to the condition that any set of fiducial points chosen by the surgeon are asymmetric.

6.4 Effects of Spatial Error on Transformations

6.4.1 Selection of Parameters

In order to evaluate the effects of spatial error on the transformation processes and compare the performance of the Tensor Method and the RMS Method, suitable parameters had to be chosen. These parameters had to be able to quantify what took place when transformations were applied to sets of points and give some measure of the changes that took place in the presence of spatial error. Two sets of parameters were selected; both had merit. These sets of parameters were:

SET 1: Mean Translational Error (MTE)

Mean Rotational Error (MRE)

SET 2: Root Mean Squared Error (RMSE)

Because of its better suitability to enhance the visualization of errors created by the addition of spatial error, the parameters of Set 1 were chosen to study the transformation process. However, the usefulness of the root mean squared error was not dismissed. Root

mean squared errors were addressed in Section 6.5.

As was mentioned earlier, some spatial error always exists between two corresponding sets of measurements taken from the same physical points. This was due to the inaccuracies of human handling of probes, human subjectivity in the alignment of probes with points and the finite resolution of the measuring process. The intent of this thesis was to observe the effects of spatial error, as the independent variable, on the resultant errors in the transformation process. The effects of varying the number of fiducial points, N, were also studied. These resultant errors were quantified using the selected parameters: mean translational error (MTE) and mean rotational error (MRE).

Several important questions should arise here. How is the strain modeled? What is MTE? What is MRE? In addition to this, does the geometry of the fiducial point set itself affect the MTE and MRE curves?

6.4.2 The Spatial Error Model

When spatial, or random, error was added to each fiducial point to study the resulting effect on MTE and MRE, a different direction was specified for the random error added to each point. The specific method used in this study to model the spatial, or random error, which entered the robotic process when touching fiducial points with a stylus is explained below and illustrated in Figure 6.1.
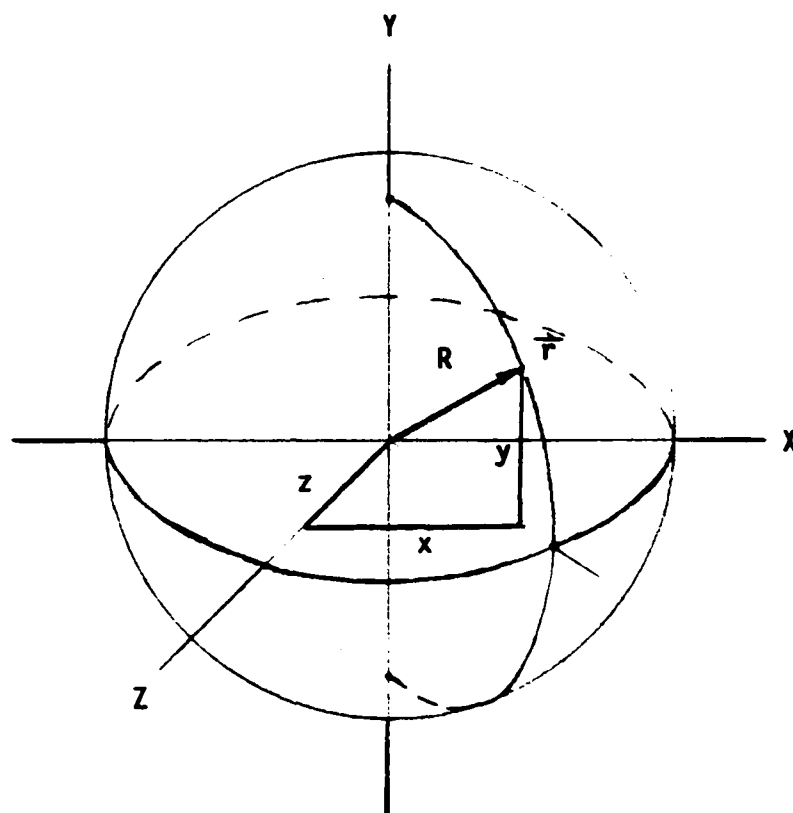
$$\vec{r} = x\,\vec{i} + y\,\vec{j} + z\,\vec{k}$$

$$|R| = SQRT\ (x * x + y * y + z * z)$$

Figure 6.1 Strain Model used in Transformation Analysis

The deviation allowed for each point is controlled by the amplitude of the random error. Random error amplitude is equal to the diameter of a circle whose origin is the fiducial point. For a given amplitude all possible points containing spatial error lie on the surface of a sphere. This means that $|\vec{r}| = R = .5 \times$ Random Error Amplitude, where $\vec{r}$ is the random error vector.

The x, y and z components of the random error vector, $\vec{r}$, were determined using a random number generator. Letting RN be a random number between +/- .5 and RS be a randomly selected +/- 1, the following equations were used to compute values for x, y, and z for each $\vec{r}$:

$$x = 2 \times R \times RN \qquad (14)$$

$$y = 2 \times \sqrt{R^2 - x^2} \times RN \qquad (15)$$

$$z = \sqrt{R^2 - x^2 - y^2} \times RS \qquad (16)$$

The random error added to each point in a given iteration was based on a uniformly distributed set of directions for the orientation of a constant magnitude random error vector. This was done because of its simplicity and ease of programming. It is noted that the distal end of the femur is highly irregular. Fiducial points selected from it will tend to be based on: (1) the surgeon's ability to easily identify the points, (2) their accessibility, and (3) the condition of the patient's knee.

The actual probability density function (PDF) of the random error direction on the femur surface could not be easily modelled. It was different for each point. The directions of the random error were more likely to be confined on a planar surface containing the fiducial point; not on a sphere surrounding it. Still, the approximations of the spatial error model were not unreasonable given the variety of other factors affecting fiducial point geometry. By selecting fiducial points surrounding the femur, the effects of random errors normal to the surface of the bone were reduced.

6.4.3 Mean Translational Error versus Random Error and N

The procedure for evaluating the effects of spatial error and the number of fiducial points used on the Mean Translational Error (MTE) required the repetitious solution of the transformation matrix equation:

$$A = {}^rT_p\ B$$

Initially, the number of fiducial points, N, was set at 4. The first 4 points out of Table 6.10 were read into the computer to establish **B**. **A** was then computed as described below. The relationship between MTE and spatial error, or random error, was then computed for random error amplitudes which varied from 0 to 5 millimeters. Upon completion of this computation, the test program incremented N by 1 and proceeded to compute the next MTE versus

Table 6.10 Set of values used in the analysis of
            the Transformation Process (Set C)

Number of fiducial points (N) - 4 to 10

Data used to form the B matrix:

Point		Coordinates	
Number	x	y	z
1	14.12381	22.83499	-42.17916
2	6.382701	-28.96292	-40.25432
3	-20.38861	-45.54621	-3.138103
4	-22.05031	-21.68828	39.28616
5	22.32864	-20.11880	39.95830
6	-1.208152	-3.073993	-49.89079
7	-40.56549	-20.12018	21.20422
8	-0.120606	-12.80411	-48.33260
9	-36.72083	32.98188	7.986022
10	-30.00000	0.000000	40.00000

Comments: A total of ten random points were generated with all points
           being on the surface of a sphere 100 millimeters in diameter.
           These points are listed above.

Usage: The Set C data above was used to assess the effects of spatial
        error between the A and B matrices on two parameters: (1) MTE
        and (2) MRE. Values for the A matrix were generated within the
        testing program and are not listed here.   The coordinate
        transformation form used to form the transformation matrix
        which pre-multiplied B to obtain A was:

                    [530, 370, 100, 10, 120, 180]

        See Chapter 3 for the definition of the coordinate
        transformation form.   This data was chosen based on its
        similarity to actual values found when utilizing the AID 600 to
        cut a plastic femur mounted in the robot work volume.

                In this test, N was also varied from 4 to 10 to assess
        the effects of random error on MTE and MRE values.

random error curve. This was done for values of N equaling from 4 to 10. The resultant curve relationships between MTE and random error were plotted.

The model of the fiducial point geometry used to establish the test data was a simple one. A total of 10 random points were used, all of which lay on the surface of a sphere 100 millimeters in diameter. The center of the sphere was designated as the origin of the coordinate system which would model, or represent, the PCS. The points generated in this coordinate system would then be used to construct the **B** matrix. By pre-multiplying the **B** matrix by an orthogonal transformation matrix, whose coordinate transformation form was:

$$[530, 370, 100, 10, 120, 180]$$

the **A** matrix was generated. The values of the parameters in the above coordinate transformation form were selected for their similarity with actual coordinates and Euler angles found in using the AID 600 to generate the cuts on the plastic femur.

Knowing both **A** and **B**, the next step in the procedure was to compute $^{r}T_{p}$. This was done by employing either the Tensor method or the RMS method. Both methods were used in the computation process.

The difference vector between the centroid of **A** and **B** was computed using the last column of $^{r}T_{p}$. The resulting magnitude of this vector was recorded and used as the control value against which

the effects of spatial, or random, error in **A** were studied.

At this point, the effect of a specified amount of spatial, or random, error was studied. This was done by adding a constant magnitude of error, random in direction, to each point in **A**. The transform, $^r T_p$, was subsequently recomputed. Finally, the difference vector between the centroids of **B** and the modified **A** matrix were recomputed. This resulted in a new magnitude value. The difference between this new value and the control value was stored. By repeating the above process many times and taking the mean value of this difference, one point on the MTE versus random error curve was computed. This mean value was termed the Mean Translational Error, or MTE.

The process of computing the MTE for random error amplitudes varying from 0 to 5 millimeters was then executed in the same manner. This was also done as N varied from 4 to 10. Both the Tensor and RMS Methods were used. The family of curves which resulted are contained in Figures 6.2 and 6.3. Standard deviation curves for the MTE were also computed and are shown in Figures 6.4 and 6.5.

6.4.4 Mean Rotational Error versus Random Error and N

The procedure used to evaluate the effects of spatial error and the number of fiducial points used on the Mean Rotational Error (MRE) was nearly identical to the previously defined procedure for computing the MTE family of curves. The only differences were the

TRANSFORMATION ERROR ANALYSIS

Figure 6.2 Mean Translational Error, mm, versus Random Error
            Amplitude, mm, using the Tensor Method
            (N = 4 to 10) and Data Set C

TRANSFORMATION ERROR ANALYSIS

Figure 6.3   Mean Translational Error, mm, versus Random Error
Amplitude, mm, using the RMS Method
(N = 4 to 10) and Data Set C

Figure 6.4 Standard deviation of the Mean Translational Error, mm, versus Random Error Amplitude, mm, using the Tensor Method (N = 4 to 10) and Data Set C

Figure 6.5 Standard deviation of the Mean Translational
Error, mm, versus Random Error Amplitude, mm,
using the RMS Method (N = 4 to 10) and
Data Set C

parameters chosen to make the comparison.

Upon achieving the ^rT_p matrix for the case of no spatial error between A and B matrices, the transformation matrix, ^rT_p, was then used to compute the rotation angle between A and B. The equation for this angle is:

$$\theta = arc\ cos\ ((Tr\ .\ T - 1)/2) \tag{13}$$

$$where\ Tr\ .\ T = n_x + o_y + m_z$$

The resultant angle, θ, was the control angle against which the effects of adding random error to the points in A were studied.

Once again, the effect of a specified amount of random error was studied. This was done by adding a constant magnitude of error, different in direction, to each point in A. Again, the transformation matrix, ^rT_p, was recomputed. The angle, θ, was recomputed. The difference between this new angle and the control angle was stored. By repeating the above process many times and taking the mean value of this difference, one point on the MRE versus random error curve was computed. This mean value was termed the Mean Rotational Error, or MRE.

The process of computing the MRE for random error amplitudes varying from 0 to 5 millimeters was then executed in the same manner. This was also the same as N varied from 4 to 10. Both the Tensor and RMS Methods were used. The family of curves which resulted are contained in Figures 6.6 and 6.7. Standard deviation curves for the
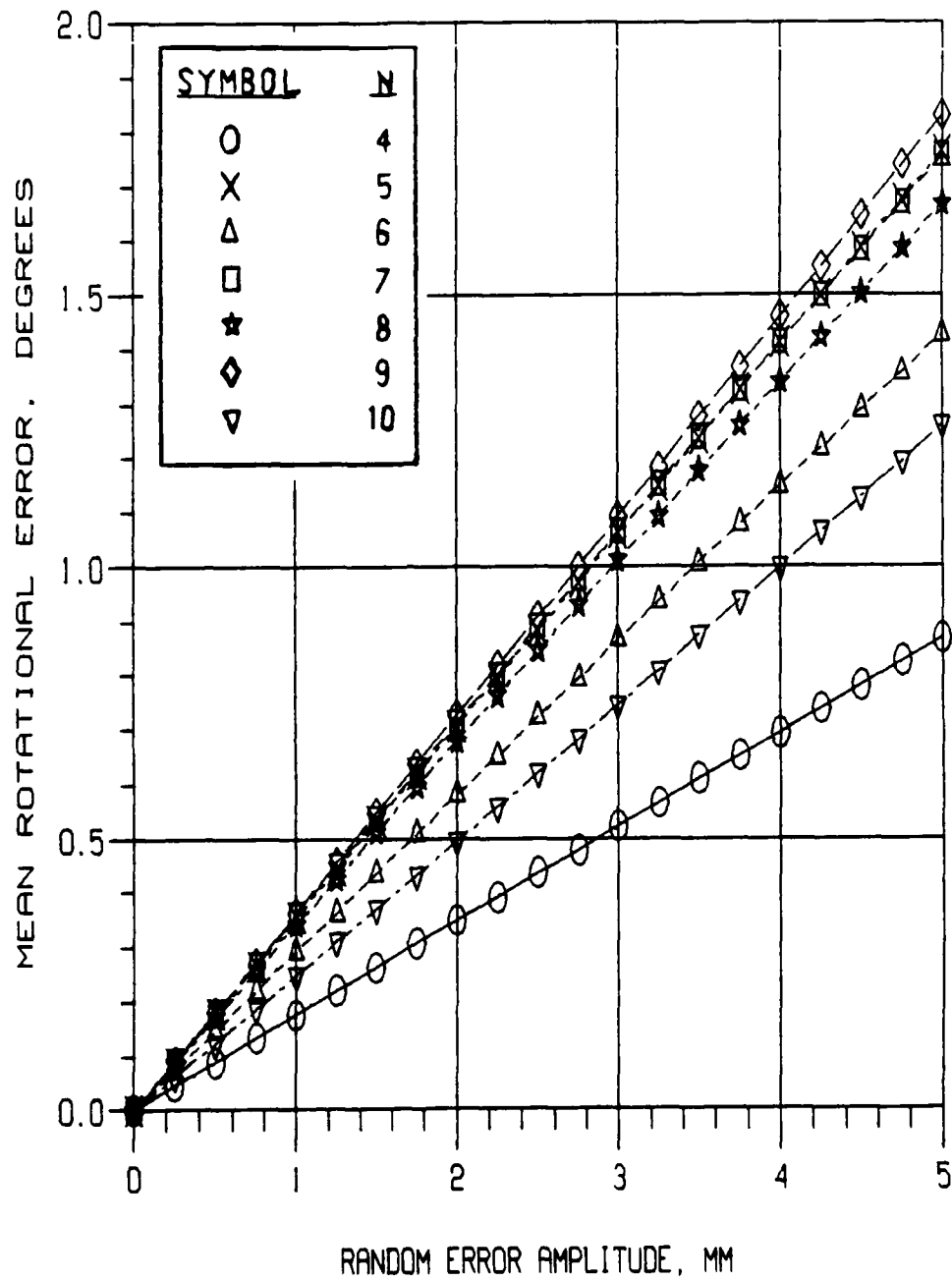
Figure 6.6   Mean Rotational Error, degrees, versus Random
              Error Amplitude, mm, using the Tensor Method
              (N = 4 to 10) and Data Set C

APPENDIX C

PROCEDURE FOR COMPUTING THE ROTATION MATRIX, R

1. To solve the equation:
$$\sum_{i=1}^{N} \vec{a_i} = \sum_{i=1}^{N} R\,\vec{b_i} \ ,$$

given $\vec{a_i}$ and $\vec{b_i}$, proceed to first make a guess for R and, then, employ an iterative process to improve this guess until the RMS error between $\vec{a_i}$ and the set of points obtained by pre multiplying $\vec{b_i}$ by R is minimized. That is,

$$\text{RMS Error} = \left[\sum_{i=1}^{N} [a_i - R\,b_i]^2 \ / \ N \right]^{1/2}$$

must be as small as possible.

2. To obtain a first approximation for R, only the first three points of A and B are used.

3. For each set of three points, a set of orthonormal basis vectors was created. The procedure for this was as follows:

- subtract point 2 from point 1 and normalize it to obtain basis vector 1.

- subtract point 3 from point 1 to obtain vector 2.

- take the cross product of basis vector 1 with vector 2 and normalize it to obtain basis vector 2.

- take the cross product of basis vector 1 with basis
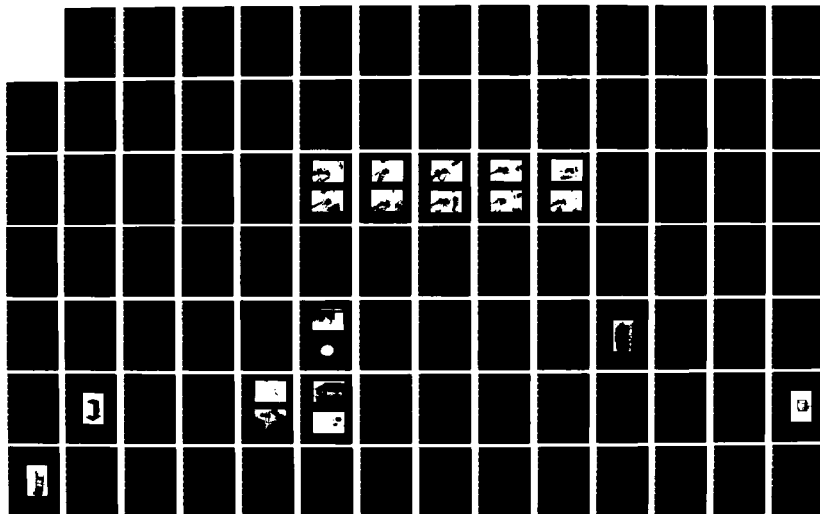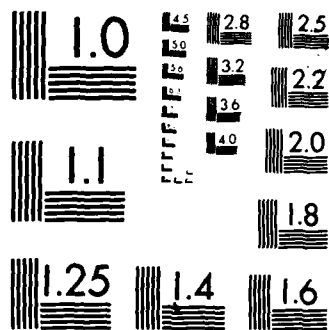
MICROCOPY RESOLUTION TEST CHART
NATIONAL BUREAU OF STANDARDS-1963-A
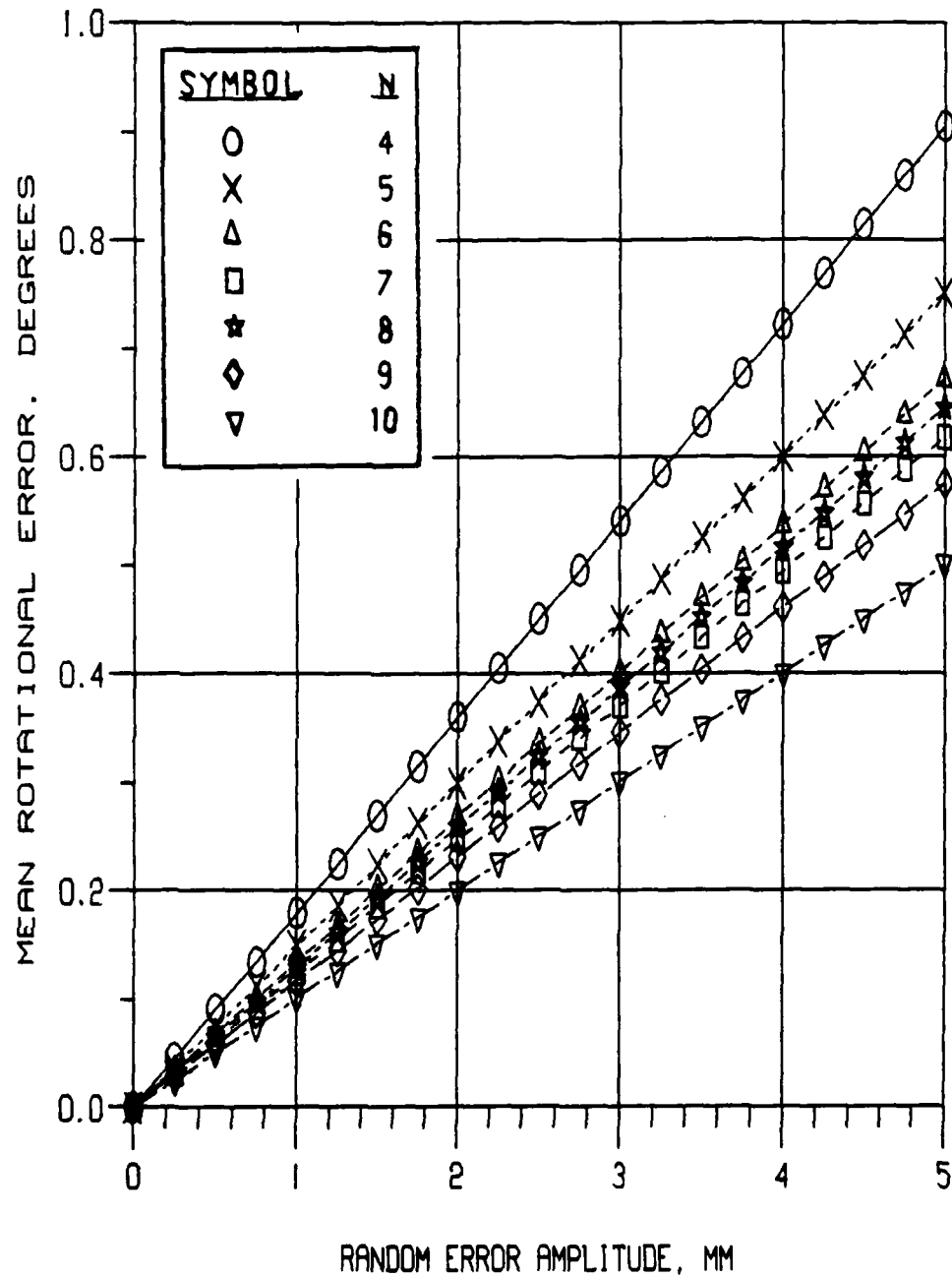
Figure 6.7 Mean Rotational Error, degrees, versus Random
            Error Amplitude, mm, using the RMS Method
            (N = 4 to 10) and Data Set C

MRE were also computed and are shown in Figures 6.8 and 6.9.

6.4.5 Comments on MTE and MRE

By evaluating the effects of varying random error amplitude on the mean translational error (MTE) and mean rotational error (MRE) several important observations concerning both the Tensor and RMS Methods can be made.

First, the lower the random error amplitude the lower the MTE and MRE values. Without exception, the smooth, positive sloped curves for MTE and MRE observed in Figures 6.2, 6.3, 6.6 and 6.7 indicate that a lower random error amplitude produced less change between the true positioning of the femur and the position the robot "perceived" the femur to be in. It can be clearly seen that if random error is totally eliminated, then the true position of the femur will be relayed to the robot without any translational or rotational error. While total elimination of random error is impossible, any procedure that increases the accuracy whereby fiducial points can be located will also improve the probability of attaining a satisfactory prosthesis emplacement.

Secondly, the results seen in Figures 6.2 through 6.9 offer a means of predicting the overall accuracy of the robotic process. The ability to make predictions concerning the level of accuracy of the robotic process is important since it would provide a means of comparison with the experimentally determined accuracy values. The
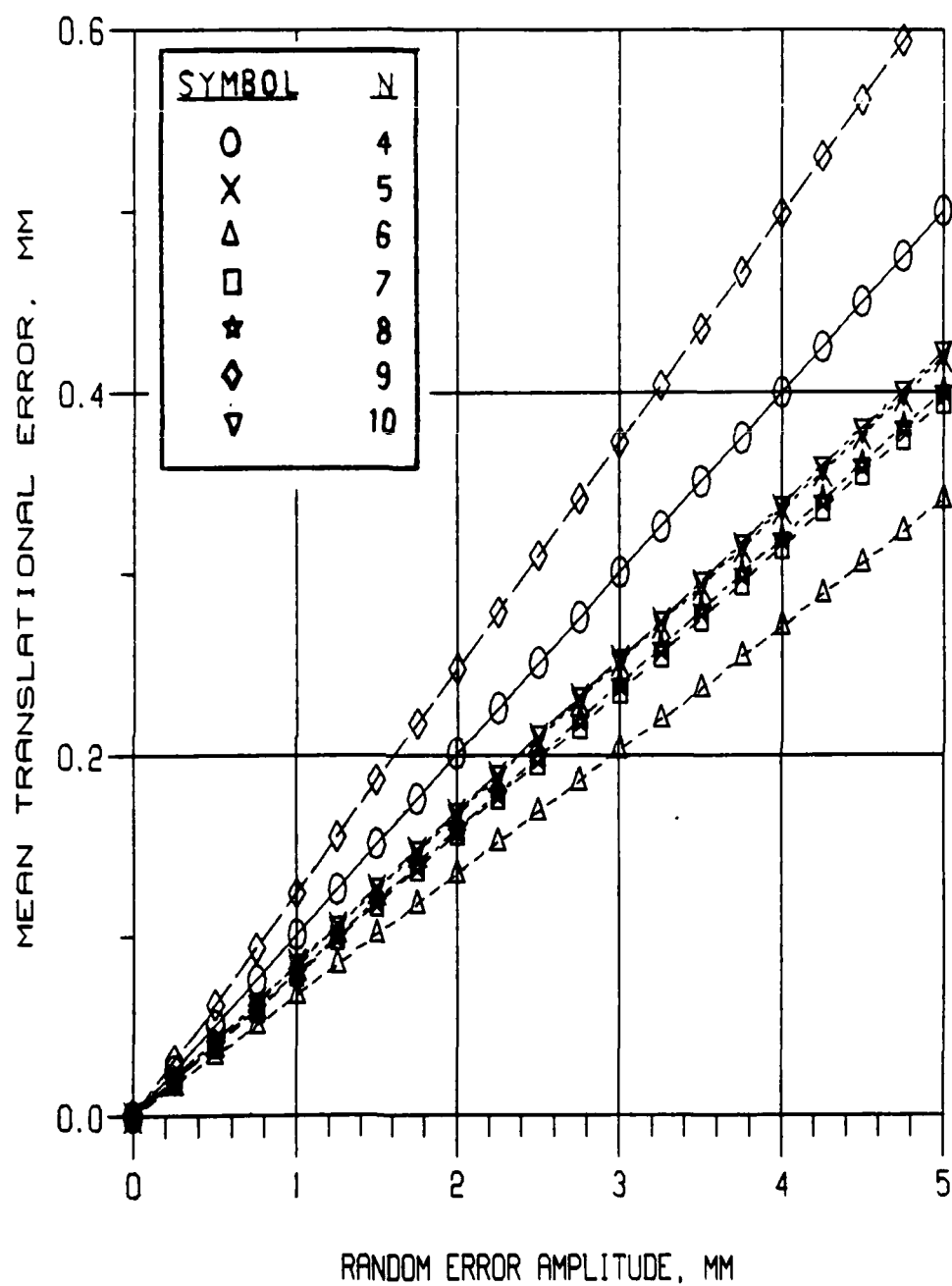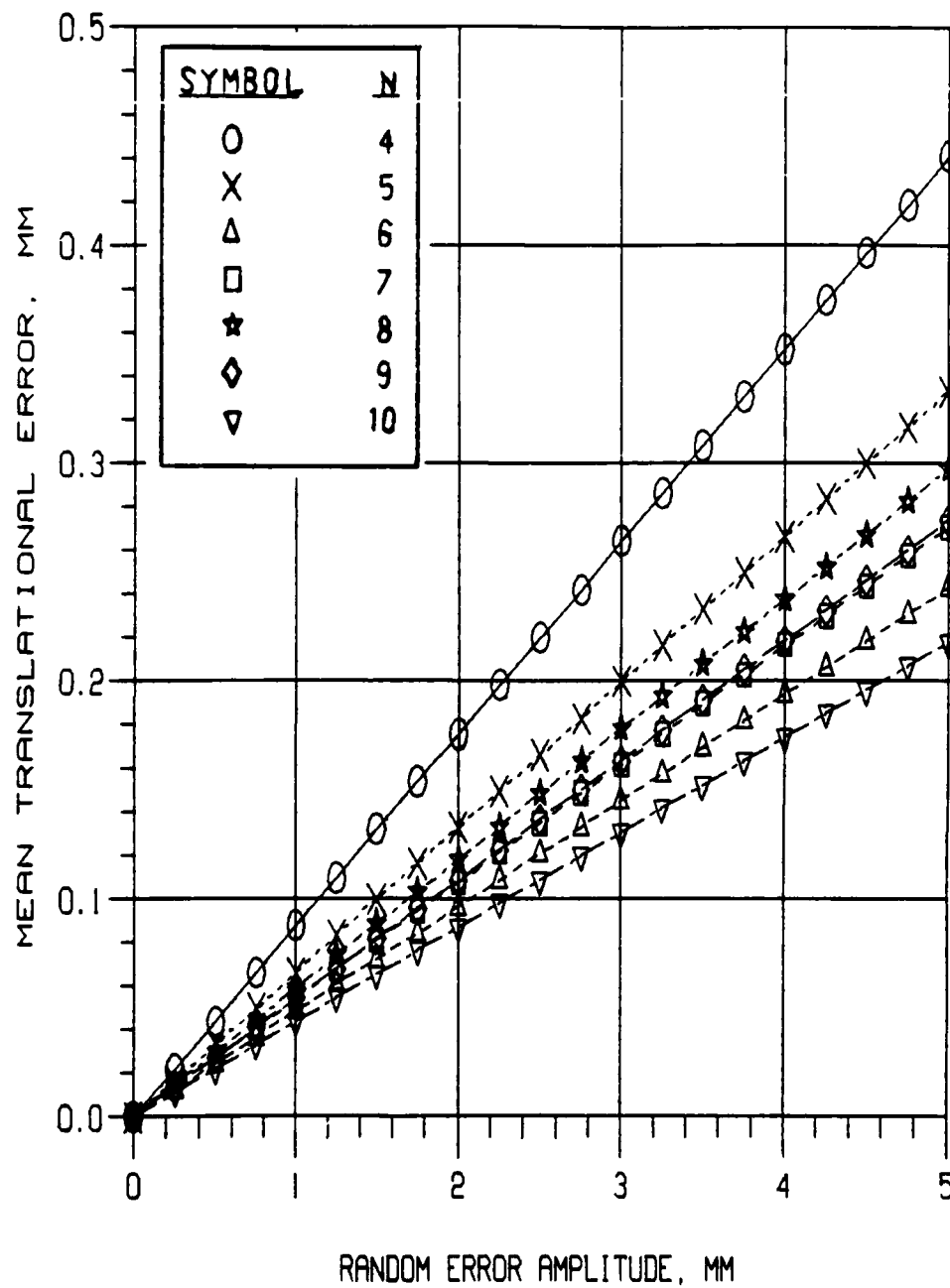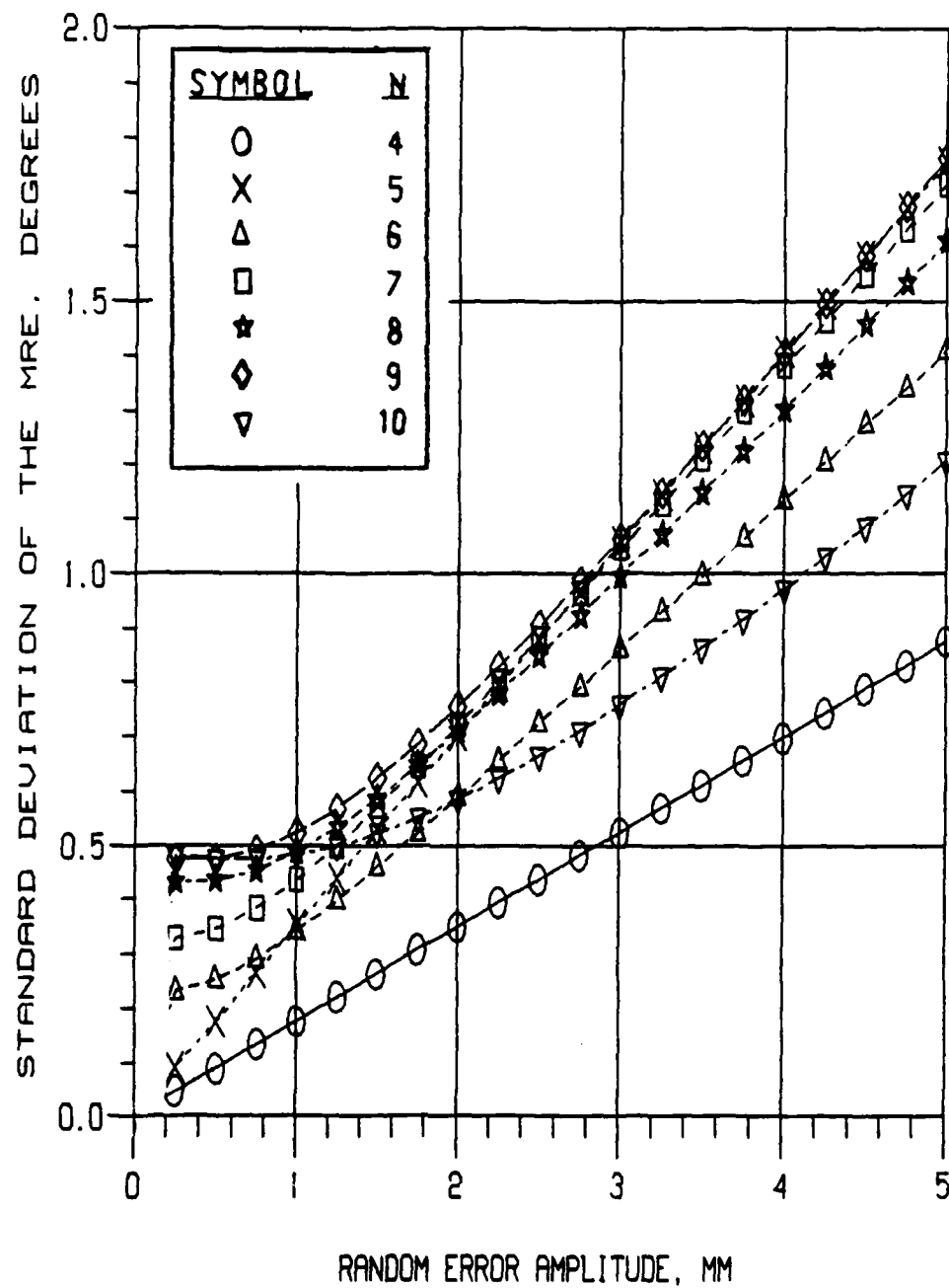
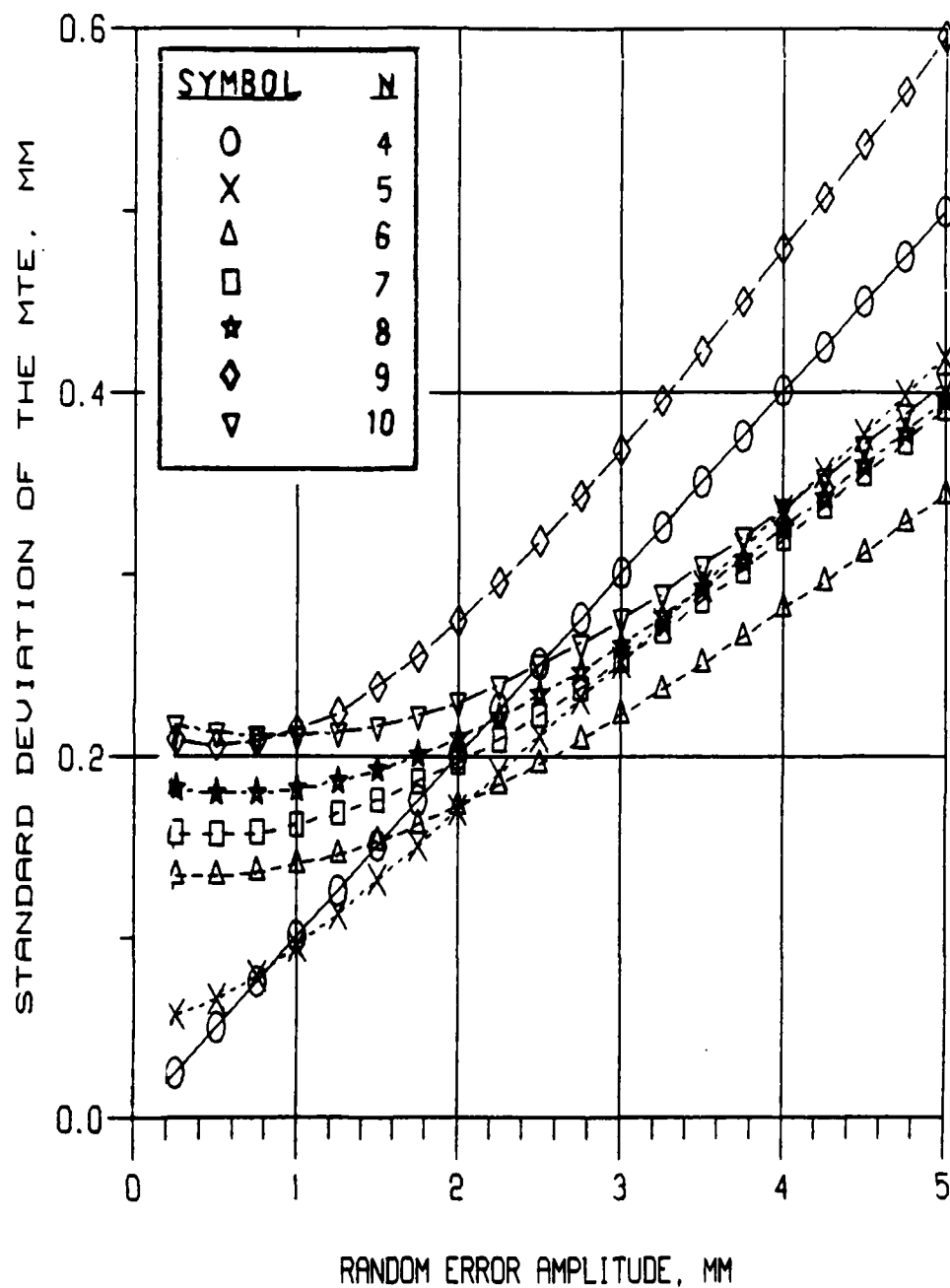Figure 6.8 Standard deviation of the Mean Rotational Error,
            degrees, versus Random Error Amplitude, mm, using
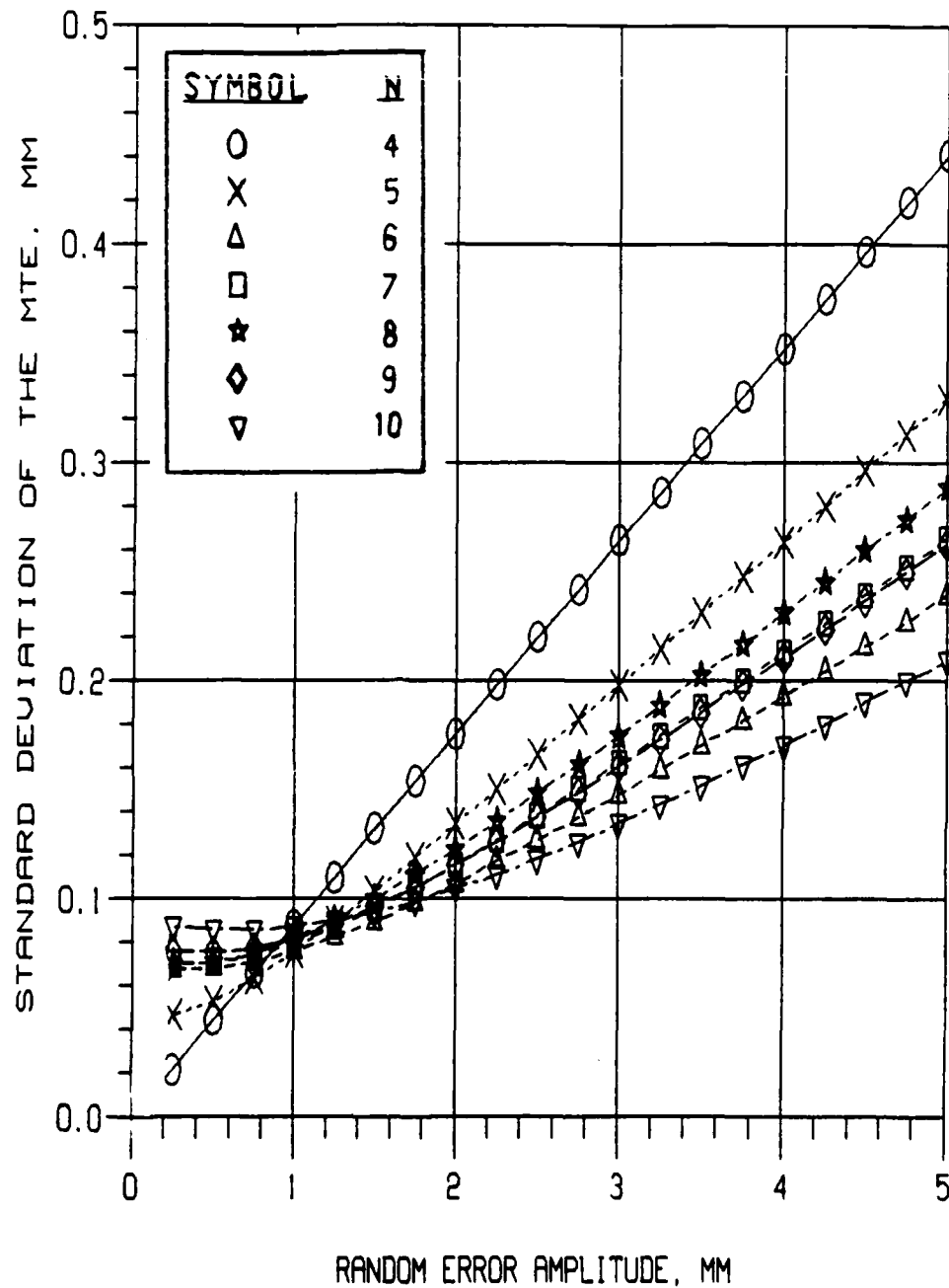   the Tensor Method (N = 4 to 10) and Data Set C
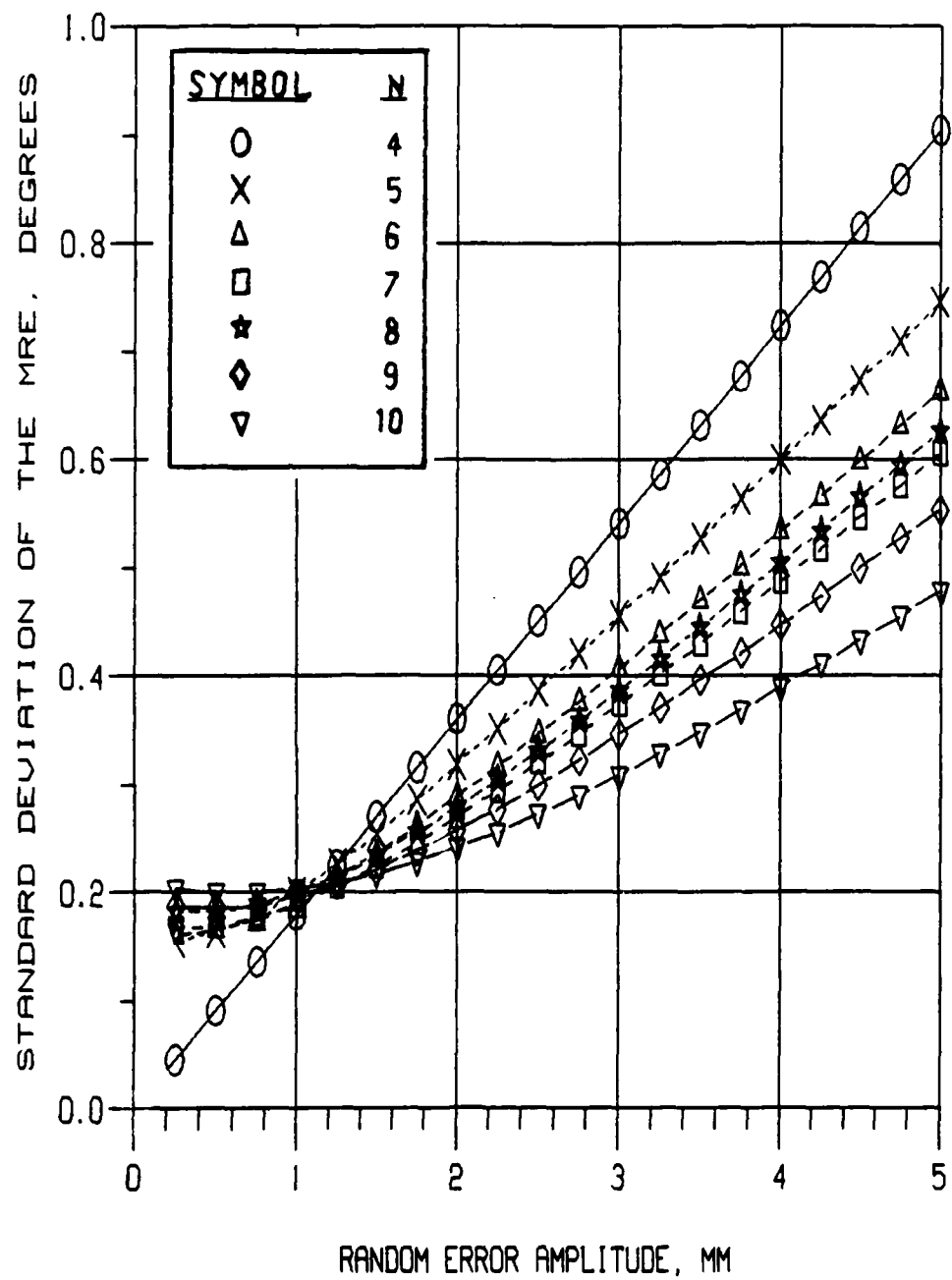
Figure 6.9 Standard deviation of the Mean Rotational Error,
degrees, versus Random Error Amplitude, mm, using
the RMS Method (N = 4 to 10) and Data Set C

procedure for using these figures is a simple one. By determining the random error in each fiducial point up to the start of computing the transformation, $^r T_d$, the above figures could be used to predict the mean translational error and mean rotational error that could be expected for the location of the center of the femur portion of the knee joint where the prosthesis was to be emplaced.

6.4.6 Impact of Fiducial Point Geometry

In the process of analyzing the Tensor Method and the RMS Method, the question of fiducial point geometry and its affect on the resultant MTE and MRE versus strain curves was raised. If fiducial point geometry did affect the MTE and MRE values, what were the implications on the selection of fiducial points?

To assess this aspect of the transformation process Table 6.11, was developed. These points were selected to see what the affects would be of using non-uniformly spaced points in the strain analysis. All points in Table 6.11 are located on one hemisphere of the surface of a sphere. Figures 6.10 through 6.13 contain the results of testing done to obtain the MTE and MRE curves for both the Tensor and RMS Methods.

It was noted that the geometry of the fiducial points had a significant impact on the resulting MTE versus strain curve. This was observed in comparing Figures 6.2, 6.3, 6.6 and 6.7 with associated Figures 6.10 to 6.13 that the MTE versus random error curves were 100% higher for the fiducial point geometry which was

Table 6.11 Set of values used in the analysis of
the Transformation Process (Set D)

Number of fiducial points (N) - 4 to 10

Data used to form the **B** matrix:

Point		Coordinates	
Number	x	y	z
1	25.00000	-42.13075	10.00000
2	00.00000	-48.98979	10.00000
3	25.00000	42.13075	10.00000
4	10.00000	47.95832	10.00000
5	25.00000	-35.35534	25.00000
6	25.00000	35.35534	25.00000
7	-25.00000	35.35534	25.00000
8	-25.00000	-35.35534	25.00000
9	30.00000	00.00000	40.00000
10	-30.00000	0.000000	40.00000

Comments: A total of ten points were chosen arbitrarily with all points being on one hemisphere of the surface of a sphere 100 millimeters in diameter.

Usage: The Set D data above was used to illustrate the effect of different point geometries on the MTE and MRE versus random error relationships. Values for the **A** matrix were generated within the test program and are not listed here. The coordinate transformation form used to form the transformation matrix which pre-multiplied **B** to obtain **A** was:

[530, 370, 100, 10, 120, 180]

See Chapter 3 for the definition of the coordinate transformation form. This data was chosen based on its similarity to actual values found when utilizing the AID 600 to cut a plastic femur mounted in the robot work volume. In this test, N was also varied from 4 to 10.
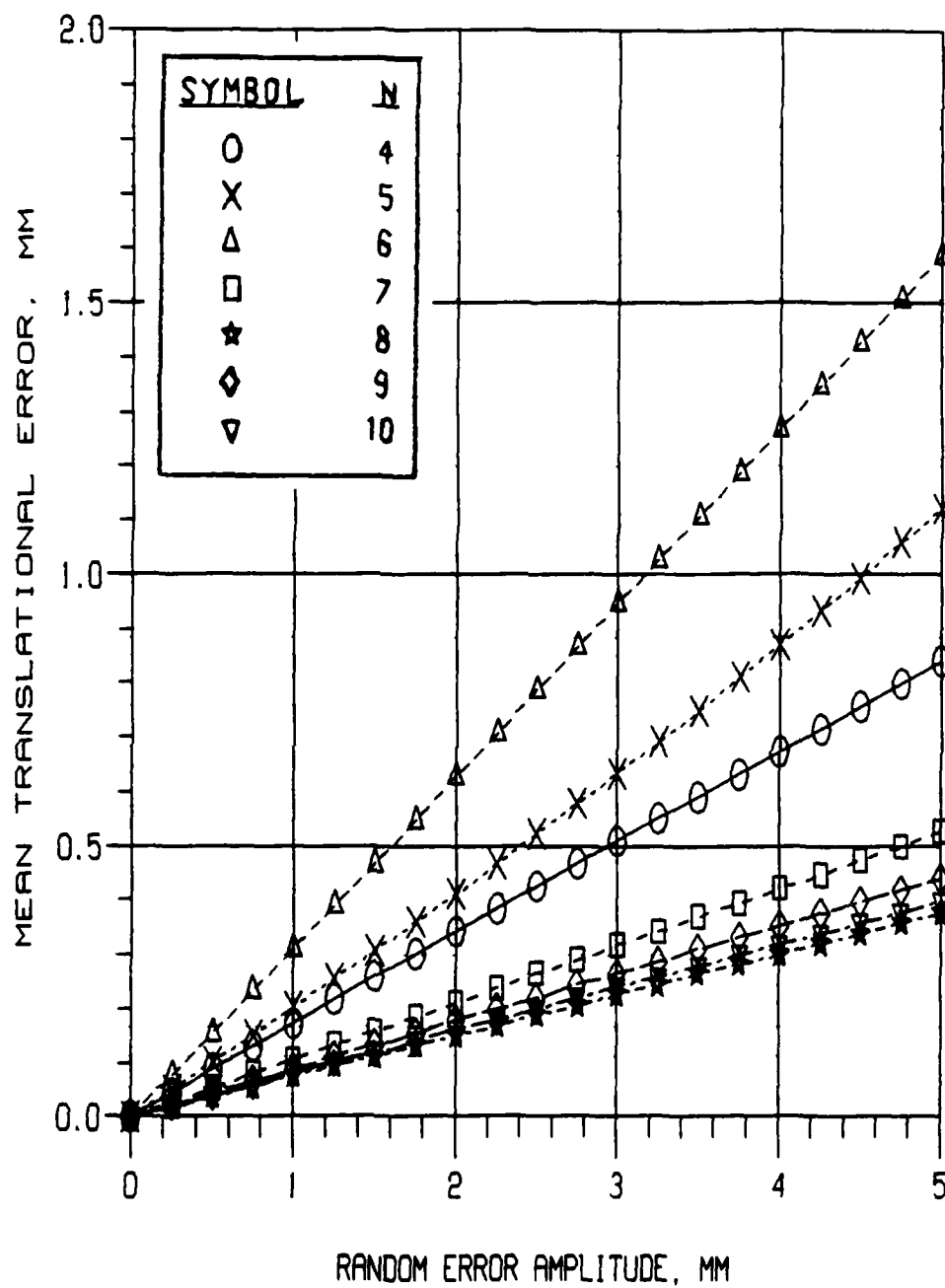
Figure 6.10 Mean Translational Error, mm, versus Random Error
Amplitude, mm, using the Tensor Method
(N = 4 to 10) and Data Set D

TRANSFORMATION ERROR ANALYSIS
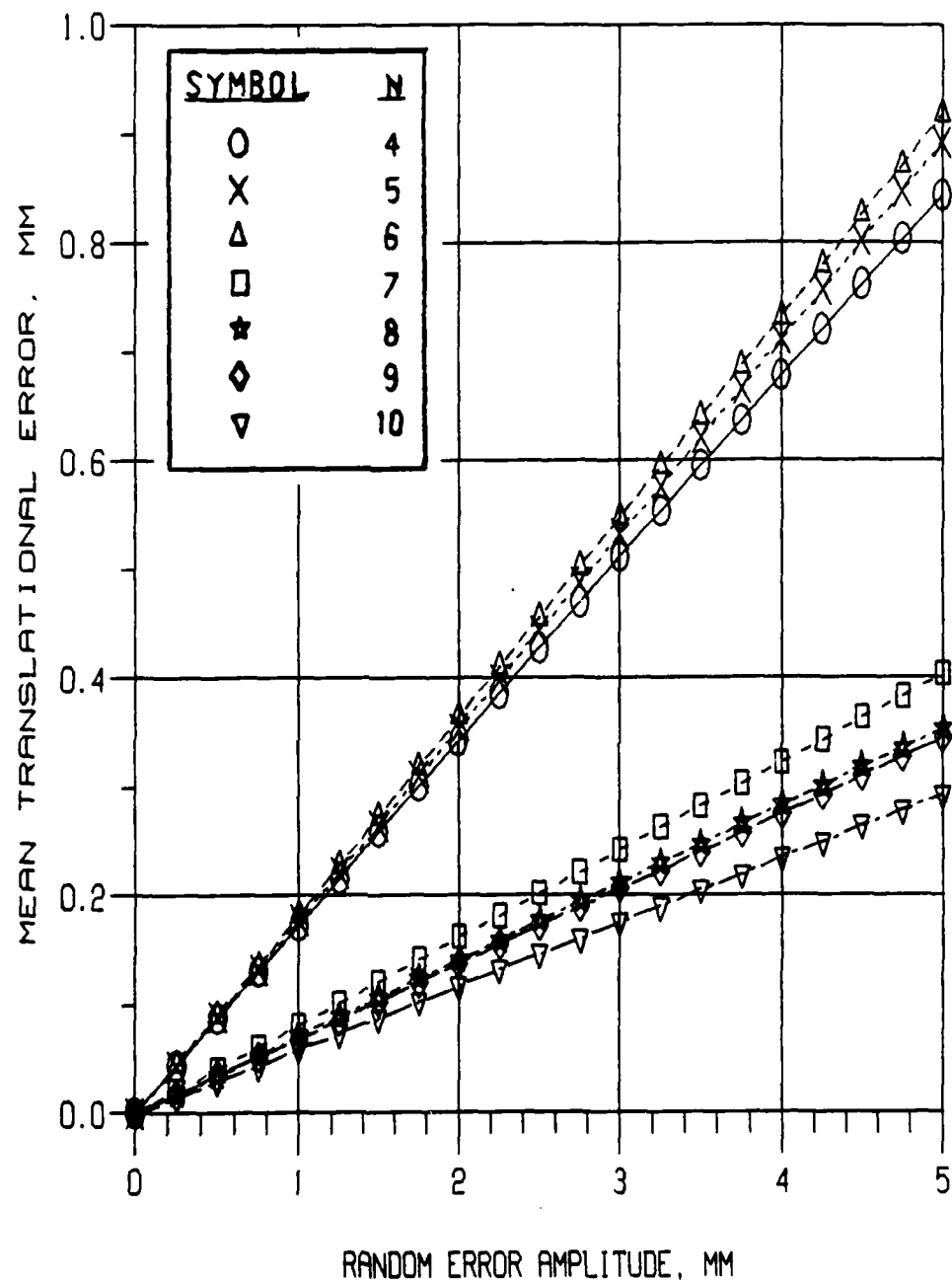
Figure 6.11   Mean Translational Error, mm, versus Random Error
Amplitude, using the RMS Method (N = 4 to 10) and
Data Set D

TRANSFORMATION ERROR ANALYSIS
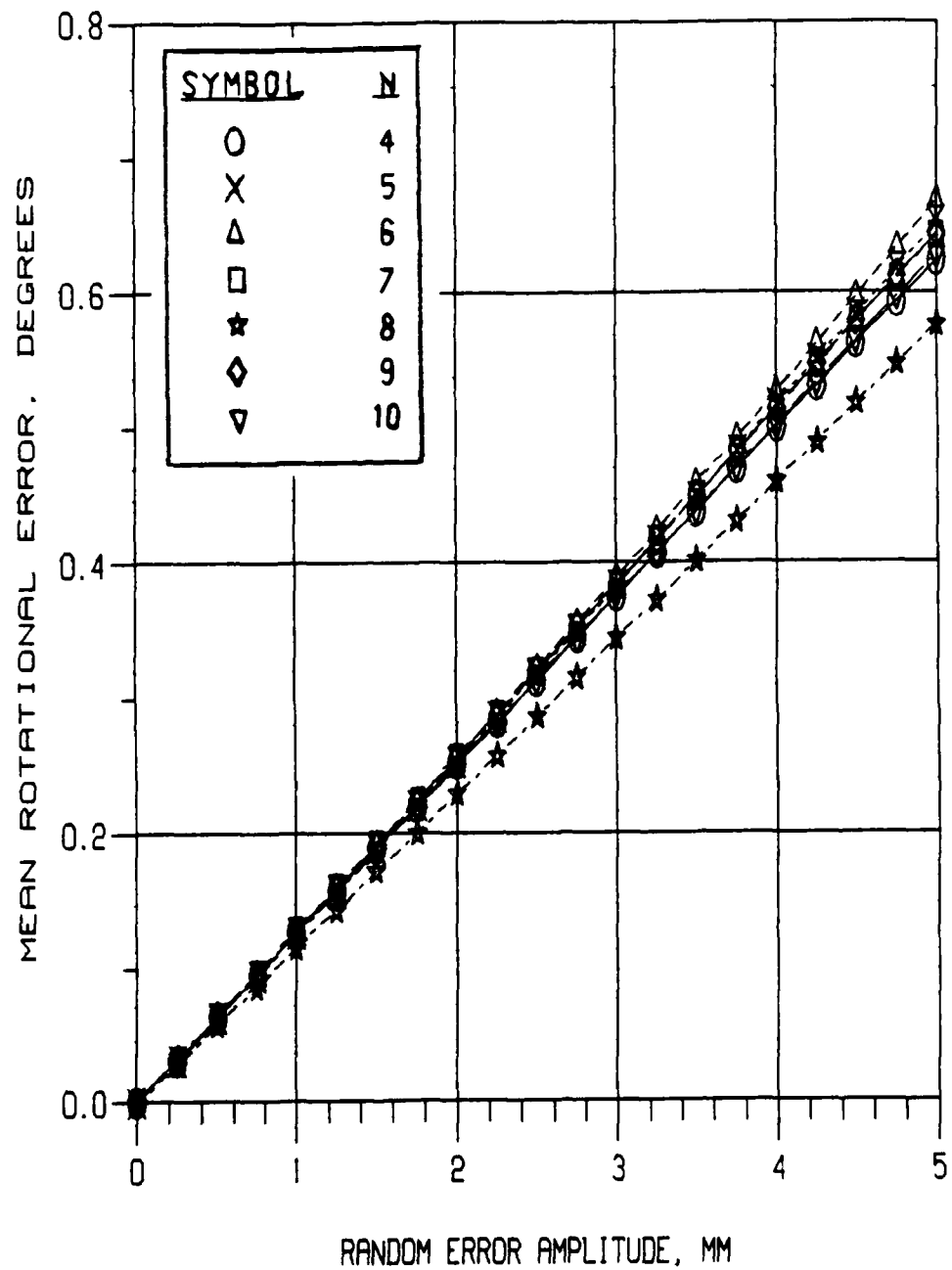
Figure 6.12   Mean Rotational Error, degrees, versus Random Error
Amplitude, mm, using the Tensor Method (N = 4 to 10)
and Data Set D
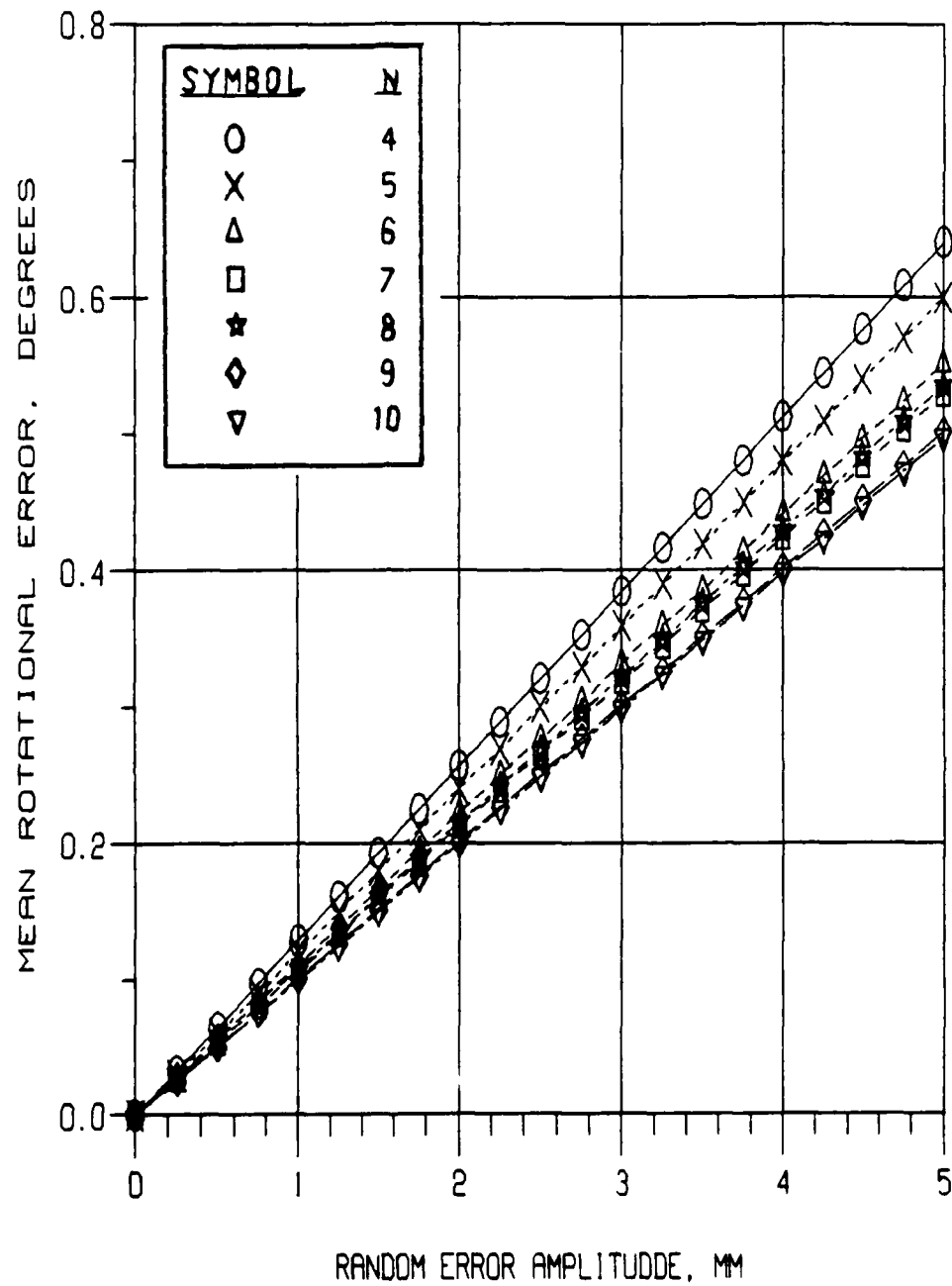
Figure 6.13 Mean Rotational Error, degrees versus Random Error
Amplitude, mm, using the RMS Method (N = 4 to 10)
and Data Set D

biased (all fiducial points were located on one hemisphere of the spherical femur model used). MRE values, however, showed no significant changes between the random set of fiducial points and the biased set of fiducial points.

6.5 Root Mean Squared Errors

An excellent comparison of how well the Tensor and RMS Methods computed transformations between the PCS and the RCS was made by computing the root mean squared errors for each of the methods. The equation which expressed this error was:

$$\text{RMS Error} = \left[\sum_{i=1}^{N} \left[\vec{a}^i - {}^r T_p \vec{b}^i \right]^2 / N \right]^{1/2} \tag{17}$$

The procedure used to compute the RMS error was a simple one and required post multiplying the transformation, ${}^r T_p$, produced in the process by the matrix, **B**. The corresponding column vectors in ${}^r T_p$ **B** were subtracted from **A** and the magnitudes of the resulting difference vectors squared and summed. The sum was divided by N and the square root of the result was taken. This final value was the RMS Error.

Set A data, listed in Table 6.1, was used to generate RMS Error values for the Tensor and RMS Methods.

The resultant values for the RMS error along with the deviation between **A** and ${}^r T_p$ **B** are displayed in Table 6.12 for the case when no spatial error was present and in Table 6.13 for the case where spatial error did exist.

Table 6.12   Comparison of RMS Error for Tensor and RMS
              Methods without spatial error in points

Deviation(x 10^{-5} mm)

Method Used	PT 1	PT 2	PT 3	PT 4	RMS Error ($x10^{-10}$ mm)
Tensor	.514	.572	.191	.477	.855
RMS	.191	.633	.095	.668	.892

Table 6.13   Comparison of RMS Error for Tensor and RMS
              Methods with spatial error in points

Deviation(mm)

Method Used	PT 1	PT 2	PT 3	PT 4	RMS Error (mm)
Tensor	.377	.212	.383	.517	.601
RMS	.373	.211	.404	.502	.596

The root mean squared errors computed showed that the Tensor and RMS Methods produced transformations which were comparable to each other. Moreover, the errors did not seem to favor either method. In the case where four fiducial points were used to test the two methods and with no spatial error between the two sets of points, the Tensor Method produced the lower RMS error value. On the other hand, the RMS Method produced the lower RMS error value for the case where some spatial error existed between the two sets of points. Based on the results of the RMS error assessment both the Tensor and RMS Methods performed equally well.

6.6 Execution time

The speed with which a program reaches a desired answer is often a critical concern of the user. Programs which require too much time to solve problems are undesirable unless the result is significantly more beneficial than the results produced by faster, more efficient algorithms. The average execution times for the Tensor Method versus the RMS Method for a specified set of points were recorded in Table 6.14. These times were the result of computing the mean value of ten execution times. Both cases where spatial error was and was not present were considered. The PDP-11 computer was used to compute the execution times.

Clearly, the Tensor Method was faster than the RMS Method for cases where spatial error was induced between the two sets of points

for which the transformation was calculated. This was understandable since the Tensor Method was not nearly as reliant on an iterative approach to computing the direction cosines of ^rT_p. The RMS Method, on the other hand, was an algorithm which iterated to a solution. For no spatial error between the two sets of points the RMS Method was as fast as the Tensor Method. However, with spatial error induced between the two sets of points, the RMS Method's execution time jumped one order of magnitude while the Tensor Method's execution time only tripled. As was mentioned earlier, although time is important, the difference in execution times was not significant enough in this instance to effect the outcome of the robotic process. Nevertheless it is an aspect of interest, especially if cost considerations are to play a role in determining the final structure of the robotic process.

Table 6.14 Comparison of Average Execution Time for Tensor and
RMS Methods with and without spatial error in points

Method	w/o Strain	w/ Strain
Tensor	37 ms	98 ms
RMS	43 ms	490 ms

CHAPTER 7

CUT GENERATION PHASE

7.1 General Comments

The procedure for computing the path of points the cutting tool would follow was described in Chapter 3. However, reference was made to a set of coordinates which defined the path of the cutter with respect to the origin of the RCS. How were these coordinates derived? How do they assist in the control of the cutting tool? These questions as well as those concerning the protocol used for tool movement and how the tool was controlled are now addressed.

7.2 Degrees of Freedom versus Constraints

The relationship between the number of degrees of freedom of a rigid body in three-dimensional space and the number of axes of movement possessed by the Automatix AID 600 robot had to be understood before tools used in the robotic process would be employed.

A total of six parameters are required to adequately describe the location of an object (rigid body) in the three-dimensional space in which the robot operated. An unconstrained object located in the work volume of the robot might therefore exhibit six degrees of freedom: three translations and three rotations. However, because

the wrist flange of the robot, on which tools would be mounted, was constrained to rotate about only two axes (x and y) any tool mounted to it was also constrained to rotate about two axes and hence would possess only five degrees of freedom. The practical result of this situation was that the Automatix robot being used could not align all three designated axes of a tool mounted on its wrist with any arbitrary set of axis established by a set of Euler angles.

This did not mean that the 5 axis robot was inappropriate for its intended task. On the contrary, the AID 600 was chosen for this investigation because it offered a simpler configuration with which to work and because of its high degree of structural stiffness. The positioning of the tool in the work volume of the robot was dependent on the wrist constraint discussed above. This relationship between the tool and the wrist was determined by first noting that the tools used were all symmetrical with respect to their longest axes of construction. This meant that if the long axis of the tool was selected as the z axis of the tool, the orientation of the remaining x and y to axes would not affect the function of the tool.

7.3 Orienting the Tool

The control over position and orientation of tools which the robot used in executing its programming was based on the simple goal of being able to move the tool tip to a point in space and align the z axis of the tool with an imaginary line running from the tool tip

through a second point designated elsewhere in the coordinate system of the robot.

In determining the position of the tool tip, the robot merely used the coordinates of the first point supplied to it to establish the position components x, y, and z. Determination of the correct orientation angles aligning the tool with the imaginary line running between the second and first points required a more complex procedure.

First, the difference between the first and second points was computed. If the two points given are $\vec{s}$ and $\vec{t}$ where:

$$\vec{s} = (x_1, y_1, z_1) \text{ and } \vec{t} = (x_2, y_2, z_2)$$

Then:

$$\vec{u} = \vec{t} - \vec{s} = (x_2-x_1, y_2-y_1, z_2 - z_1) = (x, y, z)$$

By recognizing that the vector, $\vec{u}$, as the desired direction for the z - axis of the tool, the first Euler angle, ϕ, may be calculated using equation (6) so that:

$$\phi = \arctan(y/x)$$

Similarly, θ may also be calculated using equation (7):

$$\theta = \arctan((x.\cos\phi + y.\sin\phi)/z)$$

Since the wrist of the robot was constrained so that it could not rotate about the z - axis of the robot coordinate system, the inverse kinematic equation for ψ was not used. Instead, the value of ψ would have to be related to this constraint so that the final

orientation of the tool would be correct.

The wrist reference frame location is defined in Appendix A and illustrated in Figure A.1. Figure A.1 shows the positive axis of this reference frame to be an imaginary line extending outward perpendicularly from the center of the surface containing the wrist flange. It was noted that no matter where the wrist was moved, the value of its ϕ orientation angle was always 90°. This was because the z axis of the wrist could not be moved out of the $y - z$ plane of the robot. With this fact known, the relationship between the angle, ψ, of the tool being used and the 90° ϕ angle of the wrist was established. Therefore, the problem was to search for the value of ψ for the tool tip location which would make the ϕ angle of the wrist reference frame location equal to 90°. Two possible values were expected, since the tool axis extended from the tool tip in two opposite directions along the imaginary z-axis of the tool. Because the directions the tool pointed would be opposite to each other, the two values for ψ would be located in different parts of the angular search range: one value located between 0° and 180°, the other located between -180° and 0°.

The search takes place initially in the first interval. The resultant ψ angle is then combined with the other 5 previously determined parameters (x, y, z, ϕ, θ) to produce a final tool location. This tool location is analyzed to see if the associated joint angle configurations are attainable by the robot. The

associated joint angles of any location specified for a tool are checked by using the built-in Automatix function, WORLD_TO_JOINT, which converts the input location and current tool definition into joint angles. Because the range of joint angles is known, an immediate determination of the acceptability of any location can be made. If the first tool location is not attainable, the search then proceeds to the second search interval. The angular movement capabilities of the wrist on the AID 600 robot insured that one final tool location would be attainable.

7.4 Illustrating the Search Technique

As was stated in the previous section, a definite mathematical relationship does exist between the ϕ angle of the wrist reference frame and the ψ angle of the tool. Because the ϕ angle of the wrist reference frame is constrained to always be 90°, only the value for ψ of the tool which satisfies this constraint and which allows the joint conditions of the AID 600 to remain within their specified limits will be acceptable.

The equation which relates the wrist ϕ angle with the tool ψ angle is:

$$^{r}T'_{w} = {}^{r}T'_{t}({}^{r}T_{t})^{-1}\,{}^{r}T_{w}$$

where

(1) ^rT_w is the transformation matrix which relates the wrist reference frame to the RCS and which does not change, and

(2) $(^rT_t)^{-1}$ is the inverse of the transformation matrix which defines the location of the tool tip relative to the wrist reference frame in the RCS and which defines the orientation of the tool reference frame in relation to the RCS when the robot is in the HOME position. See Figure 3.1 for an illustration of the tool reference frame and Chapter 3 for the definition of a tool. This matrix is constructed from the coordinate transformation form of the tool in use.

(3) $^rT'_t$ is the transformation matrix describing the desired location to which the tool in use is to move. All parameters necessary to construct this matrix are known, except the Eular angle, ψ. This angle is the independent variable in the equation and will be varied from -180° to $+180$.

(4) $^rT'_w$ is the resultant transformation matrix describing the location of the wrist reference frame based on the tool being positioned in its desired location. This matrix will change for each value of ψ for the tool. The parameter of interest in this matrix is the Euler

angle, ϕ, which is screened to determine if it is identically 90°.

To illustrate this search, two arbitrary points were chosen in the RCS and the resultant relationship between ψ and ϕ plotted in Figure 7.1. Note that, as predicted, two ψ values were found which produced the resultant 90° ϕ angle for the wrist. Their values were -112.09^o and 66.74^o. These angles were each substituted into the transformation, $^rT'_t$. The corresponding joint angles necessary for the tool in use to achieve the location described by $^rT'_t$ were then computed using the built-in RAIL function WORLD_TO_JOINT [8]. It was determined that the only ψ angle which allowed all robot joints to operate within their limits was the angle -112.09^o.

7.5 Tool Movement Protocol

7.5.1 General Comments

A formal protocol had to be developed which would facilitate the establishment of paths which the robot could follow in accomplishing its cuts. Two types of paths were required. First, a path was needed which would make planar, straight cuts on the surface of the femur. Second, a path was needed which would drill two holes in the femur required for the fit of the studs on the prosthesis. The following protocols were adopted.

7.5.2 Planar Cut Protocol

Each planar cut was be specified as three points in a Cartesian coordinate system. Figure 7.2 illustrates the spatial arrangement of
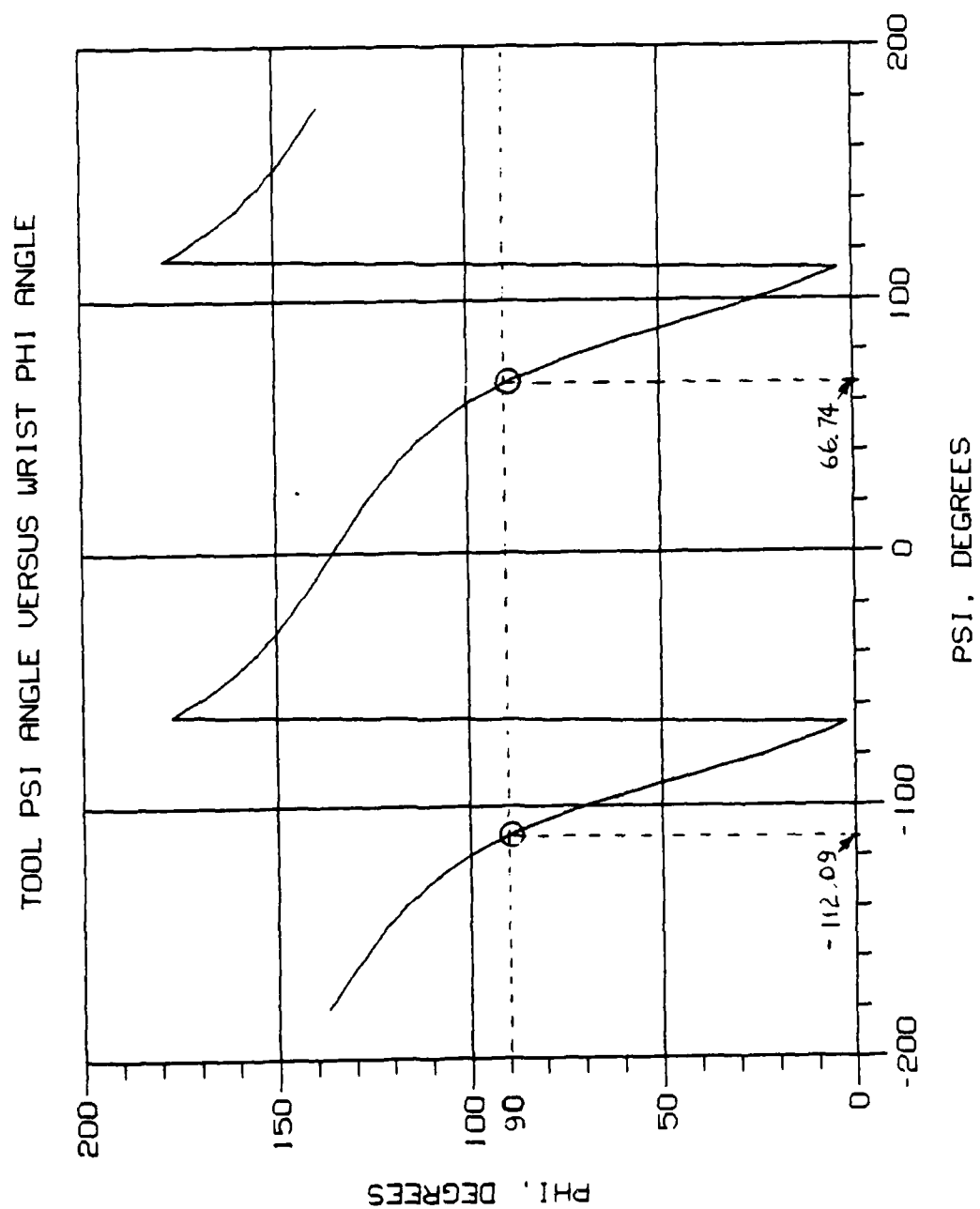
Figure 7.1 Tool ψ angle versus Wrist φ angle Relationship
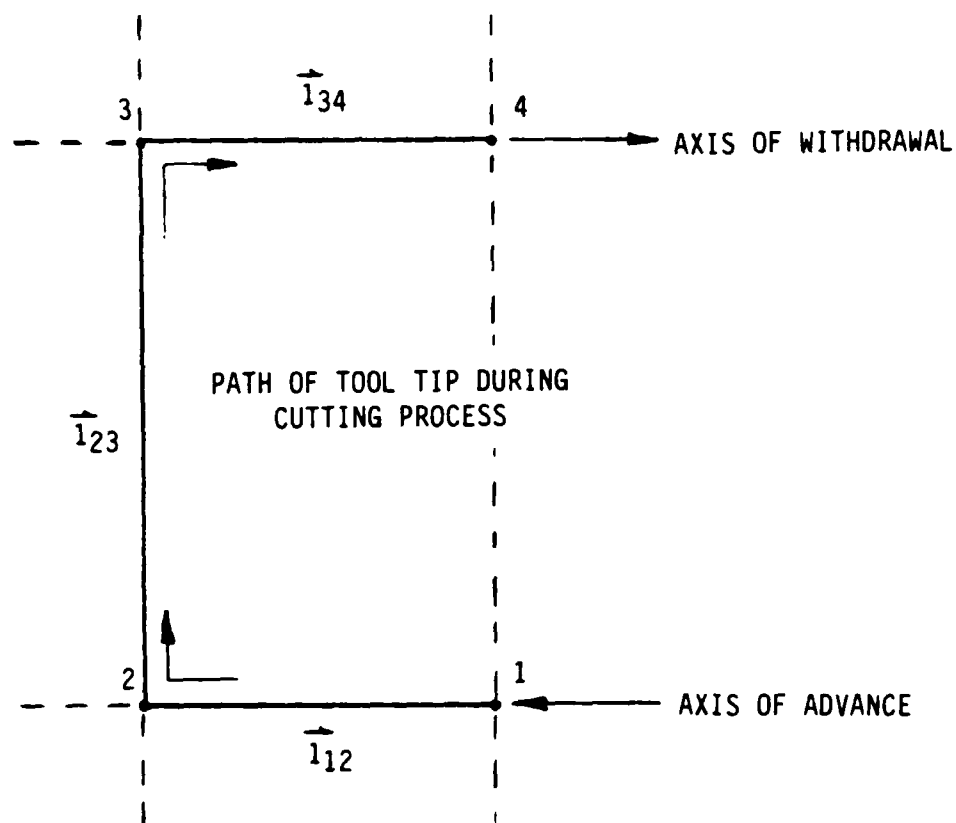
Figure 7.2 Planar Cut Protocol

these points. At a safe distance, the tool was positioned so that the axis of the cutter was aligned with $\vec{1}_{12}$ pointing from 1 to 2. The orientation of the wrist was then held constant. Using only the three Cartesian motions (x, y, z) the cutter tip moved to 1. Using only the three Cartesian motions, the cutter tip moved from 1 to 2 until the tip stopped at 2. The cutter tip then moved from 2 to 3 maintaining its established orientation. Upon reaching 3, the cutter withdrew along a path parallel with its orientation and away from 3.

Using this approach, a matrix of points was established which contained all the information required for the definition of each cut. For the five planar cuts established in this study only a 5 x 3 matrix of points was required. The points were specified with respect to the coordinate system of the robot and later transformed to the Bone Reference Frame where the execution of the cuts was made.

7.5.3 Stud-hole Cut Protocol

A somewhat more complex set of data was developed for the cutting of the stud holes for the prosthesis. However, the concept for the orientation of the tool remained the same. Each stud hole was specified by a group of 14 points. Figure 7.3 illustrates the spatial arrangement of these points. At a safe distance, the tool was positioned such that the axis of the cutter was aligned with $\vec{1}_{12}$.

With the orientation then held constant, the tip of the cutter was moved in succession to points 2, 3, 4, 5, 6 and back to 3. This

OBLIQUE VIEW
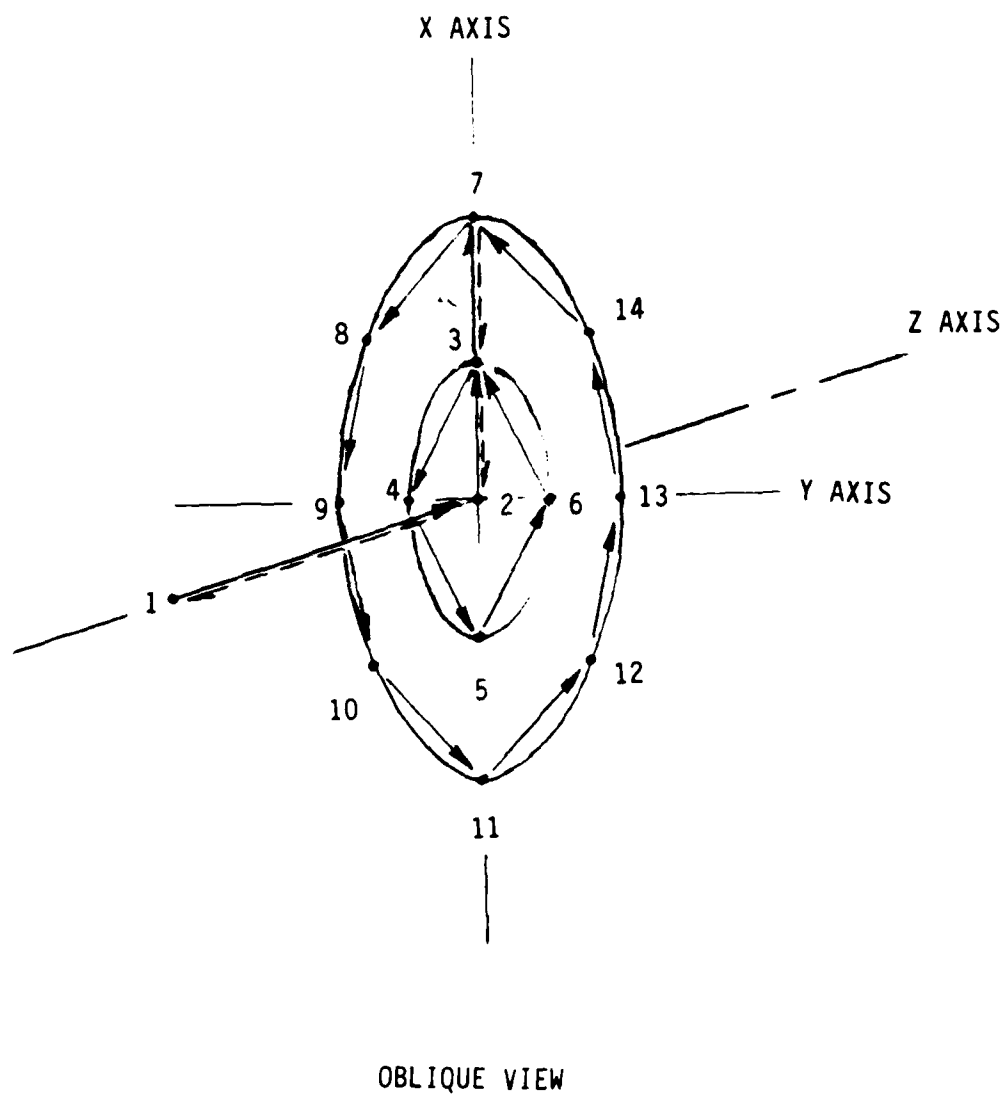
Figure 7.3   Stud Hole Cut Protocol

series of moves hollowed out the inside of the hole and prepared the bone for the outer hole cut movements. The tip of the cutter, orientation unchanged, then moved to points 7, 8, 9, 10, 11, 12, 13, 14 and back to 7, then 2. At this point the cutter was withdrawn and the hole completed.

Once again, a matrix of points was established which contained all the information required for the definition of each cut. For the two stud holes established on this study a 2 x 14 matrix of points was required.

7.3.4 Cutter Compensation

Because the tool tip of the cutter was defined to be at the center of the tip of the end mill, the location of the cutting surface relative to this tip had to be accounted for. This was done by selecting the data points for the cutter tip so that the cutting surface mills out the correct plane or hole on the surface of the femur. Figure 7.4 illustrates this compensation. The tip of the cutter was commanded to move from point 1' to 2' and 3' as described in the protocol established earlier. These points were computed so that the cutting surface of the end mill removed the correct amount of bone to form each of the planar cuts on the femur. A similar procedure was used in the computation of the stud hole data points.

105
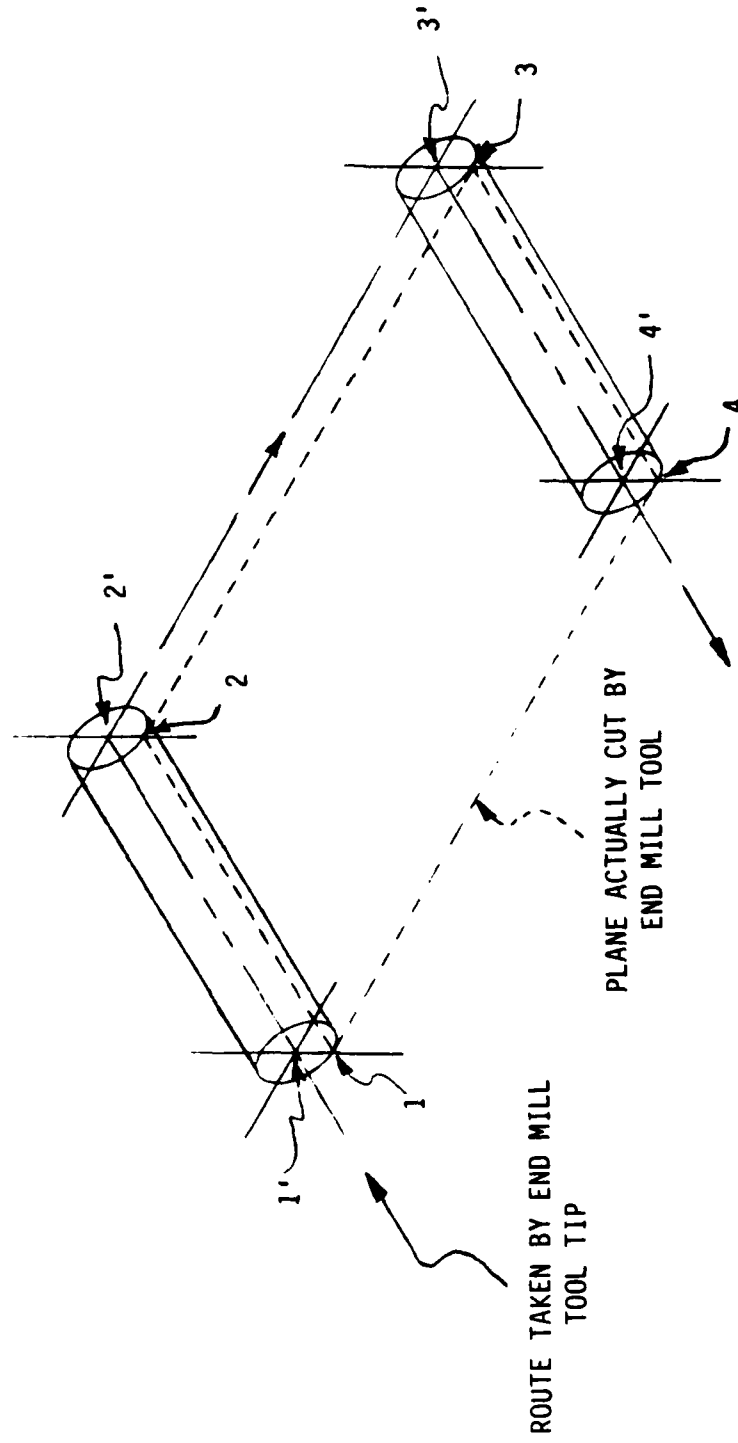
Figure 7.4 Cutter Compensation

PLANE ACTUALLY CUT BY
END MILL TOOL

ROUTE TAKEN BY END MILL
TOOL TIP

7.6 Cutter Design Comments

Because of the unique approach taken in this investigation with regard to the cutting tool used, several observations must be made.

7.6.1 Excessive Heat Generation

First, in using the routing cutter to remove material from the plastic femur, a significant amount of heat was generated. This heat causes concern because of the potential threat of damage to healthy bone cells on the cut surface which are expected to ingraft into the porous surface of the prosthesis. Destruction of healthy bone cells due to excessive heat is considered a major detractor to this ingrafting process. A possible solution to this would be the incorporation of an irrigation system into any robotic process which employs this type of cutter. Moreover, studies into the effects a routing cutter has on bone as well as establishing the material properties of bone would prove invaluable to furthering the development and use of this tool in orthopaedic surgery.

7.6.2 Size

Secondly, the size of the present cutter was considered rather large in order to be cutting the posterior condyle surfaces of the femur. The thickness of the routing cutter shaft and the restricted space between the posterior surfaces of the condyles and the tibia were the two reasons why. It was questionable whether or not cut generation in this area was desired using the cutter given its

extremely close proximity to several critical arteries, nerves and soft tissue. Possible modifications to the tool used would include the fabrication of a special tool and tool holder which would allow the surgeon to move the tool while the robot holds the tool tip in a prescribed plane. Current methods employ a flat, oscillating saw blade which may be adapted to such a tool holder. This would certainly be safer in terms of responsiveness to the surgeon and allow for increased interaction between man and machine. This observation had many implications about the direction this research could take, but was outside the scope of this thesis.

7.6.3 Tool Chatter

The cantelever-like orientation of the cutting tool mounted on the end of the robot wrist resulted in vibration of the tool at certain loads and speeds. The length of the tool from its top to the center of the wrist of the robot was approximately 85 millimeters. At certain times in the cut generation phase, the entire fluted portion of the end mill was engaged in milling out a particular planar cut. This portion of the end mill was 50 millimeters in length. Because of the large forces encountered by the tool when being drawn through the femur, the end mill occasionally encountered sufficient resistance to slow its rate of rotation, which was approximately 18,000 RPM. The end mill would then start increasing its speed again when sufficient air pressure in the die grinder

holding the tool was built up. This sudden speeding up of the tool resulted in tool chatter, or vibration.

The resulting vibrations caused a rough scoring of the cut surfaces of the bone on the order of .5 millimeters peak roughness. Efforts to prevent this tool chatter, which included the fabrication of a rigid femur fixation device, proved to be partially successful. The elimination of tool chatter was considered possible with this tool design. Some possible solutions include:

(1) use of a more powerful motor to turn the cutter,

(2) reduction of the material cut in any given pass of the tool through the femur (spring cutting),

(3) shortening of the length of the tool (end mill),

(4) slower tool translation speeds, and

(5) faster tool rotation speeds

7.6.4 Evaluation of the Prosthesis-to-Femur Fit

The demonstrated ability of the robotic process to reproduce the same set of planar cuts and stud-hole cuts was considered one of the most important features of this process. Moreover, the robotic process produced close press-fit cuts. Prostheses mounted to cut femurs without any adhesives could not be pulled apart without the aid of pry bars or other similar tools. Surface gaps between the femur and the porous surfaces of the prosthesis were less than 1

millimeter. These gaps could be completely eliminated if the geometry of the inner porous surfaces of the prosthesis were more accurately known.

Because the inner, porous surface geometry of a femoral prosthethic component can be characterized by matrices, cut data in matrix form for prostheses of many different sizes can be developed. This allows flexibility in selecting the appropriate size prosthesis for a patient. The only additional consideration in the robotic process would be insuring that the appropriate cutting data was employed to make the correct cuts.

7.7 Demonstration of the Robot-assisted Total Knee Arthroplasty

The feasibility of using robots to assist surgeons in total knee arthroplasty was demonstrated by the development and execution of the robotic process described in this thesis. The demonstration conducted utilized all phases of the robotic process. The following series of plates show the interaction of robot and femur at various stages in the orientation and cut generation phases. The plates (I through X) are shown in order of their occurrence.
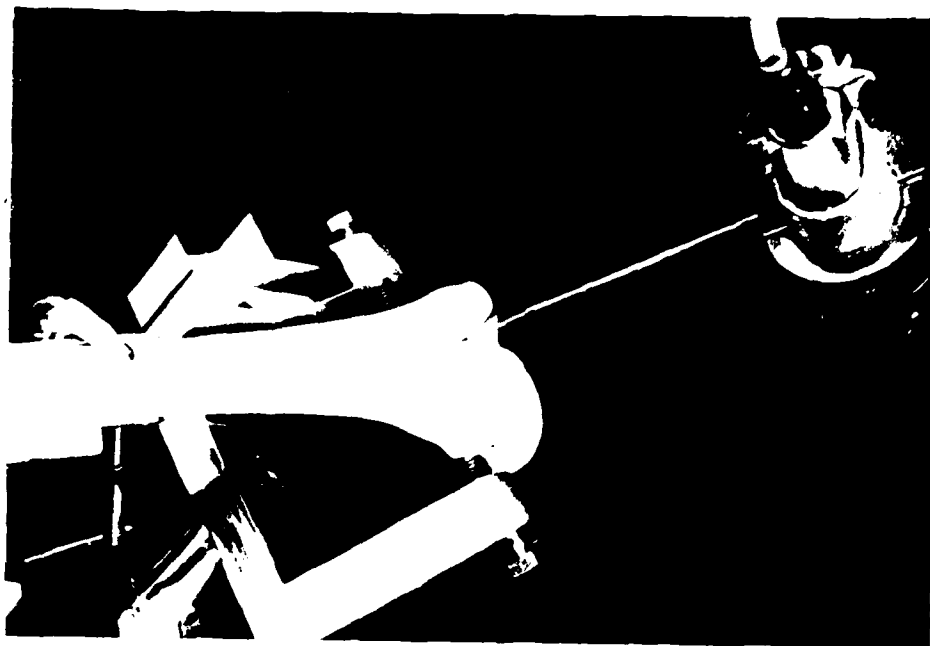
Plate I   Demonstration: Stylus is used to touch and identify
          predesignated fiducial points

Plate III   Demonstration: Cutter is at the midpoint of its first
pass in making the distal cut
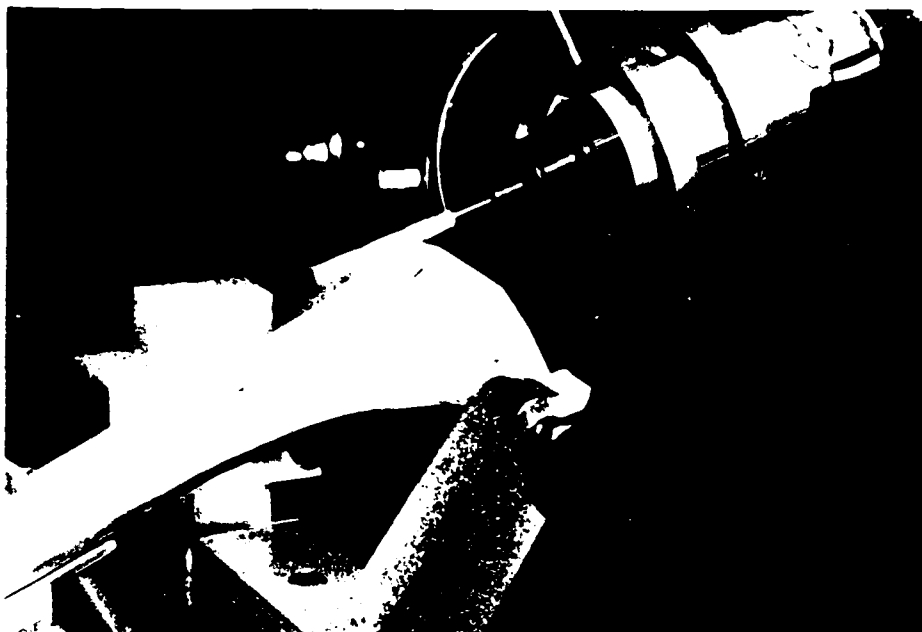
Plate V Demonstration: Cutter is near the end of completing
its third pass in making the anterior cut

Plate VII   Demonstration: Cutter is midway through its fifth
pass in making the posterior cut

Plate VIII   Demonstration: Cutter is finishing the making of
the sixth pass cut
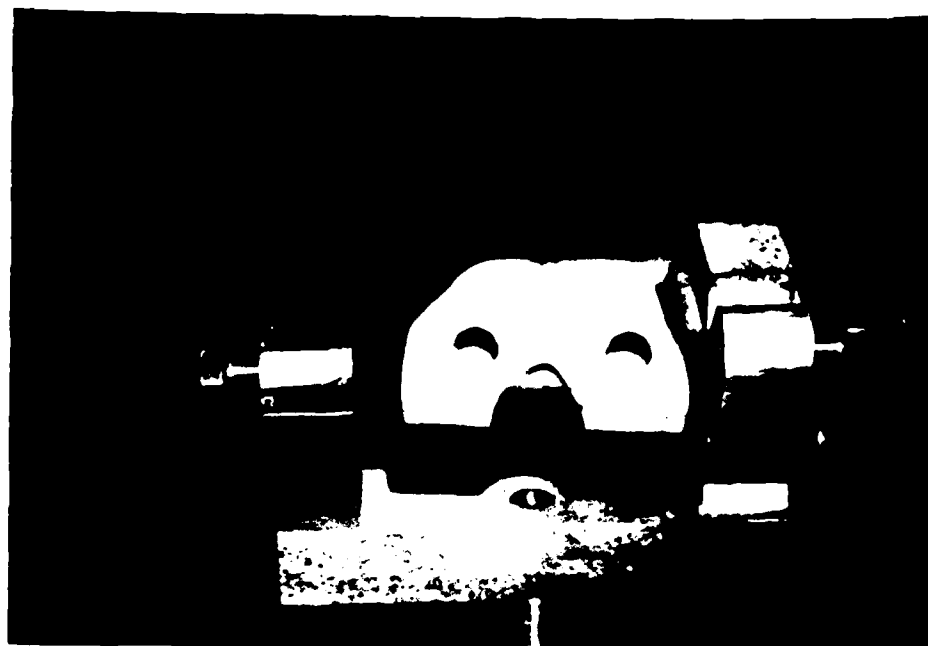
Plate IX Demonstration: The distal end of the femur is shown
after the completion of the robotic process

Plate X Demonstration: The femur is shown with the prosthesis
mounted with a near press fit

CHAPTER 8

ACCURACY EVALUATION

8.1 General Comments

The overall accuracy of the robotic process depended on a number of factors which contributed both directly and indirectly tc this accuracy.   Some of these sources of error produced overlapping influences which tended to minimize their effect.   Others had to be experimentally assessed to gain a better understanding of their values.   Some sources of error were deemed negligible through the realization that their magnitudes were insignificant provided that factors which influence them were controlled.

8.2 Sources of Error

The following sources of error were identified as having potential effect or influence on the accuracy of the robotic process:

(1) faults in the structure of the robot and construction tolerances.

(2) variation in the kinematics of the robot resulting from wear.

(3) deformations of linkages and robot parts due to temperature change.

(4) elastic deformation of the axes, segments, motor parts and the transmission devices.

(5) backlash.

(6) precision and linearity of positional sensors.

(7) system resolution of the robot and digitizer.

(8) repeatability of the robot.

(9) human error in the process of aligning crosshairs and reading dial indicators.

8.3 Assessment of Errors

Backlash, resolution and linearity characteristics of the Automatix robot were known quantities which were obtained from the current product specification sheet of the robot (see Figure 2.1). While these values gave some indication of the order of magnitude of the precision associated with the robot, the overall repeatability of the robot depended on the overlapping influences of all these error sources. Because of this, a general value for the repeatability of the robot had to be experimentally assessed.

Sources of error, whose effects were assumed to be negligible, included wear, temperature changes and elastic deformation of the robot parts. The amount of wear which took place during one cycle of the robotic process was considered insignificant given the short duration of this process. Furthermore, repeated calibration of the

robot served to minimize this source of error over long periods of time. The robot working environment was maintained at room temperature. The effects of variation in room temperature were considered minimal due to the short duration of the robotic process and the periodic nature of the calibration procedure, which served to check and adjust tool position and orientation. Elastic deformation of the robot's parts was assumed to be insignificant. The motions of the robot during the actual robotic process were contained within a relatively small portion of the robot work envelope. The working weight of the routing cutter and stylus mounted on the wrist of the robot was approximately 5% of the maximum weight specified as allowable by Automatix, Inc. Forces exerted on the tool mounted on the robot during the operation were directed in nearly identical, horizontal directions when the tool was in contact with the femur in an effort to minimize the effects of backlash. Moreover, the Automatix robot used in this thesis possessed a high degree of structural stiffness [10].

Faults in the structure of the robot and in its construction tolerances introduced bias into the readings made by tools mounted to the Automatix robot. However, care taken in the calibration procedure eliminated this bias leading to the conclusion that any residual errors were due to the precision characteristics of the robot.

The overall repeatability of the robot as well as the alignment errors introduced into the robotic process by human operators had the greatest effect on the resultant accuracy of the robotic process. The repeatability, or precision, of the robot depended on numerous mechanical and electrical factors. Values for repeatability and human induced alignment errors had to, therefore, be attained through the experimentation process.

8.4 Interaction of Error Sources

An important question in investigating the accuracy of the robotic process centered on the impact of the errors whose sources had been identified in Section 8.3. How did the various errors feed into the robotic process to produce the overall system error? In order to explain the answer to this question, the illustration in Figure 8.1 is used.

From Section 8.3, it was determined that the most significant sources of error were those related to the alignment of stylus' with fiducial points. Both the Planning Phase and the Orientation Phase required human operators to control the alignment process. The resulting errors could be represented by a random error amplitude. Once these errors reached the stage in the process where the transformation, $^{r}T_{p}$, was computed, their total effect on the robotic process could be characterized using the MTE/MRE parameters described in Section 6.4. Only the repeatability of the robot induced any
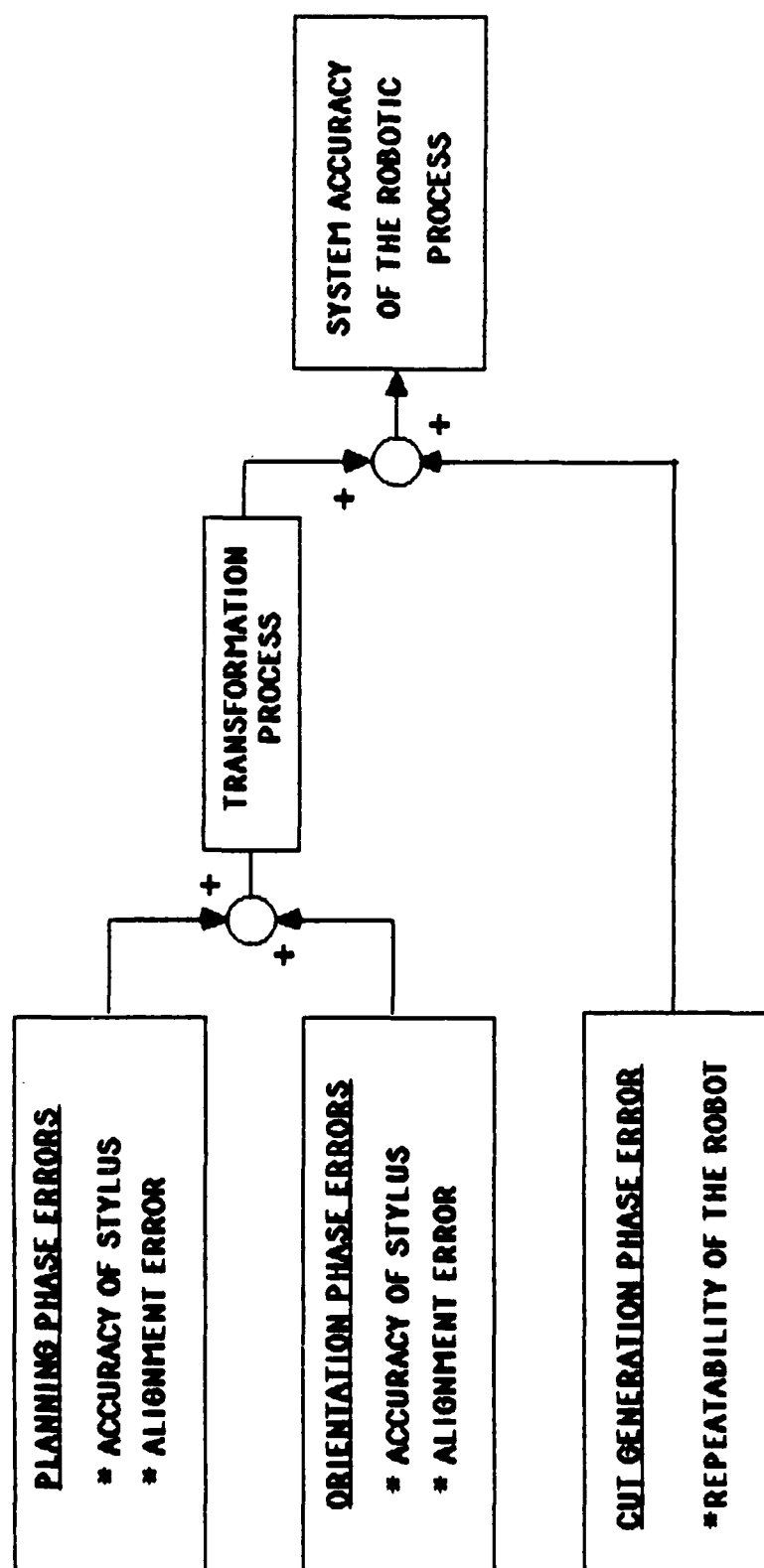
Figure 8.1 Error Source Contribution to Accuracy Determination

further errors in the robotic process after the transformation was computed. The complete interaction of errors in the Planning Phase and the Orientation Phase of the robotic process took place when the transformation was computed between the PCS and RCS.

In Figure 8.1, it can be seen that errors stemming from the alignment processes of the Planning and Orientation Phases as well as the accuracy of the stylus' geometries all affected the resultant transformation, ^rT_p. After this point, however, only the repeatability of the robot impacted on the accuracy of the robotic process.

8.5 Accuracy Experimentation

8.5.1 General Comments

The accuracy of a given process is generally quantified in terms of its bias and precision. If the instrument of the process can be calibrated, the bias can be removed and the only remaining inaccuracies are those related to the precision of the instrument. This is the case with the AID 600 robot in this investigation. The precision of the AID 600 is characterized by its repeatability. Hence, the accuracy of the robot may be roughly approximated by the repeatability.

The repeatability of the robot used in this investigation was experimentally determined using the procedure contained in Appendix B. Estimates for the amount of random error added to the fiducial

points in the alignment process were also obtained experimentally for both the Planning and Orientation Phases. The impact of the alignment errors on the transformation process were evaluated to provide a means of comparing the actual experimental MTE/MRE errors with those predicted by Figure 6.2 through 6.9.

The control set of fiducial points used in analyzing the alignment errors and determining the MTE and MRE values was the set of points in the CCS listed in Table B.2. These points corresponded to the set of points marked on the Measurement Test Cube and were known to be accurate within +/- .02 millimeters. In the Planning Phase, the points marked T1 through T4 were used to identify the CCS into which all raw data from the digitizer would be transformed. The stylus touched all fiducial points designated on the Measurement Test Cube and the points marked T1, T2, T3 and T4. The set of coordinates which resulted were then transformed, so that the resulting coordinates for T1, T2, T3 and T4 matched those contained in Table B.2. The transformed fiducial points were then analyzed. In the Orientation Phase, the points T1 through T3 were used to construct a reference frame whose representative transformation was used to transform the points contained in Table B.2 into the RCS. The BUILDFRAME function was used to accomplish this. Once the control points were established, the fiducial points of the cube could be touched with the stylus of the robot and the data recorded and analyzed.

8.5.2 Repeatability

Procedures described in Appendix B were used to determine the repeatability of the AID 600 robot. The final value for this repeatability was .03 millimeters. This value applied to the robot in the configuration which it was utilized during this investigation.

8.5.3 Stylus Alignment Error

Experimental procedures for establishing a mean value for the stylus alignment error in both the Planning and Orientation Phases of the robotic process are described in Appendix B. The results of these experiments are contained in Tables B.3 and B.4. The average alignment error values were .34 millimeters for the alignment procedures in the Planning Phase and .41 millimeters for the alignment procedures in the Orientation Phase. The alignment error for the two phases, computed using the Root-Sum-Squared Rule, was .53 millimeters. This alignment error represents the total alignment error for the Planning and Orientation Phases.

8.5.4 Actual MTE/MRE Experimental Results

In addition to calculating the alignment error, the experiments described in Appendix B also computed the MTE and MRE values between the control set of fiducial points and the set of fiducial points established using the stylus to touch the points of the Measurement Test Cube. Because the spatial orientation of the control set of fiducial points was known, the calculation of separate MTE/MRE values

in both the Planning Phase and the Orientation Phase were possible. Thus, information about the development of errors in each phase was made available, whereas in an actual operation only a single MTE/MRE estimate would be available. In the Planning Phase, the MTE was computed to be .37 millimeters and the MRE was computed to be .32 degrees. In Phase 2, the MTE was computed to be .31 millimeters and the MRE was computed to be .55 degrees.

The experimental MTE and MRE values should be no greater than the RSS values for the MTE and MRE.

8.6 Discussion

8.6.1 The Predicted MTE/MRE Values

As suggested in Section 6.4.5, the figures developed in Chapter 6 using computer simulation of the effects of spatial error on the transformation process could be utilized to predict the accuracy of the robotic process. This required knowing the random error amplitude of the fiducial points for both Phases 1 and 2.

The alignment error computed in Section 8.5.3 was used as the value for the random errors amplitude required by Figures 6.2, 6.4, 6.6 and 6.8. By entering each figure, a mean value and standard deviation for both the MTE and MRE could be obtained. The following values were established as the predicted MTE/MTE values for the experiment conducted in Appendix B. For a random error amplitude of .53 millimeters and N = 8:

$$MTE = .05 \text{ millimeters}$$

$$MTE_{S.D.} = .18 \text{ millimeters}$$

$$MRE = .20 \text{ degrees}$$

$$MRE_{S.D.} = .45 \text{ degrees}$$

For a perfect Gaussian distribution, 99.7% of the actual MTE/MRE results should fall within +/- three times the standard deviation of the mean MTE/MRE predicted values. Using this assumption, the actual MTE/MRE results for the experiment were predicted to be contained in the following intervals:

MTE = 0 millimeters to .59 millimeters

MRE = 0 degrees to 1.55 degrees

8.6.2 Comparison of Predicted and Actual MTE/MRE Values

The RSS error values for MTE and MRE obtained from the experiments in Appendix B were:

$$MTE = \sqrt{(.37)^2 + (.31)^2} = .48 \text{ mm}$$

$$MRE = \sqrt{(.32)^2 + (.55)^2} = .64 \text{ degrees}$$

These results compare favorably with those of Section 8.6.1.

The experimental MTE and MRE values fell within the ranges predicted for them by the figures developed in Section 6.4.

When the repeatability of the robot was considered in the robotic process, the overall system accuracy which resulted showed a

femur-prosthesis alignment error of .51 millimeters in translation and .64 degrees in rotation.

CHAPTER 9

CONCLUSIONS

The feasibility of using a precision motion control device, or robot, to generate the cuts on the femur component of the knee joint was successfully demonstrated. The robotic process developed and described in this investigation offers a reasonable procedure for the generation of surgical cuts on the femur using current equipment technology and mathematical theory. Robot-assisted total knee arthroplasty as envisioned in this thesis is a logical next step toward quality improvement of knee arthroplasties. This is especially true in light of current research developments which underscore the need for more accurate techniques. The three phase explanation of the robotic process, (1) planning, (2) orientation, and (3) cut generation, represents a sequential approach to the problem of improper position and alignment of the femoral prosthetic component on the distal end of the femur.

The accuracy of the robotic process developed in this investigation was experimentally established. The sources of error found to most significantly affect the accuracy of the robotic process were those related to (1) human subjectivity, (2) human handling of stylus', (3) the discrete nature of the measurement systems used, and (4) the repeatability characteristics of the robot. The results of experimentation showed that upon completion of the cut

generation phase of the robotic process, a femur-prosthesis alignment error of .51 millimeters in translation and .64 degrees in rotation was obtained. These accuracy results were supported by a numerical simulation and analysis of the transformation process. These results indicate that the robotic process developed in this study offers a potential means of significantly improving the quality of total knee arthroplasties by increasing the accuracy of the cut generation process.

Alignment errors between stylus' and marked fiducial points were found to be less than .5 millimeters. These errors were attributed to the direct handling and subjective alignment of probes with fiducial points by human operators. Alignment errors between stylus' and unmarked fiducial points were found to be significantly higher with errors of up to 4 millimeters encountered.

Three different methods for computing the transformation matrix between two corresponding sets of points were developed, explained and evaluated. These were the Tensor Method, the Best Approximate Solution Method and the Root Mean Squared Method. Only the Best Approximate Solution Method, due to its failure to produce orthogonal matrices, was not acceptable in its application to the robotic process. The relative merits of the remaining methods were discussed. Both the Tensor and Root Mean Squared Methods proved to be highly efficient and accurate. Both were able to take into account the spatial error which existed between two sets of

corresponding points. Either method is acceptable for use in the robotic process.

The spatial error model developed to simulate the random error induced into the robotic process was able to correctly predict the positional and rotational error ranges in which the final experimental values for the translational and rotational errors fell.

The protocol established for the cut generation phase of the robotic process provides a realistic approach to the cutting of the surfaces of the femur. The resulting near press-fit of the femoral prosthetic component on to the distal end of the femur provides further evidence in support of the assertion that robot-assisted total knee arthroplasty is feasible and capable of significantly higher levels of accuracy than are currently possible.

Several problem areas associated with the employment of the helically-fluted routing cutter were identified. These included significant heat generation, tool size and tool chatter. The effects of each of these problem areas was discussed and possible solutions offered.

Procedures for calibration of the AID 600 robot and its tools were developed which minimized system bias in tool definitions. These procedures, even though specifically developed for this investigation, may be used in a variety of other applications.

CHAPTER 10

RECOMMENDATIONS

Clearly, further study of the robotic process developed in this investigation is warranted. Several problems encountered in this study have been noted within the text of this thesis. Many of these points bear repeating.

(1) Improvement to the spatial error model used in the analysis of the transformation process would increase the correlation between predicted and actual experimental values obtained for MTE and MRE. An improved model would also serve to make a better assessment of the behavior of transformation processes under conditions in which spatial error exists.

(2) The design of the cutter used to generate the cuts on the femur must be improved. Problems of heat generation, tool size and tool chatter must be investigated in order to eliminate their resultant undesirable effects. The interaction between tool and surgeon could be improved through a more flexible mounting design for the cutting tool.

(3) An investigation into the material properties of bone would greatly aid the design process in terms of

selecting turning speeds, routing cutter design and rate of feed speeds for the cutter.

(4) A means of accurately marking selected fiducial points to be used in the orientation process should be developed. The accuracy of the robotic process was directly related to the ability of the operator to locate fiducial points with a specified certainty.

LIST OF REFERENCES

1. Gordon, S.L. Evaluation of the Musculoskeletal Diseases Program, NIH Publication No. 84-109, March 1984.

2. Matsen, F.A., Brackett, R.B., Garbini, J.L., Larson, R.V., Sidles, J.A., "Effect of component position on function in total knee arthroplasty" submitted for presentation to 38th Annual Meeting of the Association of Bone and Joint Surgeons.

3. Lotke, P.A., and Ecker, M. (1977) Influence of positioning of prosthesis in total knee replacement. Journal of Bone and Joint Surgery, 59-A(1), pp. 77-79.

4. Bryan, R.S. and Rand, M.J., (1982) Revision total knee arthroplasty. Clinical Orthopaedics and Related Research, 170, 141-146.

5. Kobrinski, E.J., and Prevost, C.A., in Length of Stay by Operation (United States), compiled by the Commission on Professional and Hospital Activities, p. 72, Ann Arbor, Michigan, October 1984.

6. Kwoh, Y.S., A New Computerized Tomographic-Aided Robotic Stereotaxic System, in Robotics Age, Vol. 7, No. 6, pp. 17-22, June 1985.

7. Abstract, Experimental Robot System for Microsurgery, in The Japan Robot News, Vol. 4, No. 10, October 1985.

8. Rail Software Reference Manual, Document No. MN-RB-07, Rev. 5.00, by Automatix, Inc., October 1983.

9. Cybervision III Installation Manual, Document No. MN-CB-02, by Automatix, Inc., p. 1-4, June 1982.

10. AID 600 Technical Specification, in Product Specification Document No. PS-CB-01, June 3, 1981.

11. Rail Software Reference Manual, Document No. MN-RB-07, Rev. 5.00, p. 2-31, by Automatix, Inc., October 1983.

12. Paul, Richard P., Robot Manipulators: Mathematics, Programming,

and Control, pp. 43-45, MIT Press, 1981.

13. Paul, Richard P., Robot Manipulators: Mathematics, Programming and Control, pp. 65-70, MIT Press, 1981.

14. The Tensor Method was developed in consultation with Joseph L. Garbini, Ph.D., Associate Professor, Department of Mechanical Engineering, University of Washington, 1986.

15. John Greenstadt, The Determination of the Characteristic Roots of a Matrix by the Jacobi Method, in Mathematical Methods for Digital Computers, edited by A. Ralston and H. S. Wilt, Chapter 7, John Wiley and Sons, New York, 1962.

16. Lancaster, Peter and Tismenetsky, Miron, The Theory of Matrices, pp. 435-438, Academic Press, Inc., Orlando, Florida, 1985.

17. Lancaster, Peter and Tismenetsky, Miron, The Theory of Matrices, pp. 432-435, Academic Press, Inc., Orlando, Florida, 1985.

18. The RMS Method was developed in consultation with John A. Sidles, Ph.D., Assistant Professor, Department of Orthopaedics, University Hospital, Seattle, Washington, 1985.

19. Concept for the calibration procedure of the POLHEMUS stylus was developed by John A. Sidles, Ph.D., Assistant Professor, Department of Orthopaedics, University Hospital, Seattle, Washington 1985.

20. Koren, Yoram, Robotics for Engineers, pp. 18-19, McGraw-Hill Book Company, New York, 1985.

21. Doebelin, Ernest O., Measurement Systems: Application and Design, 3rd Edition, p. 50, McGraw-Hill Book Company, New York, 1983.

22. Liegeois, Alain, Performance and Computer-Aided Design, Volume 7 in the Series, Robot Technology, translated by Meg Tombs, p. 34, Kogan Page Ltd, London, 1985.

23. Testing of the stylus alignment accuracy for Phase 1 of the robotic process was conducted by Dr. John A. Sidles. The results of the analysis are pending publication.

APPENDIX A

CALIBRATION PROCEDURES

A.1 General Comments

The calibration of tools used in the Orientation Phase of the robotic process required the development of a procedure which would define the position of a tool tip and the orientation of the tools' z - axis.   Although   the   AID   600   possessed   self-calibrating capabilities, the necessary hardware for tool calibration was not present.

It was determined that several software instructions contained in the RAIL Software Reference Manual, Document Number MN-RB-07, would aid in the tool calibration process. These were:

(1) HERE, a built-in variable, which gives the current location of the tool mounted at the end of the robot wrist.

(2) Appendix H, which describes a method for modifying tool definitions.

(3) CALIB, a built-in function which moves the robot's joints to a standard position which is then defined in the robot work space. This position is constant.

The procedure outlined in Appendix H of the RAIL Software Reference Manual required the use of a known point in the robot's

work volume. The establishment of this known point would require the development of programming steps and fabrication of equipment which would:

> (1) determine the physical location of the wrist reference frame.

> (2) create the extension, from the wrist reference frame, of a more accessible location which was known accurately by the robot.

> (3) establish a physical reference location in the work volume of the robot and subsequently define this location using the known, extended wrist location.

> (4) allow tool definitions to be obtained for a stylus, cutter, and dial indicator.

A.2 Determination of the Wrist Reference Frame Location

A.2.1 General Comments

The first objective in the calibration procedure was to determine physically where the wrist reference frame was located. This task proved to be difficult as no physical point on the robot wrist existed which marked the exact location of the origin of the wrist reference frame. The only physical surface available for tactile analysis was the surface gained when the wrist flange disk was mounted to the wrist flange of the robot. It was this surface

which was used to determine the x - y plane of the wrist reference frame.

The location of the origin of the wrist reference frame was a point supposedly in the plane defined by the wrist flange surface of the robot. The intersection of this plane with the axis of revolution of the wrist roll axis was the specified origin location. However, initial testing upon completion of tool calibration indicated that this might have been slightly in error. Figure A-1 shows the wrist of the AID 600 robot. The specified location of the wrist reference frame is indicated. The exact location of the origin will be on the physical roll axis of the wrist. This must be true, since if all other joints are held in place and only the roll joint rotated, the actual roll axis will be readily observed and can be just as readily confirmed by using a dial indicator to check for any rotational deviations. This confirmation was actually done after the wrist extension was mounted on the wrist. Thus, the determination of the x - y plane of the wrist reference frame became the only unknown which was tested for in this part of the calibration procedure.

A.2.2 Apparatus

The following equipment was used in this portion of the calibration procedure.

(1) AID 600 robot with AI32 controller manufactured by Automatix, Inc. (Plate XI)

WRIST REFERENCE FRAME

2.500

X AXIS

Y AXIS

Z AXIS

WRIST FLANGE SURFACE

ALL TOOLS USED ON THE
AID 600 ROBOT ARE DEFINED
FROM THE ORIGIN OF THE
WRIST REFERENCE FRAME
WITH RESPECT TO THE RCS
WHILE THE ROBOT IS IN THE
'HOME' POSITION.
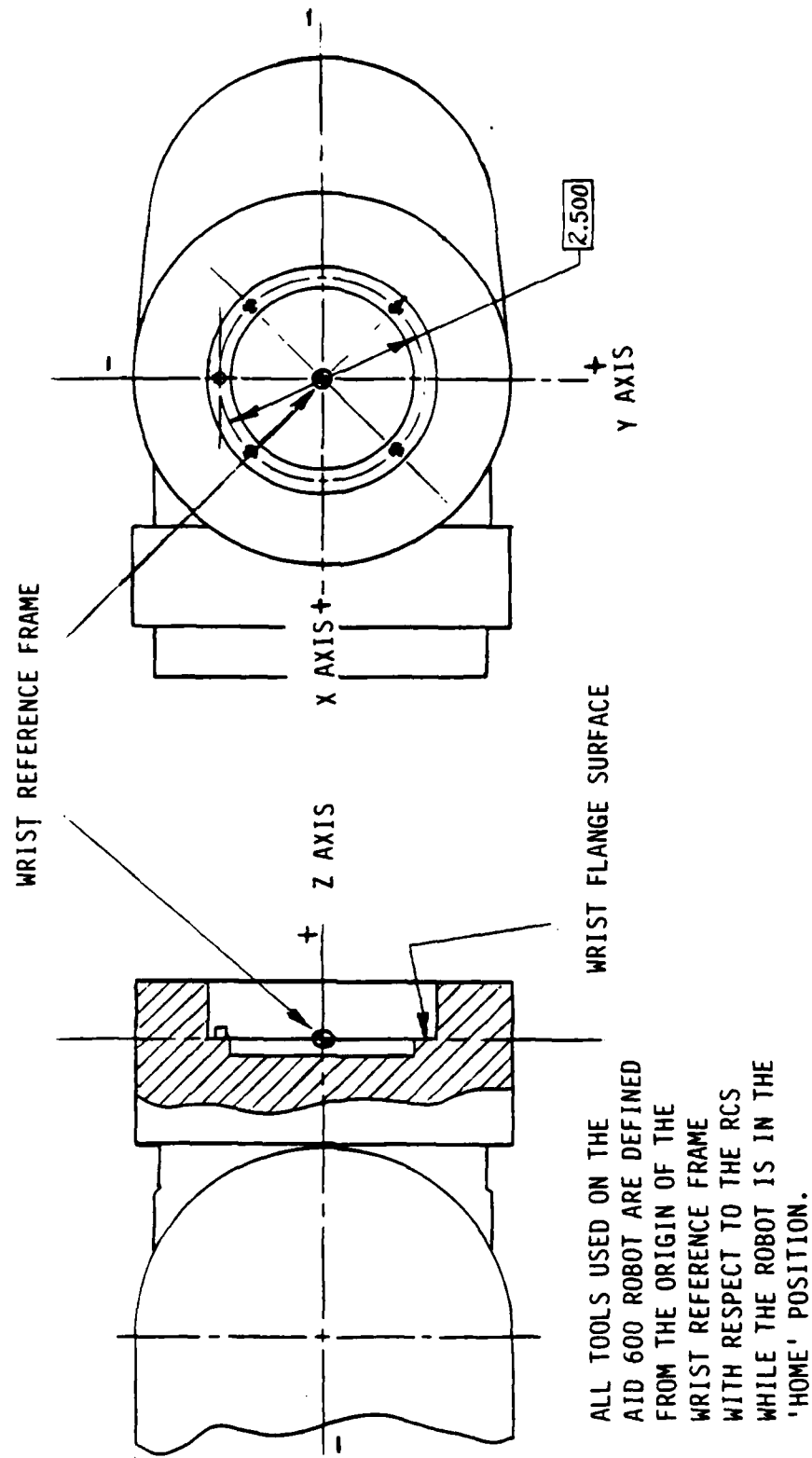
Figure A.1 Diagram of Robot Wrist Indicating Wrist Reference Frame

(2) Wrist Flange Disk. (Plate XII)

(3) Dial indicator with 0.01 millimeter precision.

(4) No special software was required to conduct this test.

A.2.3 Procedure

The following test procedure was employed to determine the distance from the x - y plane of the wrist reference frame to the outer surface of the wrist flange disk.

(1) Start up the AID 600 robot as per the instructions in the Operator's Manual.

(2) Mount the wrist flange disk to the wrist flange of the robot.

(3) Mount a dial indicator, probe up, on a standard dial indicator stand. Place the dial indicator in the center of the work space of the robot so that the tip of the probe, when zeroed on the dial indicator, is approximately 17 inches above the table surface of the robot. This height allows the surface of the wrist flange disk to be oriented facing both down, and later up, at the same position. Why this is important will be explained later.

(4) Define the TOOL using the default tool definition:

$$TOOL = [0., 0., 0., 90., 90., -90.]$$

Plate XI Automatix AID 600 robot with AI32 controller and
          fixtures set up for the conduct of a demonstration
          of robot-assisted knee arthroplasty
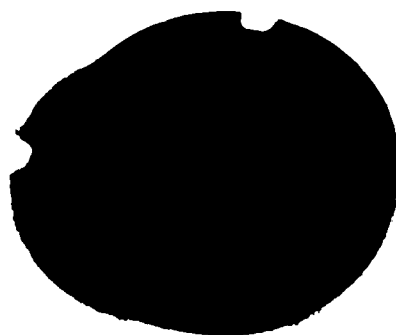
Plate XII

Note that this is the initial definition assigned to the wrist reference frame after completion of start-up procedures.

(5) Orient the wrist flange so that its outer surface is facing downward. This can be done using the ICM pendant to rotate the wrist downward. To insure the wrist flange surface is parallel to the x - y plane of the RCS, type the following command: on the AI32 keyboard:

```
A = HERE  <CR>
LOC_TO_COORD (A, AA) <CR>
AA [1,5] = 180. <CR>
COORD_TO_LOC (AA, A) <CR>
MOVE A <CR>
NOTE:  <CR> means carriage return key
```

This will jar the wrist of the robot into the desired orientation.

(6) Using only the x, y, z translation buttons of the ICM and insuring the ICM is moving using joint motion, position the surface of the flange over the probe of the dial indicator so that it is roughly centered and so that the dial indicator registers 0.

(7) Type HERE <CR> on the AI32 keyboard and record the z

component of the resulting point that is displayed.

(8) Move the wrist flange away from the dial indicator using the ICM pendant.

(9) Reposition the probe of the dial indicator so that it is pointing down and so that its tip is zeroed out at the exact height previously used. For this experiment, a height gage with precision surfaces that could be maintained at constant height was utilized. Various attachments to the height gage allowed the dial indicator to be set and zeroed in both directions at the exact same height.

(10) Place the dial indicator back into the work volume of the robot in the same general area of the table.

(11) Re-orient the surface of the wrist flange so that it now faces up. Using a similar procedure described in step (5) above, jar the wrist flange surface into its proper orientation. This is done by typing the following commands on the AI32 keyboard:

```
A = HERE <CR>
LOC_TO_COORD (A, AA) <CR>
AA [1,5] = 0. <CR>
COORD_TO_LOC (AA, A) <CR>
MOVE A <CR>
```

(12) Using x, y, z translation buttons of the ICM pendant and joint motion, position the surface of the flange under the probe of the dial indicator so that it is roughly centered and raise the wrist flange surface so that the dial indicator registers 0.

(13) Type HERE $\langle CR \rangle$ on the AI32 keyboard and record the z component of the resulting point that is displayed.

(14) The distance between the x - y plane of the wrist and the surface of the wrist flange disk is equal to one half the difference between the two z component readings. For this calibration a distance of 16.73 millimeters was obtained.

A.3 Establishment of a Wrist Extension Location

A.3.1 General Comments

Having established the distance from the x - y plane of the wrist reference frame to the surface of the wrist flange disk, the next step was to fabricate an extension to the wrist whose purpose was to aid in establishing a known reference location in the RCS. To do this, a simple design was selected. This design would seek to establish a new location, a fixed, known distance from the wrist reference frame. The origin of this new location would lay on, or close to, the z - axis of the wrist reference frame. The x, y, z axes of this new location would be parallel to the x, y, z axes of

the wrist reference frame. In essence, the new location was translated along the z axis of the wrist reference frame to a more accessible and identifiable position. This new position would allow the establishment of the desired reference location.

A.3.2 Apparatus

The fabrication of the wrist extension took place in the machine shop of the Mechanical Engineering Department using standard shop equipment which included mills, lathes, drills and various other instruments. The resultant wrist extension is shown in Plate XIII. Additional equipment required included:

(1) AID 600 robot with AI32 controller.

(2) Dial indicator with 0.005 millimeter precision.

(3) Wrist Extension. (Plate XIII)

A.3.3 Procedure

Knowledge of the exact location of the new wrist extension reference frame was achieved by testing the wrist extension at various stages in its fabrication and mounting.

The symmetry of the wrist extension shaft was assured by the lathe turning process used to fabricate it. An aluminum collar was placed on the base of the wrist extension to aid in its placement and centering on the wrist flange disk. The plastic disk which was used to establish the x - y plane of the new location was mounted to the
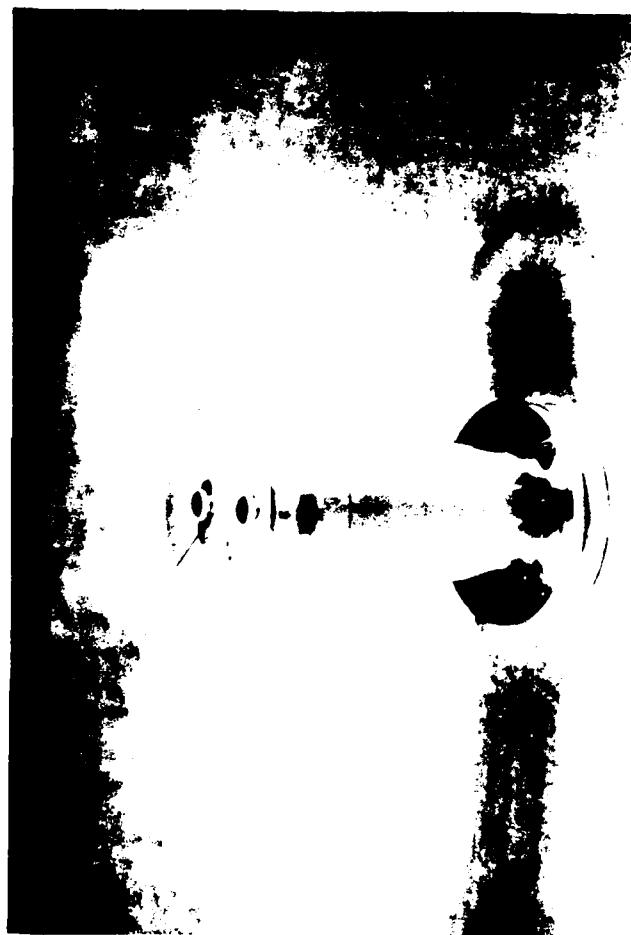
Plate XIII Wrist Extension

wrist extension using pins and screws to prevent any movement or change in its position. The plexiglass surface was then milled to insure it was parallel to the surface of the wrist flange disk. Tolerances used were less than .02 millimeters.

The crosshairs marked on the surface of the plexiglass disk were checked for correct positioning using height gages to determine the axial center of the wrist extension shaft. These checks produced a wrist extension whose mean effective length was 3.9815" or 101.13 millimeters when measured with a micrometer. By adding this distance and the preceeding distance between the wrist reference frame and the wrist flange disk surface (16.73 mm), the following initial tool definition was established for the wrist extension (CALEXT):

$$CALEXT = [0., 117.86, 0., 90., 90., -90.]$$

As seen above, the y component of CALEXT was determined by measurements made with a micrometer. The alignment of the z axis of the wrist reference frame with the long axis of the wrist extension was assured by the construction of the wrist extension. However, the x and z values of the wrist extension reference location reference location had to be verified. The following steps were then taken.

(1) Mount the wrist extension to the wrist flange disk.

(2) Move the robot to the HOME position by typing on the AI32 keyboard:

MOVE HOME <CR>

(3) Mount a dial indicator on its stand and place it in contact, perpendicularly, with the shaft of the wrist extension near the plexiglass surface. The probe should be parallel to the table surface of the robot and oriented so that it lays on an imaginary axis bisecting the shaft.

(4) Zero the dial indicator.

(5) Using only the Ry button of the ICM pendant and joint motion rotate the wrist extension clockwise and counterclockwise.

(6) Each time the crosshairs on the plexiglass align themselves with the axis of the probe, stop motion and record the readings on the dial indicator. Do this several times and compute an average readings for each spoke of the crosshair pattern. Then return the robot to its HOME position.

(7) Note that when the robot is in the HOME position, the crosshairs are aligned with the x and z axes of the RCS. By taking the two average values for the crosshairs aligned with the x axis of the RCS and subtracting the value associated with the right cross hair from the value associated with the left crosshair and dividing by 2 an x - component correction to CALEX

is obtained. Similarly, by taking the average values of the crosshairs aligned with the z axis of the RCS and subtracting the value associated with the lower crosshair from the value associated with the upper crosshair and dividing by two a z - component correction to CALEXT is obtained.

The final, corrected tool definition for the wrist extension was, within an accuracy of .02 mm:

$$CALEXT = [.04, 117.86, .06, 90., 90., -90.]$$

A.4 Establishment of a Reference Location

A.4.1 General Comments

The establishment of a known reference location (REFLOC) in the RCS was the next step in the calibration procedure. By establishing this known reference location, the operator of the robot could then make use of procedures outlined in Appendix H of the RAIL Software Reference Manual.

A.4.2 Apparatus

The following equipment was used in this portion of the calibration procedure.

(1) AID 600 robot with AI32 controller.

(2) Wrist Flange Disk.

(3) Wrist Extension.

(4) Reference Location Platform. (Plate XIV)

A.4.3 Procedure

The following procedure was utilized to establish the REFLOC of the RCS.   It is assumed that this is a continuation of the calibration process and that the normal startup procedures for the AID 600 have already been executed.

(1) Mount the reference location platform in the work volume of the robot in such a manner that its location will not obstruct future usage of the robot.   The design of the platform is a simple one which establishes a planar surface with crosshairs indicating an origin and two perpendicular axes.   The surface height of the platform is approximately 10" above the table surface of the robot and parallel to that same surface.

(2) Define the TOOL definition to be that of the wrist extension, CALEXT. This can be done by typing on the AI32 keyboard:

TOOL = CALEXT <CR>

(3) Using the ICM and joint motion, move the wrist extension to the surface of the REFLOC platform and bring the plexiglass surface of the wrist extension
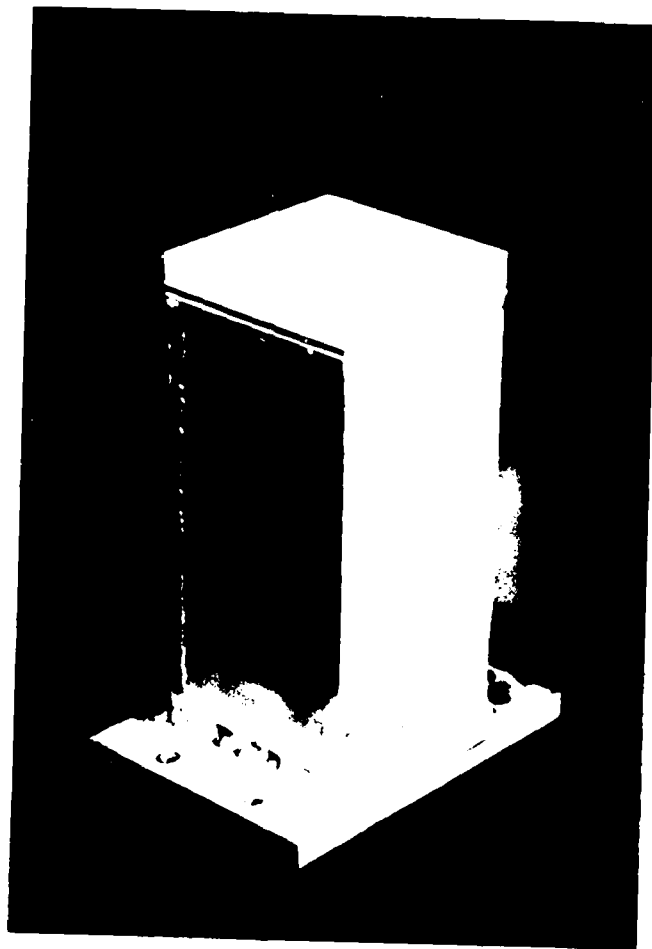
into flush contact with the surface of the platform. Insure that their crosshairs are aligned and that the surfaces are just touching. A useful method to use in checking for contact is to slide a small piece of paper back and forth between the two surfaces while bringing them into contact. At the point where the paper ceases to slide, stop the wrist extension. Then, remove the paper. With a speed of 1 registered on the ICM pendant, press then z- button of the ICM pendant once very briefly. The surfaces are now in contact.

(4) Type HERE   CR   on the AI32 keyboard to see the definition of the REFLOC location.   Record this location by typing:

$$REFLOC = HERE \langle CR \rangle$$

The REFLOC location defined in this study was:

REFLOC = [1272.88, 276.28, -83.18, 89.996, -179.969, -90.004]

A.5 Establish Tool Definitions for a Stylus, Cutter and Dial Indicator

A.5.1 General Comments

The final step in the calibration procedure was to establish tool definitions for each of the tools to be used in the Orientation Phase and the Cut Generation Phase of the robotic process.   The principles involved were identical for all three tools and involved

the use of calibration disks to aid in centering the tips of each tool. The procedure outlined in Appendix H of the RAIL Software Reference Manual was used.

It must be stated that the established REFLOC provided both position and orientation constraints which served to define each of the tools used in later procedures. The position was established by the crosshairs and the surface of the platform; the orientation established by alignment of the crosshairs alone.

A.5.2 Apparatus

The following equipment was used in this portion of the calibration procedure.

(1) AID 600 robot with AI32 controller.

(2) Wrist Flange Disk.

(3) Mechanical Fuze. (Plate XV)

(4) Stylus, cutter mounted on a fixture. (Plate XVI)

(5) Calibration disks for stylus, cutter and dial indicator. (Plate XVII)

(6) Stylus, dial indicator mounted on a fixture. (Plate XVIII)
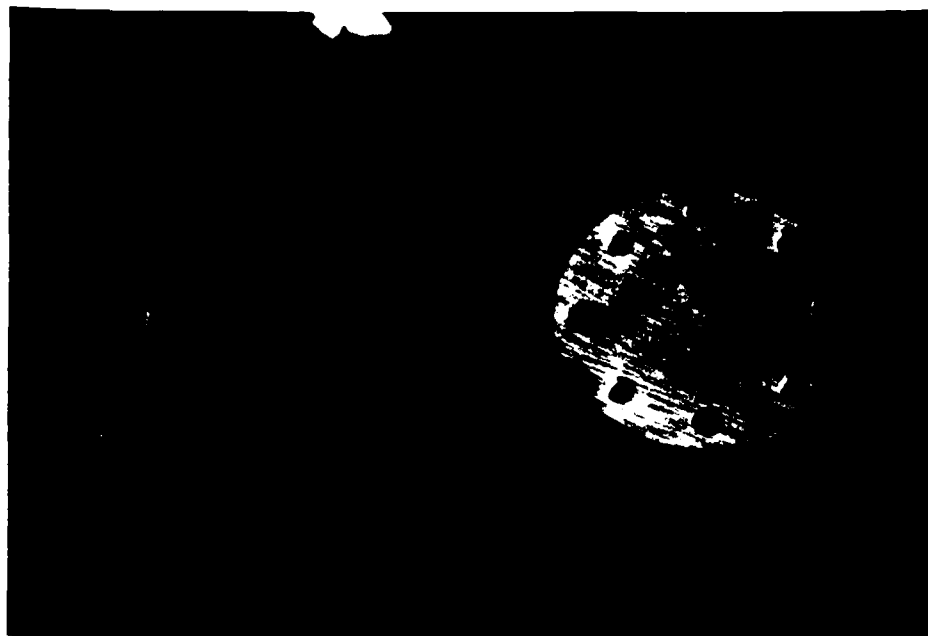
Plate XV Mechanical fuze used to interface between the wrist
flange disk and tool fixtures. Top and bottom views
shown
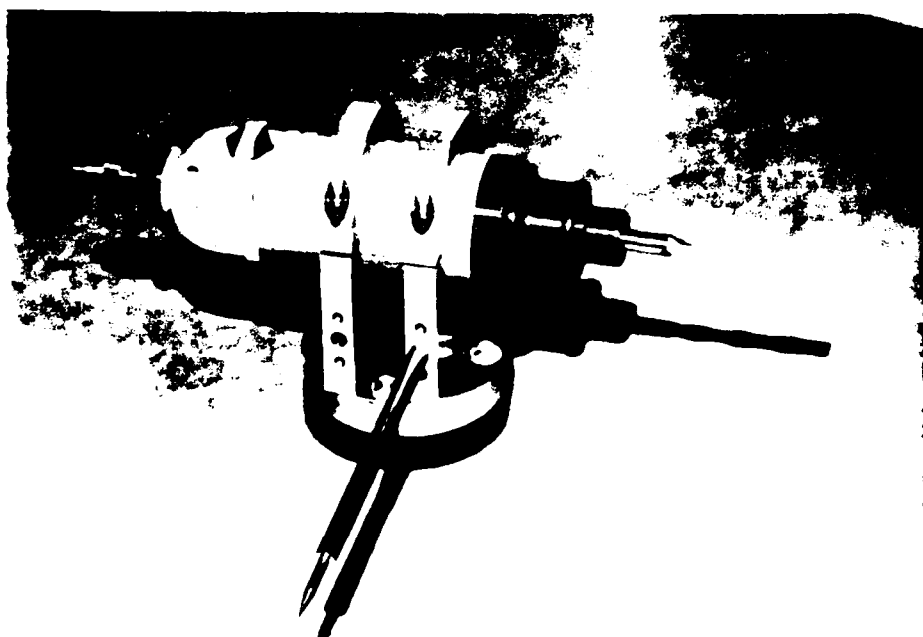
Plate XVI Stylus and pneumatic tool with end mill mounted to a
tool assembly and mechanical fuze; used in actual
demonstration of robotic process
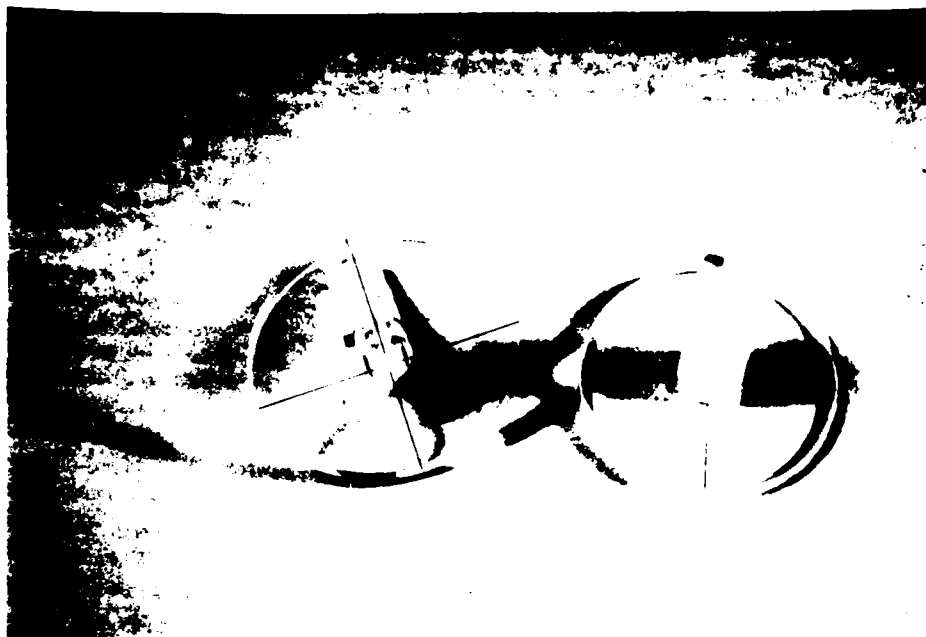
Plate XVII Calibration Disks
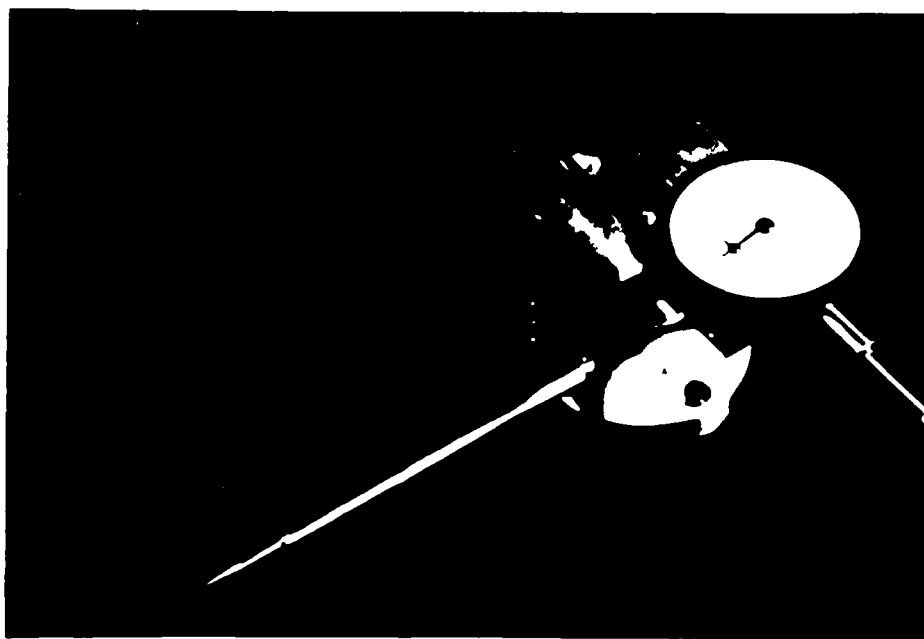
Plate XVIII   Stylus and dial indicator mounted to a tool
assembly; used in accuracy study

A.5.3 <u>Procedure</u>

The following steps were utilized to establish the definition of tools mounted to the robot wrist flange. Prior to these steps, it is assumed that the wrist extension has been removed and that a REFLOC location has been established.

(1) Mount the mechanical fuze to the wrist flange of the robot.

(2) Mount the tool fixture with the stylus and cutter attached to the mechanical fuze so that the stylus and cutter both point to the left when the robot arm is in the HOME position. To move the robot to the HOME position, simply type:

MOVE HOME ⟨CR⟩

(3) Insure that the current TOOL definition is the same as that for CALEXT.

(4) Mount the calibration disks for the stylus and cutter to their appropriate tools. Insure that the tip of each tool is flush with the surface of its calibration disk. For the stylus, insure that the tip of the stylus is centered with the crosshairs of its calibration disk.

(5) Using the ICM pendant and joint motion, move the

calibration disk of the stylus so that it is flush and centered on the REFLOC platform and so that their crosshairs are aligned. Type on the AI32 controller:

STYLUS = HERE ⟨CR⟩

(6) Repeat step (5) for the cutter calibration disk. Note in both cases that since each tool is symmetrical about its z - axis, the calibration disks may be rotated by hand to aid in the alignment process. It is not necessary to use the Ry button. Type on the AI32 controller:

CUTTER = HERE ⟨CR⟩

It must be noted here that these are not the final tool definitions for each of these tools; only intermediate data.

(7) Remove the calibration disks.

(8) Establish the stylus tool definition by typing on the AI32 controller:

TOOL = TOOL: INVERSE (STYLUS): REFLOC ⟨CR⟩

STYLUS = TOOL ⟨CR⟩

(9) Establish the cutter tool definition by typing on the AI32 controller:

TOOL = CALEXT ⟨CR⟩

TOOL = TOOL: INVERSE (CUTTER): REFLOC ⟨CR⟩

CUTTER = TOOL ⟨CR⟩

(10) Using RAIL software commands, save these definitions for STYLUS and CUTTER for later use.

The dial indicator and stylus were used in another set of experiments designed to test the accuracy of the robotic process. The procedure used to calibrate the stylus and dial indicator pair was identical to that used above for the stylus and cutter pair.

The only changes were the obvious substitution of the DIALIN variable for that of CUTTER. The tip of the dial indicator also extended pass the surface of its calibration disk to allow for +/- readings to be taken using the dial indicator. Once flush with the REFLOC platform, the dial indicator was also zeroed by adjusting the outer bezel ring of the dial indicator.

The tool definitions established in both the demonstration of the robotic process and in its testing for accuracy are listed below. These are representative definitions. The point to emphasize here is that each time the tools were removed from the wrist flange of the robot, recalibration had to take place before any processes were executed, however, only the steps in this section had to be repeated. If, on the other hand, the REFLOC changed, then the procedures in both A.4 and A.5 had to be repeated.

STYLUS = [125.63, 60.29, 93.98, 179.664, -49.1, .22]

CUTTER = [85.00, 89.51, -94.12, 179.912, -138.249, -.066]

DIALIN = [78.24, 127.16, -90.20, 2.648, 139.375, -177.989]

With tool definitions for each of these tools established, the calibration procedure was complete.

APPENDIX B

EXPERIMENTAL PROCEDURES

B.1 General Comments

The accuracy of the robotic process was determined using the experiments in this appendix. The final determination of accuracy hinged on establishing values for the repeatability of the robot and determining the translation and rotation errors introduced by human factors in both the Planning and Orientation Phases. To accomplish this, additional fixtures were designed and fabricated which served to establish a standard against which the robot's performance could be measured. As was addressed in Chapter 8, the most significant errors introduced into the robotic process were those associated with human subjectivity in regard to the alignment of probes, or stylus', with fiducial points. These errors were introduced in both the Planning and Orientation Phases. The impact of these errors was to induce inaccuracies in the perceived spatial arrangement of the physical fiducial points used to compute the transformation between the PCS and the RCS. These inaccuracies resulted in the addition of random error to the two sets of measurements taken from the one set of physical fiducial points of the femur.

In Chapter 6, a relationship between the spatial, or random error, and the shifts in the perceived position and orientation of the centroid of the RCS fiducial points with respect to a constant,

control centroid was proposed based on simulation results. The family of MTE and MRE curves shown in Figures 6.2 through 6.9 predicted these resultant shifts. In the final experiment, an attempt was made to establish the actual value of these alignment errors for a specific spatial error model.

The experiments described in this appendix:

(1) Established the repeatability characteristics of the robot, and

(2) Determined the actual value of the alignment errors introduced during the robotic process and the actual values for MTE and MRE for a Measurement Test Cube similar in size to the knee portion of the femur.

B.2 Determine Robot Repeatability

B.2.1 General Comments

As was explained in Chapter 8, when the bias of an instrument can be reduced or rendered insignificant through the calibration process, the accuracy of that instrument may be characterized by its precision. Precision is the randomness, or repeatability of the instrument and cannot be eliminated by calibration. Therefore, the accuracy of the robot used in the robotic process may be approximated by its repeatability. The two terms are not, however, the same. A clear understanding of the meaning of repeatability is required. If

a robot is instructed to move to a specific location in its work volume a given number of times, it will be found that the resultant motions of the robot lead to different displacements. Repeatability is, then, related to the positional deviation from the average of these displacements [19]. If it is assumed that the deviation of the displacements is a perfect Gaussian distribution, then 99.7% of the displacements will fall within +/- three times the standard deviation of the displacement error [20]. The convention commonly used to define repeatability is to equate it to three times the sample standard deviation of the displacement error mentioned above [21]. This convention was adopted in this study.

B.2.2 Apparatus

The following equipment was used in this experiment.

(1) AID 600 robot with AI32 controller

(2) Wrist Flange Disk

(3) Wrist Extension

(4) Reference Location Platform

(5) Stylus, dial indicator mounted on fixture

(6) Measurement Test Cube (Plate XIX)

(7) Robot Utility Mounting Fixture (Plate XX)

(8) Mechanized Fuze
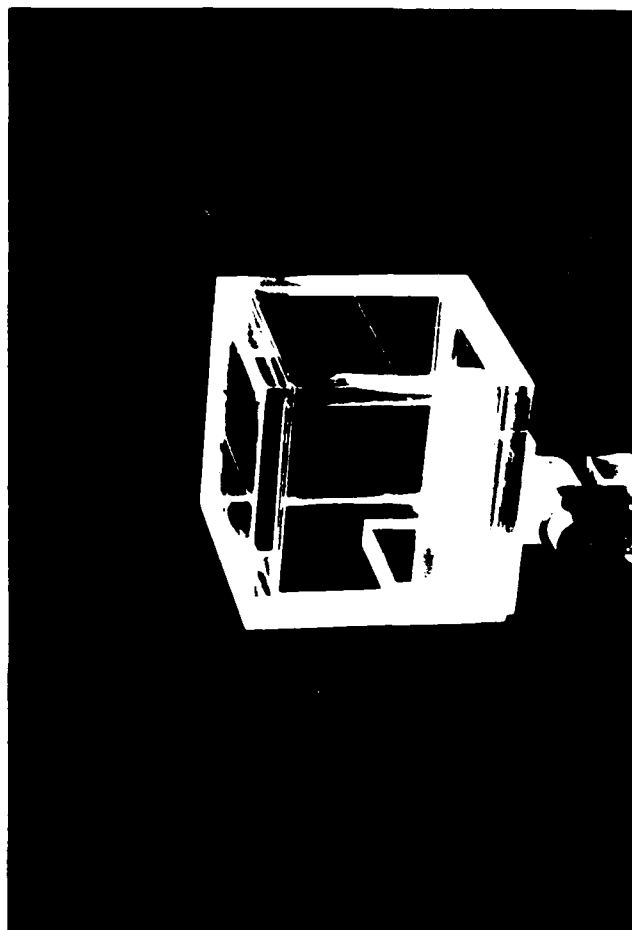
Plate XIX Measurement Test Cube used in accuracy study

Plate XX   Utility Mounting Fixture used in performing
           demonstration and accuracy studies

(9) Calibration disks for stylus and dial indicator

B.2.3 <u>Procedure</u>

The following procedure was used to establish a value for the repeatability of the AID 600 robot.

(1) Using the procedures established in Sections 3 and 4 of Appendix A, mount the wrist extension to the wrist flange disk of the robot and verify its tool definition. Then, determine the location of the REFLOC platform.

(2) Mount the Measurement Test Cube in the Robot Utility *Mounting Fixture attached to the table of the AID 600.*

(3) Insure that the surface of the Measurement Test Cube which contains the points F4 and T6 is facing the rear of the robot and that the surface of the cube containing the points F1, F2, F3, T4, T5 is facing upward.

(4) Remove the wrist extension and mount the mechanical fuze and the stylus/dial indicator fixture to the wrist flange disk.

(5) Calibrate the stylus and dial indicator in accordance with procedures contained in Section 5 of Appendix A.

(6) Define TOOL to be equal to DIALIN.

(7) Using the ICM pendant and joint motion, position the dial indicator so that its probe is pointing downward and resting on the top surface of the cube. The dial indicator should read zero.

(8) Record the location of the dial indicator by typing on the AI32 keyboard:

$$A = HERE \langle CR \rangle$$

(9) Using the ICM pendant, move the dial indicator to a random location in the work volume of the robot.

(10) Command the robot to return to point A by typing on the AI32 keyboard:

$$MOVE\ A \langle CR \rangle$$

(11) Once the robot has positioned the dial indicator at point A, record the deviation, from 0, found on the dial indicator.

(12) Repeat steps (9) through (11) twenty times. Insure that random locations throughout the work volume of the robot are used to prevent incorrect computation of the repeatability value. Table B.1 contains a list of the dial indicator readings found in this experiment.

(13) Compute the sample standard deviation value using the equation:

Table B.1 Results of Repeatability Experiment

Reading #	Reading (mm)
1	+ .002
2	- .01
3	- .008
4	- .005
5	- .005
6	- .017
7	- .012
8	.0
9	- .01
10	- .013
11	- .011
12	+ .005
13	.0
14	+ .019
15	- .013
16	- .005
17	- .01
18	+ .005
19	.0
20	+ .005

$$s = \sqrt{\dfrac{\displaystyle\sum_{i=1}^{N} x_i^2 - \dfrac{(\displaystyle\sum_{i=1}^{N} x_i)^2}{N}}{N-1}}$$

(14) The computed value of the sample standard deviation of x was:

$$s = 8.66 \times 10^{-3} \text{ mm}$$

(15) The repeatability was therefore found to be:

$$\text{Repeatability} = 3 \times s = 0.026 = 0.03 \text{ mm}$$

B.3 Determination of Alignment Error Introduced due to Human Factors in the Orientation Phase

B.3.1 General Comments

In order to establish a value for the alignment error introduced into the Orientation Phase of the robotic process by human factors such as handling of probes and subjective judgement in the alignment of those probes with the fiducial points of the femur a test was designed which duplicated the touching of fiducial points on the femur. This experiment required the fabrication of a Measurement Test Cube, whose dimensions were known to within +/- 0.02 mm. The cube was constructed of plexiglass material in such a manner that the perpendicularly of adjacent sides and parallelity of opposing surfaces was assured. Points, marked with etched crosses, were then selected on the surface of the cube in specific locations. These

points included six test points, which could be used to align the cube, and eight fiducial points which would be used to test the effects of human factors on the transformation process. Table B.2 lists the coordinates of these points with reference to the measurement test cube coordinate system, or CCS, with the reference frame designated by the points T1, T2 and T3. T1 marked the origin of the CCS. T2 marked a point along the positive x axis of the CCS. T3 marked a point in the first quadrant of the CCS.

B.3.2 Apparatus

The following equipment was used in this experiment.

    (1) AID 600 robot with AI32 controller

    (2) Wrist Flange Disk

    (3) Mechanical Fuze

    (4) Stylus, dial indicator mounted on fixture

    (5) Measurement Test Cube

    (6) Robot Utility Mounting Fixture

B.3.3 Procedure

Prior to executing these steps in the experiment it is assumed that the REFLOC location had been established and that the stylus and dial indicator have been calibrated.

    (1) Mount the Measurement Test Cube on the Robot Utility

Table B.2 Location of CCS Fiducial and Test Points

Point #	Coordinates
F1	(50., -30., 70.)
F2	(50., 30., 70.)
F3	(50., 0., 50.)
F4	(0., 50., 50.)
F5	(20., -50., 30.)
F6	(-20., -50., 70.)
F7	(20., -.30., 0.)
F8	(-20., 30., 0.)
T1	(0., 0., 0.)
T2	(40., 0., 0.)
T3	(10., 40., 0.)
T4	(50., 30., 80.)
T5	(50., -30., 20.)
T6	(20., 50., 50.)

Mounting Fixture so that its surfaces are horizontal and vertical in the robot work volume. The top of the cube should be the surface containing points F1, F2, F3, T4 and T5. The surface facing the front of the robot should contain points F5 and F6.

(2) Build a Cube Reference Frame in the RCS by using the LEARNFRAME command contained in the RAIL language. The three points required to be entered into this command are, in order, T1, T2 and T3.

(3) Transform the fiducial point coordinates given in Table B-2 from the CCS into the RCS by pre-multiplying them by the transformation created in step (2) using LEARNFRAME. The resultant points represent the known locations of each fiducial point in the RCS.

(4) Define the tool to be the stylus by typing on the AI32 keyboard:

$$TOOL = STYLUS \langle CR \rangle$$

(5) Using the ICM pendant and joint motion, contact each fiducial point, in order, from F1 to F8 with the stylus tip. Record the location for each fiducial point obtained using this method.

(6) Calculate the deviation between the known location of

each fiducial point and the corresponding location found using the stylus.

(7) Compute the average of the deviations.

(8) Compute the transformation between the two sets of points and calculate the translational difference and the rotational difference between the centroids of both sets of points.

A total of three runs were made using this sequence of steps. The results are contained in Table B.3. As can be seen from the table, an average value of 0.41 millimeters was obtained for the alignment error induced by human handling of probes and subjectivity.

Significantly, the values indicated for the differences between corresponding sets of fiducial points agree with the results of analysis conducted earlier in Chapter 6. For random error amplitudes of 0.41 mm, this experiment indicated an average translational error and an average rotational error of .31 mm and 0.55 degrees respectively which fell within the predicted MTE and MRE values.

B.4 Determination of Error Introduced due to Human Factors
in the Planning Phase

Actual experimentation used to determine the amount of error introduced by human factors in the Planning Phase of the robotic process was conducted by Dr. John A. Sidles.

Table B.3 Results of the Investigation of Stylus Alignment Accuracy
in the Orientation Phase

(1)	Fiducial PT #	Deviation Run 1 (mm)	Deviation Run 2 (mm)	Deviation Run 3 (mm)
	1	.326	.391	.390
	2	.563	.421	.399
	3	.504	.483	.455
	4	.689	.483	.455
	5	.835	.393	.185
	6	.364	.453	.448
	7	.262	.140	.181
	8	.202	.418	.553
(2)	Mean Value of Deviations	.399 mm	.424 mm	.405 mm
(3)	Translational Error	.33 mm	.31 mm	.29 mm
(4)	Rotational Error	.584 degrees	.527 degrees	.537 degrees
(5)	Average Alignment Error	.41 mm		
(6)	Average Translational Error	.31 mm		
(7)	Average Rotational Error	.55 degrees		

171

Using equipment and software developed in research which extensively investigated the Planning Phase of the robotic process, Dr. Sidles established the calibration accuracy of the stylus used with the POLHEMUS to be within .2 millimeters. Dr. Sidles also produced three sets of locations corresponding to the known fiducial points locations of the measurement test cube. The results of the above experimentation are contained in Table B.4 [23].

Table B.4   Results of the Investigation of Stylus Alignment Accuracy
in the Planning Phase

(1)	Fiducial PT #	Deviation Run 1 (mm)	Deviation Run 2 (mm)	Deviation Run 3 (mm)
	1	.308	.505	.332
	2	.401	.438	.562
	3	.475	.115	.074
	4	.409	.306	.468
	5	.586	.168	.389
	6	.380	.213	.344
	7	.379	.342	.231
	8	.266	.312	.245
(2)	Mean Value of Deviations	.400 mm	.300 mm	.331 mm
(3)	Translational Error	.21 mm	.31 mm	.61 mm
(4)	Rotational Error	.324 degrees	.355 degrees	.180 degrees
(5)	Average Alignment Error	.34 mm		
(6)	Average Trans- lational Error	.37 mm		
(7)	Average Rota- tional Error	.32 degrees		

vector 2 to obtain basis vector 3.

- care must be taken to insure corresponding points are used in the same order when creating the basis for each set of points.

4. By taking the sum of the outer products of the corresponding basis vectors of each set, the rotation matrix was obtained.

5. Mathematically, this can be shown as follows.

- let column vectors $\vec{a_1}$, $\vec{a_2}$ and $\vec{a_3}$ be a basis in **A**

- let column vectors $\vec{b_1}$, $\vec{b_2}$ and $\vec{b_3}$ be a basis in **B**

- *then,*

$R = [a_1 \cdot (b_1)^T + a_2 \cdot (b_2)^T + a_3 \cdot (b_3)^T]$

- to verify this, note that

$$\vec{a_1} = R\ \vec{b_1}$$
$$\vec{a_2} = R\ \vec{b_2}$$
$$\vec{a_3} = R\ \vec{b_3}$$

- This is true because the **A** basis vectors as well as the **B** bases vectors are orthonormal. The inner product of any orthonormal basis with itself is 1. The inner product of any orthonormal basis vector with any other basis vector is 0.

6.   Once a first guess is obtained for **R**, the next phase is to iterate to a rotation vector which, when converted to a corrective rotation matrix and post-multiplied by the old **R**, will produce a new **R** matrix which is closer to the final, desired rotation matrix.

7.   To show how this process works, the relationship between **A**, **B** and $\vec{\theta}$, must be derived. As was discussed previously, the goal of the RMS Method was to produce a transformation matrix which minimizes the RMS error.

8.   In reaching this derivation, the small angle approximation for the **θ** to **R** relationship is used. This means

$$\sum_{i=1}^{N} R\,\vec{b_i} = \sum_{i=1}^{N} (\vec{b_i} + \vec{\theta} \times \vec{b_i})$$

9.   Substituting into the equation for the RMS error:

$$\text{RMS Error} = \sum_{i=1}^{N} [\vec{a_i} - (\vec{b_i} + \vec{\theta} \times \vec{b_i})]^2$$

10.   To find $\vec{\theta}$ which minimized this error, differentiate the above equation and set equal to zero. This yields:

$$0 = \sum_{i=1}^{N} [\vec{b_i} \times (\vec{a_i} - \vec{b_i} - \vec{\theta} \times \vec{b_i})]$$

11.   Expanding terms yields

$$0 = \sum_{i=1}^{N} [\vec{b_i} \times \vec{a_i} - \vec{b_i} \times \vec{b_i} - \vec{b_i} \times \vec{\theta} \times \vec{b_i}]$$
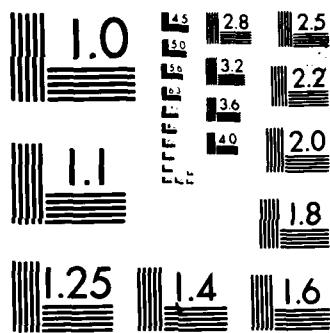
MICROCOPY RESOLUTION TEST CHART
NATIONAL BUREAU OF STANDARDS-1963-A

12. The second term is equivalent to 0.

13. By using the vector property: $\vec{a} \times \vec{b} = -\vec{b} \times \vec{a}$ the equation can be written in the form:

$$\sum_{i=1}^{N} (\vec{b_i} \times \vec{b_i} \times \vec{\theta}) = \sum_{i=1}^{N} (\vec{a_i} \times \vec{b_i})$$

14. To solve for $\vec{\theta}$, it must be isolated from the rest of the equation. This is accomplished by using the vector property:

$$\vec{a} \times \vec{b} \times \vec{c} = \vec{b}\,(\vec{a} \cdot \vec{c}) - \vec{c}\,(\vec{a} \cdot \vec{b})$$

15. Hence, the equation may be written as:

$$\sum_{i=1}^{N} [\vec{b_i}\,(\vec{b_i} \cdot \vec{\theta}) - \vec{\theta}\,(\vec{b_i} \cdot \vec{b_i})] = \sum_{i=1}^{N} (\vec{a_i} \times \vec{b_i})$$

16. To separate $\vec{\theta}$ out of the first term and isolate $\vec{\theta}$, note that the first term can be written as:

$$\sum_{i=1}^{N} \vec{b_i}\ [\ \sum_{j=1}^{3} (b_i)_j\, \theta_j\ ] \quad \text{and,}$$

$$\sum_{i=1}^{N} \sum_{j=1}^{3} [\ \vec{b_i}\,(b_i)_j\, \theta_j\ ] \quad \text{and,}$$

$$\sum_{i=1}^{N} [\ \vec{b_i} \cdot (\vec{b_i})^{T}\ ]\ \vec{\theta}$$

17. With $\vec{\theta}$ now separated, the final equation can be written:

$$\sum_{i=1}^{N} [\vec{b_i} \cdot (\vec{b_i})^T - (\vec{b_i})^T \cdot (\vec{b_i})I] \vec{\theta} = \sum_{i=1}^{N} (\vec{a_i} \times \vec{b_i})$$

18. Note that the first term is the outer product of $\vec{b_i}$ with itself while the second term is the inner product of $\vec{b_i}$ with itself.

19. This equation, when computed, will produce a relationship of the form: $A \vec{x} = \vec{b}$. This is a standard matrix equation (1) which may be solved for $\vec{x}$, given A and $\vec{b}$, using any standard matrix equation solver algorithm. The value of $\vec{x}$ is equal to $\vec{\theta_c}$, the correction required to make the RMS error equal to 0.

20. Upon computing a value for $\vec{\theta_c}$, it is converted to a corrective rotation matrix. It is then post multiplied by the last rotation matrix, R, to obtain a new R.

21. Before continuing, the magnitude of the last $\vec{\theta_c}$ is calculated: if it is smaller than a tolerance of 10^{-5} degrees, then the process is halted and R is returned to the main program.

22. If the magnitude of $\vec{\theta}$ is greater than a tolerance of 10^{-5} degrees, then B is pre-multiplied by the new R and another corrective, rotation vector, $\vec{\theta_c}$, is computed between A and RB .

APPENDIX D

COMPUTER PROGRAM DESCRIPTIONS

D.1 General Comments

This investigation required several computer programs to be written on both the AI32 controller and the PDP-11 computer. These programs solved transformation problems, ran AID 600 robot demonstrations, simulated strain studies and aided in gathering data. They were developed, written and refined by Dr. Joseph L. Garbini, Dr. John A. Sidles, and myself.

Dr. Garbini developed the Tensor Method algorithm and translated it into the RAIL language. He also aided in the development of much of the interfacing software between the AI32 and PDP-11 which is not contained in this appendix.

Dr. Sidles developed the RMS Method algorithm and was invaluable in providing assistance for its subsequent translation from its original BASIC language into RAIL.

Both the Tensor and RMS Methods proved to be highly effective and ingenious approaches to the solution of transformation problems encountered in this investigation.

D.2 Description of Program Listings

The following program descriptions and hierarchical diagrams are given. Programs are described, as much as possible, in hierarchical

order with duplication avoided by referring to common subroutines already addressed. Programs described in Sections D.2.1 and D.2.2 were written using the RAIL software computer language. Programs described in Sections D.2.3 and D.2.4 were written in Fortran 77, with extensive use made of scientific programming already contained in the PDP-11 software library. Section D.2.5 listed the subroutine programs used and their source.

D.2.1 Demonstration Programming

The program, OPN, was used to demonstrate the feasibility of robot-assisted total knee arthroplasty. This program and its subroutines are described below and with a hierarchical diagram immediately following this description.

Program Name	Description
OPN	Main program; demonstrates feasibility of robot-assisted knee arthroplasty.
SET_DATA	Subroutine; gathers data on fiducial points, bone reference points and puts it in a form which enables its processing.
DEFINE_TOOLS	Subroutine; provides tool definitions for the stylus, cutter, dial indicator, and the wrist extension; provides definition of the reference location platform.

TOOL_RETURN Subroutine; redefines the tool in use as the default tool definition.

HOM Subroutine; moves the wrist of the robot to its HOME position in the lower, right rear corner of the AID 600 work volume.

MDISPL Subroutine; displays the contents of any n x m matrix on the CRT of the AI32 controller.

BTW Subroutine; computes the transformation matrix between the corresponding sets of fiducial points.

TENSOR Subroutine; computes the inertia tensor of a given set of fiducial points and solves the associated eigenvalue problem for the principal moments of inertia and the direction vectors.

EIGENS Subroutine; computes the eigenvalues and eigenvectors of a real, symmetric matrix.

ESORT Subroutine; sorts the eigenvalues and eigenvectors of the eigenvalue problem in descending order.

DET3 Subroutine; computes the determinant of a 3 x 3 matrix.

DOTC Subroutine; computes dot product of two corresponding column vectors in two separate 3 x 3 matrices.

GMPRD | Subroutine; computes the product of two matrices and forms a resultant matrix.

CUTMOVE | Subroutine; provides the path of points describing the cuts to be made on the femur by the cutter with respect to the origin of the RCS.

DEMO_TWO | Subroutine; controls the cutter in making the five planar cuts on the femur.

CUTSPEED | Subroutine; provides modified values for the variable SPEEDSCHED which regulates the speed of the cutter movement.

POINTER | Subroutine; computes the position and orientation definition necessary to point the desired tool in a specified direction and position in the work volume of the robot.

PHIW | Subroutine; computes a value for the phi angle of the wrist reference frame given the tool definition and its euler angles.

TOOL_REVERSE | Subroutine; computes the inverse orientation angles of the current tool and returns the result.

STUD-CUT | Subroutine; controls the cutter in making the two stud holes for the two corresponding pegs of the prosthesis to be mounted to the femur.

```
OPN
      —SET_DATA
           └─DEFINE_TOOLS
      —TOOL_RETURN
      —HOM
      —MDISPL
      —BTW
           —TENSOR
                —EIGENS
                     └─ESORT
                └─DET3
           —DOTC
           └─GMPRD
      —CUTMOVE
      —DEMO_TWO
           —CUTSPEED
           —POINTER
                └─PHIW
           └─TOOL_REVERSE
      └─STUD_CUT
           —CUTSPEED
           —POINTER
                └─PHIW
           └─TOOL_REVERSE
```
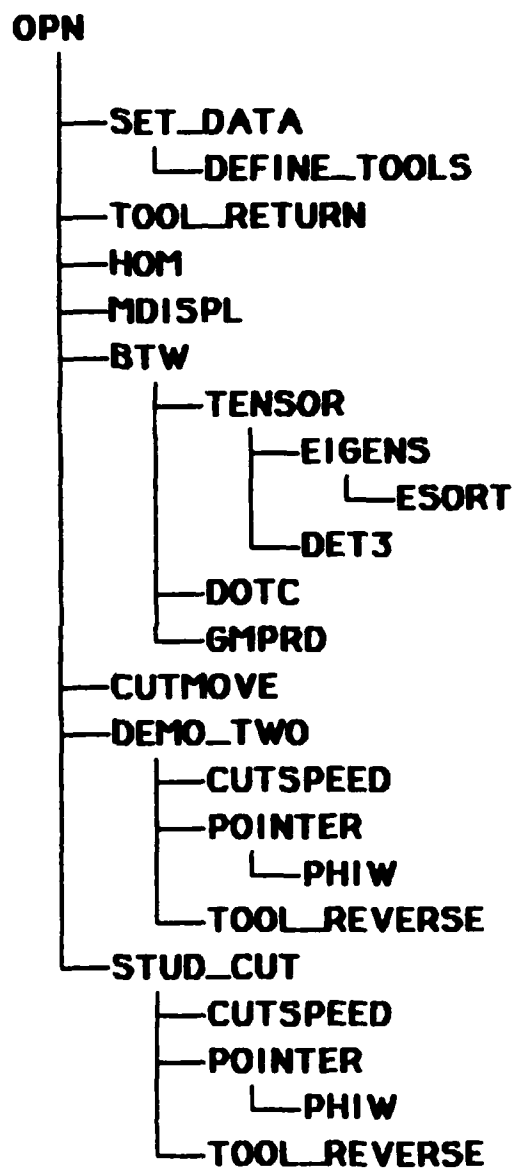
Figure D.1 Hierarchical Diagram: OPN

D.2.2 Accuracy Testing Programming

The program, ACC, was used to evaluate the amount of error induced by human control of probes and subjective alignment of probes with fiducial points. This program and its subroutines are described below with a hierarchical diagram immediately following this description.

Program Name	Description
ACC	Main program; evaluates errors in robotic process induced by human control of probes and subjective judgement.
DEFINE_TOOLS	See Section D.2.1
CUBE_DATA	Subroutine; provides actual location of fiducial points of cube in the CCS.
PRINT	Subroutine; sends variable values to a printer through port 2 of the AI32 controller.
CONFIGURE_PORT2	Subroutine; configures port 2 to 1200 baud.
BTW	See Section D.2.1

```
ACC
    ├──DEFINE_TOOLS
    ├──CUBE_DATA
    ├──PRINT
    │      └──CONFIGURE_PORT2
    └──BTW
           ├──TENSOR
           │      ├──EIGENS
           │      │      └──ESORT
           │      └──DET3
           ├──DOTC
           └──GMPRD
```

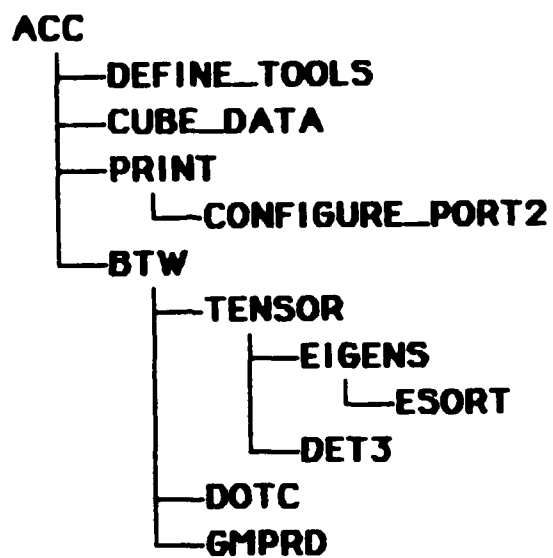Figure D.2 Hierarchical Diagram: ACC

D.2.3 Transformation Algorithm Test Programming

Programs BTW3, BTW4 and BTW5 were used to evaluate the performance of the Tensor, RMS and BAS Method algorithms. These programs are described below with a hierarchical diagram immediately following this description.

Program Name	Description
BTW3	Main program; tests the transformation solver, BTW (Tensor Method).
MDISPL	Subroutine; displays the contents of an n x m matrix on the CRT of the PDP-11 terminal.
BTW	Subroutine; computes the transformation matrix between two corresponding sets of fiducial points.
TENSOR	Subroutine; computes the inertia tensor of a given set of fiducial points and solves the associated eigenvalue problem for the principal moments of inertia and the direction vectors.
EIGENS	Subroutine; computes the eigenvalues and eigenvectors of a real, symmetric matrix.
ESORT	Subroutine; sorts the eigenvalues and eigenvectors of the eigenvalue problem in descending order.
DOT	Subroutine; computes the dot product of two vectors.

DET3	Subroutine; computes the determinant of a 3 x 3 matrix.
GMPRD	Subroutine; computes the product of two matrices and forms a resultant matrix.
MSTR	Subroutine; changes the storage mode of a matrix from a square matrix to a linear matrix of specified storage mode.
LOC	Subroutine; computes a vector subscript for an element in a matrix of specified storage mode.
BTW4	Main program; tests the transformation solver, MBTW (RMS Method).
MDISPL	Subroutine; displays the contents of an n x m matrix on the CRT of the PDP-11 terminal.
MBTW	Subroutine; computes the transformation matrix between two corresponding sets of fiducial points.
OUTPRD	Subroutine, computes the outer product of two vectors and forms the resultant matrix.
ELROMX	Subroutine; creates a differential rotation matrix from a vector.
DOTPRD	Subroutine; computes the dot product of a vector by itself and multiplies it by an identity matrix of

order 3.

VADD	Subroutine; computes the sum of two vectors.
PULLPT	Subroutine; takes a column vector from a matrix and stores it as a vector.
TSUM	Subroutine; subtracts one matrix from another and adds the results to a third matrix.
ANGROT	Subroutine; creates a rotation matrix from a rotation vector based on the small angle relationship.
TANGLE	Subroutine; creates a rotation matrix from a *rotation vector based on the small angle* relationship.
GUESS	Subroutine; computes an initial estimate of the rotation matrix between two sets of corresponding points.
CROSS	Subroutine; computes the cross product of two vectors.
BTW5	Main program; tests the transformation solver, ABTW (BAS Method).
MDISPL	Subroutine; displays the contents of an n x m matrix on the CRT of the PDP-11 terminal.

ABTW   Subroutine; computes the transformation matrix
                between two corresponding sets of fiducial points.
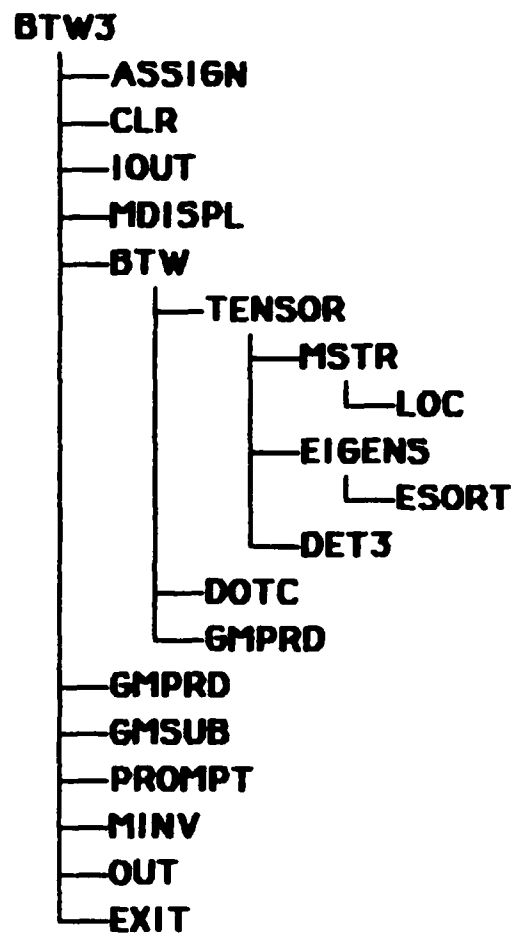
Figure D.3 Hierarchical Diagram: BTW3

```
BTW4
    ├─ASSIGN
    ├─CLR
    ├─IOUT
    ├─MDISPL
    ├─MBTW
    │      ├─OUTPRD
    │      ├─ELROMX
    │      ├─DOTPRD
    │      ├─VADD
    │      ├─PULLPT
    │      ├─TSUM
    │      ├─ANGROT
    │      ├─TANGLE
    │      └─GUESS
    │             └─CROSS
    ├─GMPRD
    ├─GMSUB
    ├─PROMPT
    ├─MINV
    ├─OUT
    └─EXIT
```
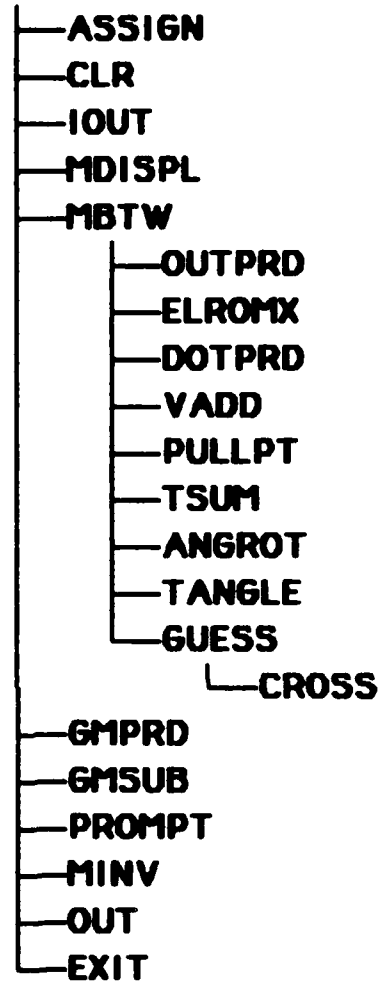
Figure D.4   Hierarchical Diagram: BTW4

```
BTW5
    ├─ASSIGN
    ├─CLR
    ├─IOUT
    ├─MDISPL
    ├─ABTW
    │       ├─GMTRA
    │       ├─GMPRD
    │       └─MINV
    ├─GMPRD
    ├─GMSUB
    ├─PROMPT
    ├─MINV
    ├─OUT
    └─EXIT
```
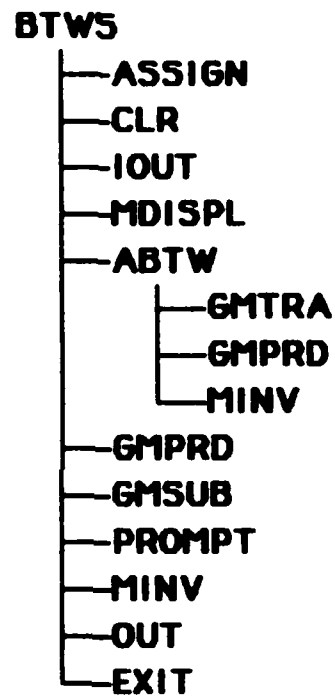
Figure D.5 Hierarchical Diagram: BTW5

D.2.4 Transformation Strain Analysis Programming

The programs TERR2 and TERR3 were used to study the effects of strain and total number of fiducial points on the MTE and MRE values. These programs are described below with a hierarchical diagram immediately following this description.

Program Name	Description
TERR2	Main program; tests the reaction of the TENSOR Method to varying levels of strain and changes in the number of fiducial points used to compute the transformation.
MDISPL	See Section D.2.4.
BTW	See Section D.2.4.
TERR3	Main program; tests the reaction of the RMS Method to varying levels of strain and changes in the number of fiducial points used to compute the transformation.
MDISPL	See Section D.2.4.
MBTW	See Section D.2.4.

```
TERR2
    ┌─CLR
    ├─ASSIGN
    ├─CLOSE
    ├─MDISPL
    ├─GMPRD
    ├─BTW
    │     ┌─TENSOR
    │     │      ┌─MSTR
    │     │      │    └─LOC
    │     │      ├─EIGENS
    │     │      │     └─ESORT
    │     │      └─DET3
    │     ├─DOTC
    │     └─GMPRD
    └─EXIT
```
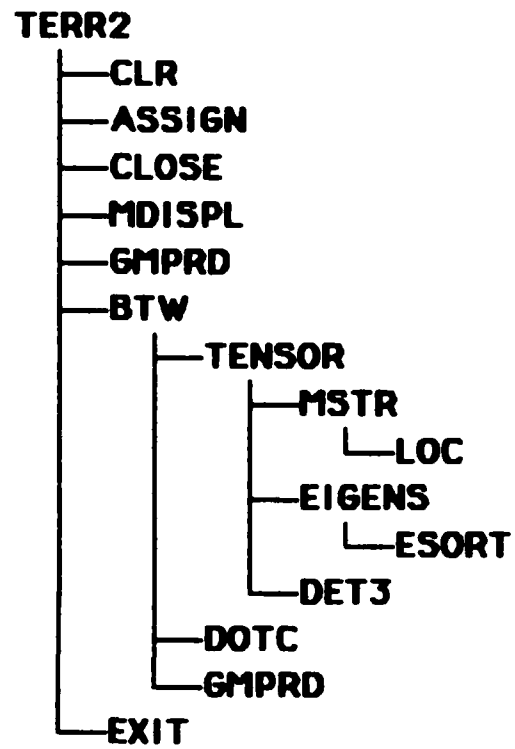
Figure D.6 Hierarchical Diagram: TERR2

```
TERR3
     └─CLR
     ├─ASSIGN
     ├─CLOSE
     ├─MDISPL
     ├─GMPRD
     ├─MBTW
     │       ├─OUTPRD
     │       ├─ELROMX
     │       ├─DOTPRD
     │       ├─VADD
     │       ├─PULLPT
     │       ├─TSUM
     │       ├─ANGROT
     │       ├─TANGLE
     │       └─GUESS
     │              └─CROSS
     └─EXIT
```
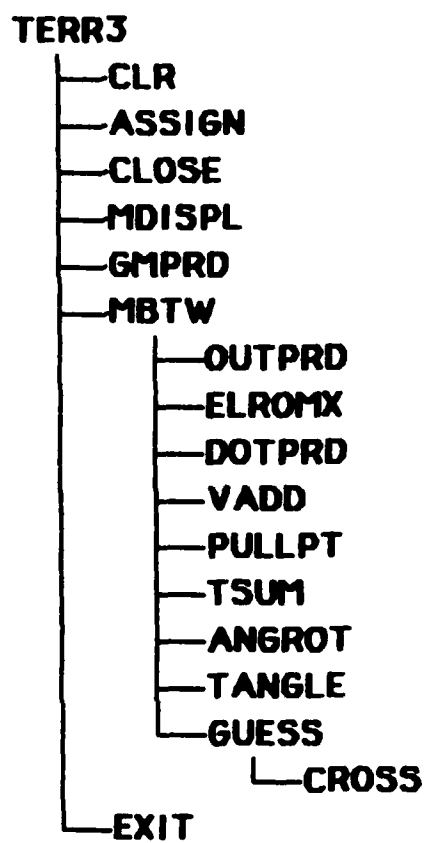
Figure D.7 Hierarchical Diagram: TERR3

D.2.5 Listing of Scientific Programs Used

The PDP-11 computer contained a number of programs in user software libraries which proved invaluable in writing Fortran 77 programs. These programs were contained in a source titled the Scientific Subroutines Package. The following listing acknowledges the programs used from this source.

EIGEN   GMTRA

GMPRD   MINV

GMSUB   SIMQ

Several other programs developed by Joseph L. Garbini were also utilized in programming the routines in this study. The following listing acknowledges these programs.

CLR   OUT

IOUT   PROMPT

Finally, a few subroutines contained in the PDP-11 computer were used that were defined by special key words and which performed simple software functions. These programs are now acknowledged.

ASSIGN   CLOSE

EXIT

END

11 — 86

DTIC